
UNIVERSIDADE FEDERAL DO CEARÁ
CENTRO DE CIÊNCIAS
DEPARTAMENTO DE FÍSICA
DOUTORADO EM FÍSICA


UNIVERSITY OF ANTWERP
PHYSICS DEPARTMENT
BACHARELADO EM FÍSICA

LUAN VIEIRA DE CASTRO

# PROPERTIES OF QUASI PARTICLES ON TWO DIMENSIONAL MATERIALS AND RELATED STRUCTURES

FORTALEZA
2019

LUAN VIEIRA DE CASTRO

# Properties of quasi particles on two dimensional materials and related structures

Tese apresentada ao Curso de Pós-Graduação em Física da Universidade Federal do Ceará como parte dos requisitos para a obtenção do título de Doutor em Física. Área de concentração: Física da Matéria Condensada.

Orientador: João Milton Pereira Jr.
Co-Orientador: Prof. Dr. François M. Peeters
Co-Orientador: Dr. Ben Van Duppen

Dados Internacionais de Catalogação na Publicação
Universidade Federal do Ceará
Biblioteca Universitária
Gerada automaticamente pelo módulo Catalog, mediante os dados fornecidos pelo(a) autor(a)

---

C351p Castro, Luan Vieira de.
Properties of quasi particles on two dimensional materials and related structures / Luan Vieira de Castro. – 2019.
93 f. : il. color.

Tese (doutorado) – Universidade Federal do Ceará, Centro de Ciências, Programa de Pós-graduação em Engenharia Civil, Fortaleza, 2019.
Orientação: Prof. Dr. João Milton Pereira Jr..
Coorientação: Prof. Dr. Ben Van Duppen.

1. Pontos Quânticos. 2. Plasmons. 3. Eléctron liquido. I. Título.

CDD 600

---

LUAN VIEIRA DE CASTRO

Properties of quasi particles on two dimensional materials and related structures

Tese apresentada ao Curso de Pós-Graduação em Física da Universidade Federal do Ceará como parte dos requisitos para a obtenção do título de Doutor em Física. Área de concentração: Física da Matéria Condensada.

Aprovada em:__/__/__ BANCA EXAMINADORA

---

Prof. Dr. João Milton Pereira Jr. (Orientador)
Departamento de Física – UFC

---

Prof. Dr. François M. Peeters
University of Antwerp – UA

---

Prof. Dr. Ben Van Duppen
University of Antwerp – UA Física – UFC

---

Prof. Dr. Diego Rabelo da Costa
Departamento de Física – UFC

---

Prof. Dr. Andrey Chaves
Departamento de Física – UFC

*Dedicated to my parents*

# Aknowledgements

I want to express my gratitude to my mother, Maria das Graças, and my father, Francisco. I know everything that I achieved so far is because of your unconditional love. I hope I can still keep you proud.

I would like to thank Prof. Milton for his supervision throughout most part of my academic years, since graduation. I am really thankful for his availability of sharing his deep knowledge of physics with me. I also would like to thank Prof. François Peeters for his support during my joint Ph.d. stay in Belgium and my incorporation in the CMT group. I also want to express my gratitute for my co-supervisor Dr. Ben Van Duppen. All the discussions we had were very fruitful and made possible for me to understand better a subject so vast and exciting as plasmonic.

I am also thankful to all the professors of the physics department of Universidade Federal do Ceará, who have contributed for my formation. In special, I would like to thank Prof. Diego Rabelo for the friendship; to Prof. Andrey Chaves for always sharing his insightful ideas.

To all my friends. In special to Duarte, Gabriel, Johnathas, Lucas, Ravenna, João Paulo. Without you guys, these years would be, for sure, less fun.

I would also like to thank all the employees of the Deparment of physics of from the Department of Physics of Universidade Federal do Ceará (UFC) and from the Department of Physics of Universiteit Antwerpen (UA). Finally, I would like to thank the Brazilian agency CNPq and the Flemish agency FWO for financial support.

[· · · ] *baixei os olhos, incurioso, lasso,*
*desdenhando colher a coisa oferta que*
*se abria gratuita a meu engenho.*
*A treva mais estrita já pousara sobre*
*a estrada de Minas, pedregosa, e a*
*máquina do mundo, repelida,*
*se foi miudamente recompondo,*
*enquanto eu, avaliando o que perdera,*
*seguia vagaroso, de mãos pensas.*

---

Carlos Drummond de Andrade

# Resumo

Nesta tese, empregamos o uso de técnicas analíticas para estudar propriedades de sistemas bidimensionais em que os portadores podem ser descritos como quasi particulas.

Na primeira parte, consideramos quasi elétrons confinados em pontos quânticos de bicamada de grafeno com empilhamento AA. Uma condição de contorno que descreve o tipo de confinamento é obtida. Em seguida, utilizamos essa condição para calcular os níveis de energia para o ponto com e sem a presença de um campo magnético externo perpendicular a estrutura. Por fim, nosso resultado analítico é comparado com cálculos númericos utilizando modelo tight-binding. Nossos resultados mostram uma dependência de $1/R$ nos níveis de energia, onde $R$ é o raio. Isto é uma consequência direta da natureza de Dirac dos níveis de energia.

Motivados por recentes observações experimentais, na segunda parte investigamos as propriedades de plasmons acústicos em estruturas bidimensionais. Plasmons são quasi partículas que surgem devido ao movimento coletivo de elétrons devido a um campo elétrico externo aplicado. Nosso sistema de estudo é composto de um material bidimensional na presença de um *gate*. Utilizando uma abordagem semiclássica calculamos a dispersão dos plasmons presentes nessa estrutura com correções que vão além da convencional RPA - *random phase approximation* (do inglês, isto é, aproximação de fase aleatória). Outro resultado importante é a obtenção do *damping* que permite uma clara observação da diferença entre regimes balístico, sem colisões, e hidrodinâmico, colisional. Por fim, calculamos o acoplamento do sistema com uma *near field probe* (do inglês, ponta de campo próximo) descrevendo como eficientemente observar plasmons nessas estruturas.

Na terceira parte, uma extensão dos resultados da segunda parte é realizada, onde calculamos as propriedades dos plasmons na presença de uma campo magnético. O mesmo gera uma hibridização dos modos devido às órbitas ciclotrônicas, conhecidos como modos de Bernstein. Por fim, mostramos que as interações elétron-elétron exercem papel fundamental na formação desses modos híbridos.

# Abstract

In this thesis, we use analytical techniques to study properties of two dimensional systems for which the carriers can be described as quasi particles.

In the first part, we consider confinement of quasi electrons on AA-stacked bilayer graphene quantum dots. In order to describe this confinment, an appropriate boundary condition is derived. Then, we use this condition for the calculation of the energy levels of the quantum dot with and without an external applied perpendicular magnetic field. Finally, we compare our analytical result with numerical tight-binding calculations. Our results show that due to the nature of the boundary conditions there is intrisic symmetry in the system related with the Dirac $\boldsymbol{K}$ and $\boldsymbol{K}'$ states. Also, we see that the dependence of the energy levels on the radius of the system is inversely proportinal to the radius, which is a direct consequence of the Dirac nature of electrons in AA-stacked bilayers.

Motivated by recent experimental observations, in the second part we investigate properties of acoustic plasmons. Plasmons are quasi particles describing a collective modes of electrons in the presence of an external electric field. Here, we consider a 2D electron liquid for which plasmon modes can be achieved in the presence of a top gate. Using a semiclassical approach we calculate the plasmon dispersion with many-body corrections beyond Random Phase Approximation. Another important result is the calculation of the damping of acoustic plasmon modes identifying the crossover between the collisionless and hydrodynamic regime. Finally, we calculate the coupling to a near-field probe. This allow the identification of how efficiently observe these modes experimentaly.

In the last part, we extend the results obtained in the second part by adding an external perpendicular magnetic field to the structure. The presence of the field generates hybridization of the plasmon modes, known as Bernstein modes. Finally, we show that electron-electron interactions have fundamental role in the observation of these hybrid modes.

# Contents

# List of Figures

# List of Tables

# 1 Introduction

## 1.1 Graphene and the growing of 2D-materials research

Two-dimensional (2D) materials are crystals for which one of their dimensions is smaller then the other tow[1]. After graphene synthesization in 2004[2], a large number of related 2D materials have been obtained[1, 3]. To list a few we have the transition metal dichalcogenides (TMDs), boron-nitride, phosphorene, silicene, germanene, etc (Fig. 1.1). The list provides a large number of materials and equally a large number of properties to investigate. As an example we have phosphorene, a monolayer of phosphorus atoms, which possess a large gap and in-plane anisotropy. Both properties useful for transport experiments[4, 5]. Other example we can cite antimonene (now an antimonium layer), which possess a large spin-orbit coupling [6, 7]. In the first part of this thesis we focus mainly in graphene. Despite sometime passed since its first observation, its simplicity keeps graphene as a relevant 2D material to investigate. In the second part we discuss general properties for any 2D material.

Since we discuss exclusively graphene, let us briefly remenber some of its main properties. Graphene is made of carbon atoms, one of the most abundant materials in the universe, which has several allotropic forms[8]. In graphene the carbon atoms connect to each order through what is called a $sp^2$ or $\sigma$ bonding - a combination between the $s$ and $p$ orbitals in plane of the valence shell of carbon. Because of these bondings, each carbon atom connects with other three inside the plane forming a honeycomb like structure. On the other hand, the $p_z$ orbital remains pratically unchanged and it is the main responsible for transport on the sheet. This structure results in some of the most interesting properties of graphene from the theoretical point of view: the linearity of the dispersion relation of graphene around some point in the corner of the brillouin zone (known as $\boldsymbol{K}$ and $\boldsymbol{K}$' points). Therefore, from that results that electrons or quasi electrons (we are going to make the distinction in the next section) behave as relativistic particles inside graphene. This is also the starting point for explaning many of the structural properties of graphene:

- Graphene possess one of the largest electronic mobility found in nature. Measure-

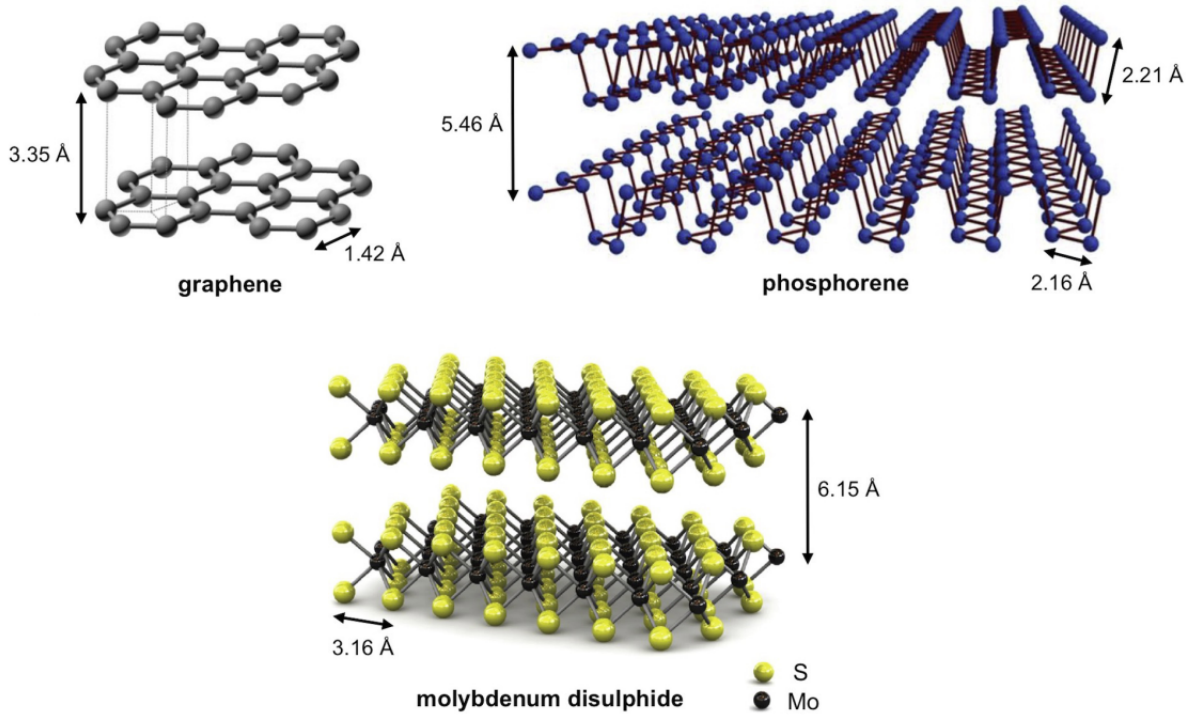


Figure 1.1: Some of the most studied two-dimensional materials: (a) graphene, (b) phosphorene and (c) molybdenium disulphide. Original figure from Ref. [1]

ments on ultraclean suspended graphene has reported values of the order of 200000 $cm^2/Vs$[9];

- Graphene has also interesting mechanical properties, possessing a high ductility which makes graphene useful for a widespread number of applications;
- Optical properties are also enhanced because of graphene linearity. In it, only a small quantity of light is absorbed, while the rest is transmitted. This absorption is independent of other parameters such as the light wavelenght and is directly related with the collective moviment in graphene.

Finally, it is worth mention that the properties of the 2D crystal can be tuned using different means, like by coupling with an electric field, application of strain, etc. Also, the combination of different 2D materials provides the possibility of obtaining structures with richer and richer properties. We expect in the near future to be able of controlling all this properties. This will correspond to a new era of electronic devices.

## 1.2 Some preliminary concepts

### 1.2.1 Quasi particles

An exact analytical solution of the many body problem is impractible for both classical and quantum physics. Indeed, when the interactions are sufficiently strong, particles

motion is completely correlated. This means that the motion of individual parts alters the complete configuration. However, if the interactions are weak enough we can make an approximation and treat the system assuming they are noniteracting. The particles treated in this framework are not the real particles however. They are what is sometimes called quasi particles and, roughly speaking, we could think of this system in the following way[10]

$$\text{quasi particles} = \text{real particle} + \begin{matrix}\text{cloud}\\ \text{of other particles}\end{matrix}. \tag{1.1}$$

The cloud referenced in Eq. 1.1 is the collective effect of the particles on each other. As an example we could cite the atractive electrostatic potential felt by an electron toward an atom. Effectively, the electron fells the potential due the nucleos and the cloud of electrons surrounding it. Therefore we can see that interactions change the particles properties. One characteristic usually changed is the mass. Normally we say quasi particles have an effective mass $m^*$. Another property is the quasi particle lifetime [10, 11, 12]. Because of interactions, after some appreciable amount of time the quasi particle loses its individuality. We say it has dispersed. In the next part of this section we give two examples of quasi particles problem. These are the examples we will be discussing during the next chapters of this thesis.

### Free quasi electrons in a solid

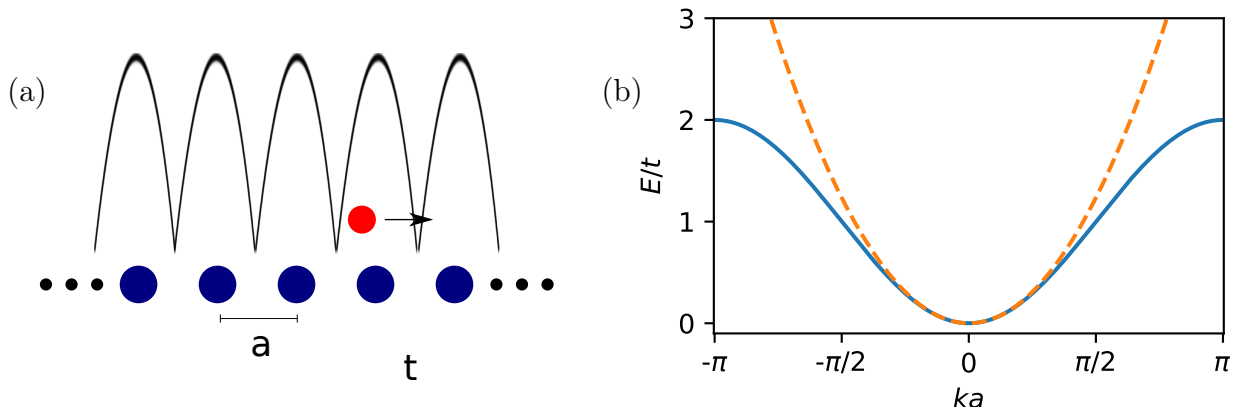


Figure 1.2: (a) Electron propagating in a periodic potential of an unidimensional crystal. Assuming all the interaction are avereaged, free electrons inside this system can be visualized as quasi particles. (b) Dispersion energy of the quasi electron in the unidimensional periodic potential. Blue solid line correspond to the exact solution of the tight-binding hamiltonian, while solid dashed gives the approximate result around $k$ close to zero.

One of the simplest examples of quasi particles on solid state physics is of electrons propagating in the periodic potential of a cristaline structure. Here, we ignore lattice vibrations and interactions with other electrons (The latter can actually be embodied in the periodic potential of the crystal). For simplicity, we consider the unidimensional case

represented in Fig. 1.2(a). In order to describe this system we are going to use the tight-binding formalism[13]. This assumes that the electron is tightly bound to the surrounded ion and therefore can only tunnel between neighbour ions. The Hamiltonian is given by

$$\mathcal{H} = E_0 \sum_i c_i^\dagger c_i + t \sum_i c_i^\dagger c_j + h.c., \tag{1.2}$$

where $t_{ij} = t\delta_{i,i+1}$ is called the hopping parameter and describe the tunneling energy of electrons between sites i and j. The operators $c_i^\dagger$ ($c_j$) creates (anihilates) electrons on site $i$ ($j$). The solution of this hamiltonian is given in terms of the Wanier functions[13, 15]

$$|\psi_W(\boldsymbol{r})\rangle = \frac{1}{\sqrt{2\pi}} \sum_i e^{i\boldsymbol{k}\cdot(\boldsymbol{r}_i)} c_{\boldsymbol{i}}^\dagger |0\rangle. \tag{1.3}$$

Here, $|0\rangle$ represents the vacuum state, $\boldsymbol{k} = (2\pi/a)\hat{\boldsymbol{x}}$ is the wavevector, $a$ is the lattice constant and $c_{\boldsymbol{k}}^\dagger$ is the Fourier transformation of the $c_i^\dagger$ operator. The Wanier wavefunction is a specific type of Bloch[1] function composed of combinations of atomic wavefunctions. By making the bracket of the solution Eq. 1.3 with the hamiltonian Eq. 1.2 we obtain the energy

$$E_{\boldsymbol{k}} = \langle \psi_W | \mathcal{H} | \psi_W \rangle = E_0 + 2t\cos(ka). \tag{1.4}$$

The dispersion relation for Eq. 1.4 is represented in Fig. 1.2(b) for $t = -1$ and $E_0 = -2t$. If we make an expansion of the energy for small values of $k$ we obtain $E_{\boldsymbol{k}} \approx E_0' + ta^2k^2$, where $E_0' = E_0 + 2t$. Comparing this energy with energy for a free particle $E = \hbar^2k^2/2m$, we obtain an effective mass $m^*$ given by $m^* \approx \hbar^2/2ta^2$. For GaAs this values is $m^* \approx 0.067m_0$ [14], where $m_0$ is the mass of electrons. As we are going to see in chapter 2, the same approach for graphene results in the massless relativistic behaviour for electrons. Since the electrons in this approach are pratically free, this results in an infinity lifetime.

The example of quasi particle addressed here is an example of a single particle excitation. The electrons fell an effective potential over it. Next subsection we talk about a collective excitation. In this case the system propagates as whole, "like a wave", generating quasi particles.

### Plasmons

It is possible to have a collective mode of electrons in a crystal if we continously excite the system with high energy excitations. The quasi particles oscillating in this system are known as plasmons. We can calculate the plasma activation frequency $\omega_\mathrm{p}$ for a three dimensional (3D) electron gas using a simple classical model. For doing so, we assume there is a uniform positive charge background $en_0$ nullifying an equal and contrary negative electronic charge. When an external electric field is applied the negative charge is displaced resulting $-en(\delta\boldsymbol{r}, t)$ electronic charge, where $\delta\boldsymbol{r}$ is the displacement of the

[1] If a particle is subjected to a periodic potential $U(\boldsymbol{r}) = U(\boldsymbol{r} + \boldsymbol{T})$, the Bloch theorem says that the wavefunction has the form $\psi(\boldsymbol{r}) = e^{i\boldsymbol{k}\cdot\boldsymbol{r}}u(\boldsymbol{r})$, where $u$ has the periodicity of the potential.

electronic charge and $t$ is the time coordinate. Therefore, the net charge over the system is given by $e(n_0 - n(\delta\boldsymbol{r}, t))$ and hence from Gauss law we obtain

$$\nabla \cdot \boldsymbol{P}(\boldsymbol{r}, t) = 4\pi e(n_0 - n(\boldsymbol{r}, t)). \tag{1.5}$$

Here, $\boldsymbol{P}(\boldsymbol{r}, t)$ is the polarizability of the system, i.e it is the induced electric field due to the charge displacement. Also, we require the electron current $n(\delta\boldsymbol{r}, t)\delta\dot{\boldsymbol{r}}$ to satisfy the continuity equation

$$-\frac{\partial n(\delta\boldsymbol{r}, t)}{\partial t} = \nabla \cdot (n(\delta\boldsymbol{r}, t)\delta\dot{\boldsymbol{r}}) \approx n_0 \nabla \cdot \delta\dot{\boldsymbol{r}}. \tag{1.6}$$

In the last step we made the approximation $n \approx n_0$ since $\dot{\boldsymbol{r}}$ is already first order in the pertubation. Integrating Eq. 1.6 and the comparing with Eq. 1.5 results in the relation

$$\nabla \cdot \boldsymbol{P}(\boldsymbol{r}, t) = 4\pi e(n_0 - n(\delta\boldsymbol{r}, t)) = 4\pi e n_0 \nabla \cdot \delta\boldsymbol{r} = \nabla \cdot (4\pi e n_0 \delta\boldsymbol{r}) \tag{1.7}$$

and hence this results in the expression

$$\boldsymbol{P}(\boldsymbol{r}, t) = 4\pi e n_0 \delta\boldsymbol{r}. \tag{1.8}$$

We can combine this expression for the electron field with the Newtonian equation of motion

$$m\delta\ddot{\boldsymbol{r}} = -e\boldsymbol{P}(\delta\boldsymbol{r}, t) = -4\pi e^2 n_0 \delta\boldsymbol{r}. \tag{1.9}$$

This expression shows that electrons describe a simple harmonic oscillation with frequency $\omega_\mathrm{p}$ given by

$$\omega_\mathrm{p} = \sqrt{\frac{4\pi e^2 n_0}{m^*}}. \tag{1.10}$$

For electrons in a metal typical values of $\omega_\mathrm{p}$ are of the order of $10^{16}$ Hz of magnitude.

We can forcibly introduce the lifetime concept in our description if we assume the system is under the influence of damping therefore resulting in a damped harmonic oscillator

$$m\delta\ddot{\boldsymbol{r}} + m\tau^{-1}\dot{\boldsymbol{r}} = -e\boldsymbol{E}(\delta\boldsymbol{r}, t). \tag{1.11}$$

Also, we have introduced the application of an external electric field over the sytem $\boldsymbol{E}(\boldsymbol{r}, t)$. Assuming the electric field is periodic with a frequency $\omega$, we can fourier transform Eq. 1.11 and finally we obtain

$$\delta\boldsymbol{r}(\omega) = \frac{e}{m(\omega^2 + i\omega\tau^{-1})}\boldsymbol{E}(\omega) \tag{1.12}$$

Using the definition of polarizability of Eq. 1.8 we obtain

$$\boldsymbol{P}(\omega) = -\frac{\omega_\mathrm{p}^2}{(\omega^2 + i\omega\tau^{-1})}\boldsymbol{E}(\omega) \tag{1.13}$$

Finally, we define the displacement field $\boldsymbol{D}(\boldsymbol{r},t)$ as the total electric field inside the material, i.e, the combination of external plus polarization field. Therefore this results

$$\boldsymbol{D} = \epsilon_0(\boldsymbol{E}+\boldsymbol{P}) = \epsilon_0\left(1 - \frac{\omega_{\mathrm{p}}^2}{(\omega^2 + i\omega\tau^{-1})}\right)\boldsymbol{E}(\omega) = \epsilon_0\epsilon(\omega)\boldsymbol{E}(\omega), \tag{1.14}$$

where we have defined the dielectric function $\epsilon(\omega)$

$$\epsilon(\omega) = 1 - \frac{\omega_{\mathrm{p}}^2}{(\omega^2 + i\omega\tau^{-1})}. \tag{1.15}$$

Plasmon modes are obtained when the total electric field inside the metal is canceled. The electrons propagate in a correlate movement in order to nullify the external field. From Eq. 1.14 we see this is equivalent to make $\epsilon(\omega) = 0$.

### 1.2.2 Graphene tight-binding

For the calculations of graphene spectrum on $\pi$ bands we can use the tigh-binding model introduced in Sec. 1.2.1. In graphene we have a triangular crystaline structure with two atoms in the base. We label these atoms $A$ and $B$. This is represented in Fig. 1.3. Therefore, this results in the hamiltonian

$$\hat{H} = \sum_i E_0(a_i^\dagger a_i + b_i^\dagger b_i) + \sum_{i,j} t_{ij}(a_i^\dagger b_j + h.c.), \tag{1.16}$$

where the operators $a_i^\dagger$ ($b_j$) creates (anihilates) electrons in sublattice $A$ ($B$). By convention, we choose $E_0 = 0$. We also assume $t_{ij} = t =$ 'first neighbours hopping' (See Fig. 1.3). Numerical calculations give values of $t \approx 2.97$ eV.

Graphene hexagonal lattice does not have a Bravais lattice structure. This means it is impossible of going from one point of the lattice to any other by a simple lattice translation. A point of the Bravais lattice is actually a combination of sublattices $A$ and $B$. And therefore we define again the Wannier wave function

$$|\Psi_W(\boldsymbol{r}_i)\rangle = \frac{1}{2\pi}\sum_i \left(c_A e^{i\boldsymbol{k}\cdot\boldsymbol{R}_{i,A}} a_i^\dagger + c_B e^{i\boldsymbol{k}\cdot\boldsymbol{R}_{i,B}} b_i^\dagger\right)|0\rangle. \tag{1.17}$$

Here, the vectors $\boldsymbol{R}_{i,A}$ and $R_{i,B}$ give the position of the A and B atoms of graphene sublattices. In order to find the exact values the eigenenergies and $c_A$ and $c_B$ coefficients we apply the hamiltonian $\mathcal{H}$ from the left side of $|\psi_W\rangle$. From the right side we multiply either $\langle 0|a_j$ or $\langle 0|b_j$. This finally results in a matricial equation given by

$$E\begin{pmatrix} c_A \\ c_B \end{pmatrix} = -t\begin{pmatrix} 0 & S(\boldsymbol{k}) \\ S^*(\boldsymbol{k}) & 0 \end{pmatrix}\begin{pmatrix} c_A \\ c_B \end{pmatrix}, \tag{1.18}$$

where the function $S(\boldsymbol{k}) = \sum_{i=1}^{3} e^{\boldsymbol{k}\cdot\boldsymbol{\delta}_i}$ is called the structure factor of graphene and $\boldsymbol{\delta}_i$ defined in Fig. 1.3 are the first neighbours distance. Solving the equation $\det|\mathcal{H} - \mathrm{E}\hat{1}| = 0$ we obtain the eigenvalues of the equation

$$E_\pm(\boldsymbol{k}) = \pm t|S(\boldsymbol{k})| = \pm\sqrt{3 + f(\boldsymbol{k})}, \tag{1.19}$$

where we have defined the function $f(\boldsymbol{k}) = 2\cos\left(\sqrt{3}k_y a\right) + 4\cos\left(\sqrt{3}k_y a/2\right)\cos(3k_x a/2)$. The energy spectrum of Eq. 1.19 inside the brillouin zone is represented on Fig. 1.3. The two energies $E_\pm$ touch in six different points of the Brillouin zone. From these six points, two are inequivalents (in total analogy with points $A$ and $B$ of the direct lattice). We define this points as $\boldsymbol{K}$ and $\boldsymbol{K}'$ and they are given by

$$\boldsymbol{K} = (\frac{2\pi}{3a}, -\frac{2\pi}{3\sqrt{3}a}) \qquad \boldsymbol{K}' = (\frac{2\pi}{3a}, \frac{2\pi}{3\sqrt{3}a}), \tag{1.20}$$

Around these points, in a low energy regime, the band structure of graphene shows a conical profile in an exactly analogy with the energy-momentum relation between massless particles in the relativistic theory. Hereafter, we are going to explore this relativistic analogy to find the infinite mass boundary conditions in chapter 2. Another interesting property we would like to highlight is the symmetry between the two solution, $E_+$ and $E_-$, around the touching points. This high symmetry is of the main factors responsible for graphene high mobility. The inclusion of high order hopping parameters break these symmetry though. These are however small contributuions to the spectrum (second neighbours hopping are $t' \approx 0.073$ eV) and therefore we can still assume the system is higly symmetric.

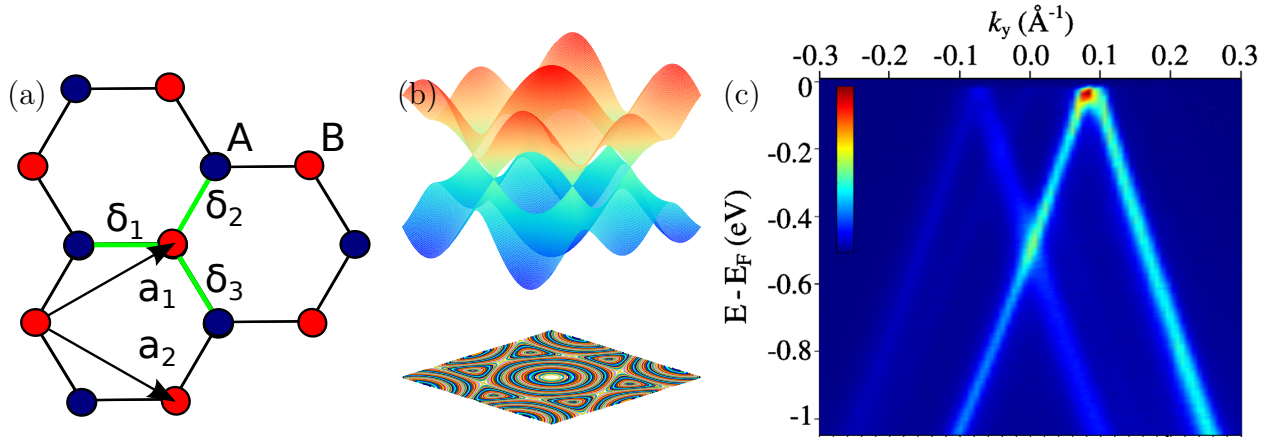


Figure 1.3: (a) Graphene crystaline structure. $A$ (blue) and $B$ (red) are the different graphene sublattices. (b) Graphene dispersion relation obtained using the tight-binding first neighbours approximations (See Eq. 1.19). (c) The valence band of a graphene structure grown on the surface of a SiC crystal. Image was obtained using the ARPES tecquinique [16].

The band structure of graphene can be observed experimently through a procedure known as ARPES (angle resolved photoemission spectroscopy). This tequinique uses the scattering of photons by the crystaline structure of graphene. The information of the scattered photons momentum and energy intensity allow us to obtain the energy distribution in the Fermi surface. Figure. 1.3 is represented the first observation of graphene band structure using this procedure[16]. Since the conduction band is empty, we can only see the valence band in the representation.

### 1.2.3 Linear-response theory

In many situations we are interested in describe a system under the influence of small pertubations. From the experimental point of view, the coupling with small probes are relevant since we look for ways of interacting with system without changing its properties. Here, we present a formal way of calculating the properties of a slightly modified system.

Consider a many particle time-independent Hamiltonian $\mathcal{H}$ and let $|\Psi_{\rm S}(t)\rangle$ be the wave function in the Schrondiger picture. Therefore it must satisfy

$$i\hbar\frac{\partial}{\partial t}|\Psi_{\rm S}(t)\rangle = \mathcal{H}|\Psi_{\rm S}(t)\rangle. \tag{1.21}$$

The time-dependent wavefunction is given by

$$|\Psi_{\rm S}(t)\rangle = e^{-i\mathcal{H}t/\hbar}|\Psi_{\rm S}(0)\rangle. \tag{1.22}$$

Now let us assume that in time $t = t_0$ we apply a small pertubation over the system $\mathcal{H}_{\rm ext}$. If $\mathcal{H}_{\rm ext}$ is sufficiently small we expect the wavefunction for $t \leq t_0$ possess some resemblance with Eq. 1.22. If $|\Psi(t)\rangle$ is the wavefunction of the system with the application of the external field, we assume it should be given by the following expression

$$|\Psi(t)\rangle = e^{-i\mathcal{H}t/\hbar}A(t,t_0)|\Psi_{\rm S}(0)\rangle. \tag{1.23}$$

where $A(t,t_0)$ must satisfy $A(t,t_0) = 1$ for $t < t_0$. Next, imposing the solution shown at Eq. 1.23 must to satisfy the Schrondiger equation for the $t > t_0$, we obtain

$$i\hbar\frac{\partial}{\partial t}\left(e^{-i\mathcal{H}t/\hbar}A(t,t_0)\right)|\Psi_{\rm S}(0)\rangle = i\hbar\frac{\partial}{\partial t}|\Psi(t)\rangle = \left(\mathcal{H}+\mathcal{H}^{\rm ext}\right)e^{-i\mathcal{H}t/\hbar}A(t,t_0)|\Psi(t)\rangle. \tag{1.24}$$

and therefore this results

$$i\hbar\frac{\partial A(t,t_0)}{\partial t} = \mathcal{H}^{\rm ext}_{\rm H}(t)A(t,t_0), \tag{1.25}$$

where $\mathcal{H}^{\rm ext}_H(t)$ is the pertubation in the Heinsenberg picture. This equation can be solved iteratively resulting in an expression for $A(t,t_0)$ as accurate as possible. Therefore we can write

$$A(t,t_0) = 1 - \left(\frac{i}{\hbar}\right)\int_{t_0}^{t}\mathcal{H}^{\rm ext}_H(t')dt' + \cdots \tag{1.26}$$

which results in the wave function

$$|\Psi(t)\rangle = e^{-i\mathcal{H}t/\hbar}|\Psi_{\rm S}(0)\rangle - e^{-i\mathcal{H}t/\hbar}\left(\frac{i}{\hbar}\right)\int_{t_0}^{t}\mathcal{H}^{\rm ext}_H(t')|\Psi_{\rm S}(0)\rangle dt' + \cdots \tag{1.27}$$

It is also possible to obtain the expected value of any observable in the presence of the pertubation. If the operator $\mathcal{O}_{\rm S}(t)$ represents an observable, its expected value can be computed using the wavefunction of Eq. 1.27. The linear response theory (LRT) correspond to taking only the first order contribution for this expression. Therefore we obtain

$$\langle\Psi(t)|\mathcal{O}_{\rm S}(t)|\Psi(t)\rangle = \langle\Psi(0)|\mathcal{O}_{\rm H}(t)|\Psi(0)\rangle + \left(\frac{i}{\hbar}\right)\int_{t_0}^{t}\langle\Psi(0)|\left[\mathcal{H}^{\rm ext}_H(t'),\mathcal{O}_{\rm H}(t)\right]|\Psi(0)\rangle dt' \tag{1.28}$$

The external pertubation $\mathcal{H}^{\rm ext}$ can usually be written as the product of two terms, namely $\mathcal{H}^{\rm ext} = F^{\rm ext}(t)\mathcal{P}_{\rm H}(t)$, where $\mathcal{P}_{\rm H}(t)$ is the observable of the system probing the system. The variation of the expected value of $\mathcal{O}_{\rm H}$ is given by

$$\delta\langle\mathcal{O}_{\rm H}\rangle = \left(\frac{i}{\hbar}\right)\int_{t_0}^{t}\langle[\mathcal{P}_{\rm H}(t'),\mathcal{O}_{\rm H}(t)]\rangle F_{\rm H}^{\rm ext}(t')dt' = -\left(\frac{i}{\hbar}\right)\int_{t_0}^{t}\chi_{\mathcal{O},\mathcal{P}}(t,t')F_{\rm H}^{\rm ext}(t')dt' \quad (1.29)$$

The function $\chi_{\mathcal{O},\mathcal{P}}(t,t')$ is named the linear response function of the system. For the situations we are interested here we calculate the response of the system to an external electric field

$$\mathcal{H}_{\rm H}^{\rm ext} = \int\frac{d\boldsymbol{r}'}{(2\pi)^3}n(\boldsymbol{r}',t)\phi^{\rm ext}(\boldsymbol{x}',t). \quad (1.30)$$

This therefore result in a modification of the density of the system given by

$$\delta n(\boldsymbol{r},t) = -\left(\frac{i}{\hbar}\right)\int_{0}^{t-t_0}\chi_{\rm nn}(\boldsymbol{r},\boldsymbol{r}',\tau)\phi_{\rm H}^{\rm ext}(\tau)d\tau \quad (1.31)$$

Here, we eliminate the brackets for making shorter the notation. We also made the variables substituion $\tau = t - t_0$ in the integral and we have defined $\chi_{\rm nn}(\boldsymbol{r},\boldsymbol{r}',\tau)$ as the density-density response function. Most cases of interest we consider the application of a periodic electric field $\phi_{\rm H}^{\rm ext}(\tau) = \phi_{\rm H}^{\rm ext}(\omega)(e^{i\omega t} + h.c.)$. Here we only focus in system that possess spatial translational invariance. This means the properties can not depend of the absolute values of $\boldsymbol{r}$ and $\boldsymbol{r}'$, but rather on the different $\boldsymbol{r}-\boldsymbol{r}'$: $\chi_{\rm nn} = \chi_{\rm nn}(|\boldsymbol{r}-\boldsymbol{r}'|,\tau)$. Therefore we can make the Fourier transformation of the spatial and temporal components resulting in the simpler equation

$$\delta n(\boldsymbol{q},\omega) = \chi_{\rm nn}(\boldsymbol{q},\omega)\phi^{\rm ext}(\boldsymbol{q},\omega). \quad (1.32)$$

By knowing the value of the density-density response function it is possible to calculate the excitations spectrum of a many particle system. The calculation $\chi_{nn}$ can be made analitaly for a free non interacting gas at zero temperature. For this case the particle density is given by $n(\boldsymbol{q}) = (1/L^2)\sum_i e^{-i\boldsymbol{q}\cdot\boldsymbol{r}_i}$, where $L$ is the dimension of the system. A detail calculation show that $\chi_{\rm nn}$ is given by[**?**]

$$\chi^0_{\rm nn}(q,\omega) = \mathcal{N}_0\frac{q_{\rm F}}{q}\left[\Sigma\left(\frac{\omega+i\eta}{qv_{\rm F}} - \frac{q}{2q_{\rm F}}\right) - \Sigma\left(\frac{\omega+i\eta}{qv_{\rm F}} + \frac{q}{2q_{\rm F}}\right)\right], \quad (1.33)$$

where $\mathcal{N}_0$ is the non interacting density of states, $q_{\rm F}$ and $v_{\rm F}$ are the Fermi wavevector and velocity and the function $\Sigma$ is given by

$$\Sigma(x) = x - \text{sign}\left(\text{Re}(x)\right)\sqrt{x^2-1} \quad (1.34)$$

for a 2D parabolic electron gas. The Eq. 1.33 is however valid for any dimension. It is also possible to obtain an analitycal equation in the case of graphene[**?**]. However, we have to be more careful since intra and inter layers contributions are included in the description.

For a significant part of this work we are going to look at response in the longwavelength limit, i.e, for $q \ll q_{\mathrm{F}}$. Therefore, is of relevance to analyse the response function Eq. 1.33 in this regime. A direct calculation results

$$\chi^0_{\mathrm{nn}}(q,\omega) = \mathcal{N}_0 \frac{q v_{\mathrm{F}}}{\omega + i\eta}. \tag{1.35}$$

This expression will be relevant for comparing the limiting cases of the expressions obtained in Chap. 3.

The inclusion of interactions in the many-body problem turn the calculation of the response function more complicated. One of the simplest possible ways of doing this is by means of the RPA approximation. Operationally, the RPA ca be defined in a number of ways. The electric field felt by a system can be defined self-consistently where the induced electron density can be used for the calculation of the generated field. The RPA is the approximation for which we replace this field by the non-interacting one in a translational invariant system generating the celebrated expression

$$\chi^{RPA}_{nn}(q,\omega) = \frac{\chi_0(q,\omega)}{1 - v_q \chi_0(q,\omega)}, \tag{1.36}$$

where $v_q$ is the electron-electron interaction potential $v_q = e^2/q$ for free electrons. Using the definition Eq. 1.32 we have

$$\frac{\chi_0(q,\omega)}{\chi^{RPA}_{nn}(q,\omega)} = \frac{\phi^{RPA}(q,\omega)}{\phi_0(q,\omega)} = \epsilon(q,\omega) = 1 - v_q \chi_0(q,\omega) \tag{1.37}$$

We used Eq. 1.37 to define the dieletric constant $\epsilon(q,\omega)$. Pasmon modes are obtained as solution of the equation $\epsilon(q,\omega) = 0$

## 1.3 Organization of the thesis

Throughout all this thesis we describe different subjects which are partially correlated. The glue connecting all this topics is that electronic system on material (here, on 2D materials) are quasi particle which can behave in differentlydepending on the way they are excited. The remaining parts of this thesis are organized as follow:

- In Chap. 2 we discuss the problem of the calculation of the infinite mass boundary condition for a graphene bilayer with AA stacking. We calculate the energy levels for a bilayer graphene quantum dot using this model and compare with tight-binding numerical calculations. Latter, we investigate the influence of an external perpendicular magnetic field over the structure;

- In chap. 3 we study the problem of the propagation of acoustic plasmon in a 2D material sample. Two different regimes are observable: ballistic or collisionless, plasmons propagate without collision in coherent movement; and hydrodynamic or collisional, where electrons collide with themselves propagating like a sound wave. Mechanisms of experimental observation are latter discussed.

- Finally, in chap. 4 we investigate the spectrum of plasmons under the influence of a magnetic field. The coupling between plasmon modes and the cyclotronic orbits generates a hybrid mode known as magnetoplasmon. Ways of controlling the magnetoplasmon spectrum through collisions are latter discussed;
- Chap. 5 is dedicated for final conclusions.

# 2 AA-stacked Bilayer Graphene Quantum Dots

## 2.1 Overview

In this chapter, we discuss the infinite-mass boundary conditions (IBMC), a simple approach for calculating the energy levels in a quantum dot. Recently, theoretical studies of energy spectrum behaviour of circular graphene quantum dots (GQD's) in the presence of an external magnetic field have been performed adpoting this type of conditions[17, 18]. For the massless Dirac equation, graphene, this condition was derived by Berry and Mondragon (Sec. 2.3) using a geometrical argument. Here, we derive a new IMBC for the bilayer graphene with AA-stacking. We use an approach similar to [19], where we take the mass-term inside the dot equal zero and infinity outside, as shown schematically in Fig. 2.2. We show that this approach result in two equations involving the components of the pseudo-spinor at the boundary of the system. The resulting solution has a clear $1/R$ dependence which is a characteristic of the Dirac behaviour of the system.

About the work presented in this chapter a small paper is being written.

## 2.2 Hamiltonian

### 2.2.1 Graphene monolayer

In order to create a quantum dot (QD) confinement has to be induced over the system. On parabolic 2D materials this can be done by means of an electrostatic potential shifting the bottom of the band. Graphene, on the other hand, has a linear spectrum and satisfies the Dirac equation for small energies around the neutrality point Fig. 2.1. One important consequence of this property is the emergency of Klein tunneling[8, 20] electrons are 100 % transmitted through a barrier and therefore can not be confined by an electrostatic potential. One way of overpassing this issue, it is by applying a potential which open a gap in the neighborhood instead of shift the system. In graphene Dirac-like hamiltonian, we will see, this can be done by introducing a mass term in the equation. This term breaks the symmetry between the sublattices of the system and consequently opens a gap

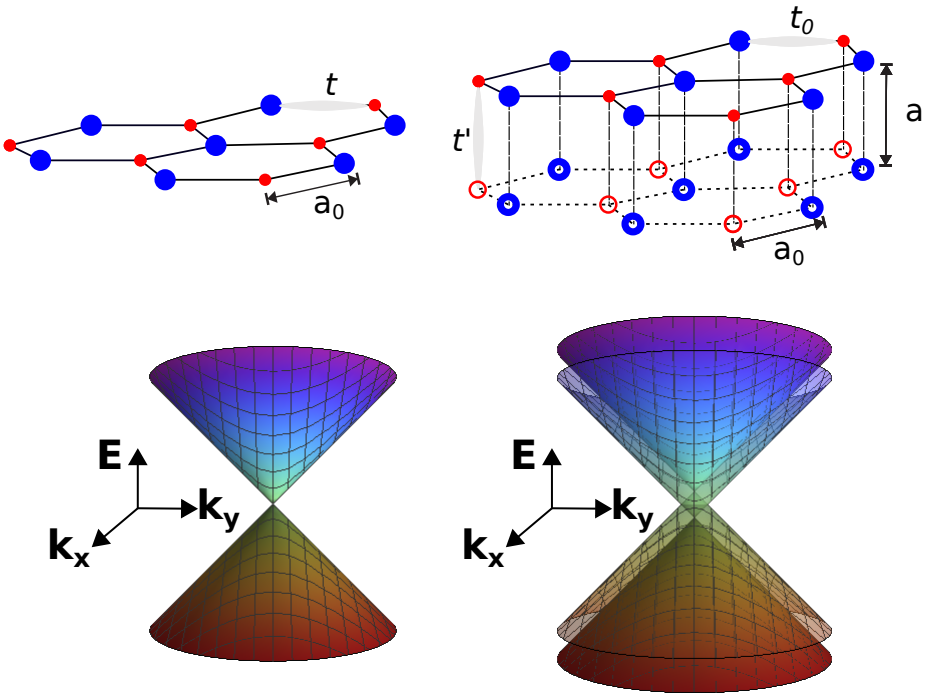


Figure 2.1: Graphene (a) monolayer and (b) AA-stacked bilayer with hoppings and lattice parameters specificated.

(Latter, we will see this is the basic idea behind the IMBC).

Next section we start discussing the IMBC conditions. Here we first obtain the appropriate hamiltonian for our system. We start with graphene and later the derive the equivalent expression for the $AA$-bilayer. Using the definition of $S(\boldsymbol{k})$ , we can make a taylor expansion around one of the $\boldsymbol{K}$ and $\boldsymbol{K}'$ points. For $\boldsymbol{K}$ we have

$$S(\boldsymbol{k}) \approx S(\boldsymbol{K}) + (\boldsymbol{k}-\boldsymbol{K}) \cdot \frac{\partial S(\boldsymbol{k})}{\partial \boldsymbol{k}}|_{\boldsymbol{k}=\boldsymbol{K}} = \frac{3at}{2}(\delta k_x - i\delta k_y)e^{i5\pi/6}. \tag{2.1}$$

The exponential factor $e^{i5\pi/6}$ has no physical meaning and can be ommitted in the expression (It is possible to consider another $\boldsymbol{K}$ where this factor does not show up). Also assuming $\boldsymbol{K}$ is the origin of our referential

$$\mathcal{H}_{\boldsymbol{K}} \approx \frac{3at}{2}\begin{pmatrix} 0 & (k_x - ik_y) \\ (k_x + ik_y) & 0 \end{pmatrix} = v_{\mathrm{F}}\boldsymbol{\sigma}\cdot\hat{\boldsymbol{p}}, \tag{2.2}$$

where the Fermi velocity $v_{\mathrm{F}}$ is given by $v_{\mathrm{F}} = 3at/2\hbar$ and in the last step we replaced the momentum components $\boldsymbol{p} = \hbar\boldsymbol{k}$ by the operators $\hat{\boldsymbol{p}} = -i\hbar\boldsymbol{\nabla}$. The $\sigma$ vector are the Pauli matrices given by

$$\sigma_x = \begin{pmatrix} 0 & 1 \\ 1 & 0 \end{pmatrix} \qquad \sigma_y = \begin{pmatrix} 0 & -i \\ i & 0 \end{pmatrix} \tag{2.3}$$

The equivalent expression for an approximation around the $\boldsymbol{K}'$ point can be obtained using the same approach. The resulting hamiltonian is directly related with Eq. 2.2 by a simple transformation $\mathcal{H}_{\boldsymbol{K}'} = \mathcal{H}^*_{\boldsymbol{K}}$.

### 2.2.2 Graphene bilayer

For a bilayer, things are a little bit more complicated. First, we have to hightlight there are different ways of stacking the two layers of graphene on the top of each other. In the first one, named $AB$ stacking, one of the sublattices is on the top of the other, while the other sublattice is in the center of the hexagonal structure of the other. This geometry was already widely studied[19]. Therefore, we only focus in the second geometry named $AA$-stacking and represented in Fig. 2.1. There, we have both atoms of both sublattices on the top of each other. Now we have four different sublattices, namely $A$, $B$, $A'$ and $B'$. Addionaly, besides the intralayer hopping $t$, we have also to consider hopping between different layers. In the minimal hopping approximation there are only hopping between the first neighbours in different layers, i.e, $A/A'$ and $B/B'$. Therefore the tight-binding hamiltonian becomes

$$\hat{H} = \sum_i E_0(a_i^\dagger a_i + b_i^\dagger b_i) - t_0 \sum_{i,j}(a_i^\dagger b_j + {a'}_i^\dagger b'_j + h.c.) + t\sum_{i,j}\left(a_i^\dagger {a'}_j + b_i^\dagger {b'}_j + h.c.\right) \quad (2.4)$$

Here, we have defined the additional creation and anihilation operators for ${a'}_i/{a'}_j^\dagger$ and ${b'}_i/{b'}_j^\dagger$ for the $A'$ and $B'$ sublattices. If we perform the analogous procedure of the case of graphene we obtain the Hamiltonian

$$E\begin{pmatrix} c_A \\ c_B \\ c_{B'} \\ c_{A'} \end{pmatrix} = \begin{pmatrix} 0 & S(\boldsymbol{k}) & 0 & t \\ S^*(\boldsymbol{k}) & 0 & t & 0 \\ 0 & t & 0 & S^*(\boldsymbol{k}) \\ t & 0 & S(\boldsymbol{k}) & 0 \end{pmatrix}\begin{pmatrix} c_A \\ c_B \\ c_{B'} \\ c_{A'} \end{pmatrix}, \quad (2.5)$$

where $S(\boldsymbol{k})$ has the same definition as before. Because of the number of sublattices, now we have a $4\times 4$ matrix. The solution of the eigen value problem results

$$E_{\boldsymbol{k}}^\gamma = \pm t_\perp^{AA} + \gamma t|g(\vec{k})| \quad (2.6)$$

where $\gamma = \pm 1$ denotes the conduction and valence bands. We can see from Eq. 2.32 that the solution for the $AA$ bilayer is very similar to the solutions obtained for graphene. Now we have four conical surfaces, two shifted of $t$ and two shifted of $-t$. Finally, if we perform the same approximations as the ones made for graphene, we obtain the Hamiltonian

$$\mathcal{H} = \begin{pmatrix} \tau\Delta & \pi & 0 & t \\ \pi^\dagger & -\tau\Delta & t & 0 \\ 0 & t & \tau\Delta & \pi^\dagger \\ t & 0 & \pi & -\tau\Delta \end{pmatrix}. \quad (2.7)$$

Here, $\tau = \pm 1$ denotes the expansion around the $\boldsymbol{K}$ and $\boldsymbol{K}'$ points respectvely and $\pi = v_{\mathrm{F}}(p_x - p_y) = -i\hbar v_F e^{i\theta}(\partial_r + i/r\partial_\theta)$ is the momentum operator. The intralayer hopping parameter is given by $t \approx 0.09t_0 \approx$ meV (See Fig. 2.1). The eigenvector for this 4x4 Hamiltonian is a pseudospinor given by $\Psi = [\psi_A, \psi_B, \psi_{B'}, \psi_{A'}]^{\mathrm{T}}$, where $A$, $B$, $A'$ and $B'$ label the sublattices represented in Fig. 2.1(b).

## 2.3 Berry Mondragon Boundary Conditions

Before describing the boundary conditions for the graphene bilayer, let us first discuss the monolayer case. We are going to present this results using some an approach first introduced by Berry and Mondragon in an article published in 1986 [**?**]. Altought it is also possible to obtain the graphene IMBC using the approach introduced in the next section, here we use Berry and Mondragon's model due to its simplicity and geometrical meaning. The model was named neutrino billiard since it was first used to describe neutrinos, considered as massless particles so far. With a mass term, graphene hamiltonian around one of the valleys is given by

$$\mathcal{H}_{\boldsymbol{K}} = -i\hbar v_F \boldsymbol{\sigma}\cdot\boldsymbol{\nabla} + \Delta(x,y)\sigma_z, \tag{2.8}$$

$v_{\mathrm{F}} \approx 10^6$ m/s is the Fermi velocity and $\sigma$ are the Pauli matrices. A major description can be done if we look to the definition of the time-reversal operator[**?**]

$$\hat{\Theta} = -i\sigma_y\hat{\eta}, \tag{2.9}$$

where $\hat{\eta}$ is the complex conjugation operator. Here, we are not interested in discussing the real physical meaning of $\Theta$, but rather how it affects Eq. 2.8. Applying the transformation defined by $\Theta$ on $H_{\boldsymbol{K}}$, we obtain

$$\hat{\Theta}\mathcal{H}_{\boldsymbol{K}}\hat{\Theta}^\dagger = -i\hbar v_F \boldsymbol{\sigma}\cdot\boldsymbol{\nabla} - \Delta(x,y)\sigma_z. \tag{2.10}$$

The only effect of $\Theta$ is changing the sign of the mass term $\Delta$. On the other hand, if $\Psi_{\boldsymbol{K}} = (\psi_A, \psi_B)^{\mathrm{T}}$ is the graphene wave-function around the $\boldsymbol{K}$-valley, the solution around $\boldsymbol{K'}$ is given by $\Psi_{\boldsymbol{K'}} = (-\psi_B^*, \psi_A^*)^{\mathrm{T}}$. By looking to definition Eq. 2.9, one can see this is equivalent to apply the time-reversal operator $\hat{\Theta}$ on $\Psi_{\boldsymbol{K}}$. Since both operations are equivalent, either modify the eigenvectors or the operators, we conclude it is possible describing the different valley by simply changing the sign of the mass term

$$\mathcal{H}_\tau = -i\hbar v_F \boldsymbol{\sigma}\cdot\boldsymbol{\nabla} + \tau\Delta(x,y)\sigma_z, \tag{2.11}$$

with $\tau = 1$ for the $\vec{K}$ valley and $-1$ for $\vec{K}'$. The IMBC for graphene can be found using a simple argument. Due to the hermiticity, for a given wave function $\Psi$, the expected value of $\mathcal{H}_\tau$ has to be real. Therefore, the following condition must be satisfied

$$\int\int_{\mathcal{S}} da\left(\Psi^\dagger\mathcal{H}\Psi - \Psi^\dagger\mathcal{H}^\dagger\Psi\right) = 0 \leftrightarrow -i\hbar\oint_{\mathcal{C}} ds\left[\boldsymbol{n}(s)\cdot\boldsymbol{\nabla}\left(v_F\Psi^\dagger\boldsymbol{\sigma}\Psi\right)\right] = 0. \tag{2.12}$$

The last step was taken by using the divergence theorem in two dimensions and integration by parts. Here, $\boldsymbol{n}(s)$ is a normal vector to the surface $\mathcal{C}$ for each point $s$ and $\boldsymbol{J} = -i\hbar v_{\mathrm{F}}\Psi^\dagger\boldsymbol{\sigma}\Psi$ is the current operator. Since the system has to be confined inside the quantum dot, the normal to surface component of the current has to be zero at each

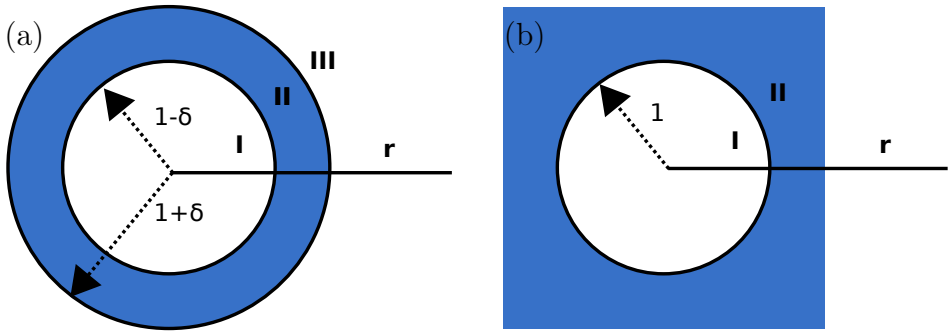


Figure 2.2: Schematic representation of the system and its boundaries. (a) Mass potential applied over a ring region and (b) potential applied over all the region outside the dot.

point of the boundary. Therefore, the integrand of Eq. 2.12 has to be zero everywhere. This implies in the following relation

$$\frac{\psi_B}{\psi_A} = iBe^{i\alpha(s)}. \tag{2.13}$$

Here, $\alpha(s)$ is the angle between $\boldsymbol{n}$ and horizontal, while $B$ is not necessarily a constant and, in general, will depend on the value of $s$ along the path. In order to obtain the value of the coefficient $B$ we can specialize our discussion for a specific situatuion. We consider $\alpha$ and the normal along the same direction and calculate the ratio between the components crossing a barrier along located at $x = 0$. If we make the potential $\Delta(x, y)$ goes to infinity, it is possible to show that $B$ goes to 1 for the $K$-valley and $-1$ for $K'$ valley. Therefore, we obtain

$$\frac{\psi_B}{\psi_A} = \tau ie^{i\alpha(s)} \tag{2.14}$$

with $\tau$ having the same meaning as previosly. The equation is called 2.14. It is possible to find the energy levels inside a quantum dot by imposing the conditions above at the solution of the Dirac equation. Next section, using a different approach than Berry and Mondragon's, we calculate the IMBC for AA-stacked bilayer.

## 2.4 Infinite Mass Boundary Conditions

Our description is based on the same formalism already used in a recent work (see Ref. [19]), in which the infinite-mass boundary condition for monolayer graphene was generalized to bilayer graphene with a AB stacking. Now we extend the work to the AA stacking BLG case. This approach is obtained by finding the correct boundary condition that solves the scattering problem of electrons trapped by a circular mass barrier. First, we consider the three separeted regions I, II and III as ilustraded in Fig. 2.2. I and III satisfy the free electron Hamiltonian, while region II is subject to a staggered potential breaking the sublattice symmetry. We solve the Hamiltonian in each and apply the usual boundary conditions, continuity of the wavefunction and its derivative. As we are going to

show, by properly manipulating $\delta$ and $\Delta$ values we can obtain the appropriate boundary conditions, i.e. the IMBC.

We start by trying to find the solutions of the eigenvector problem defined by $\mathcal{H}\Psi = E\Psi$, where $\mathcal{H}$ is defined by Eq. 2.7. Therefore, we obtain the set of coupled equations

$$\begin{aligned}
e^{i\theta}\left(\frac{\partial}{\partial\rho}+\frac{i}{\rho}\frac{\partial}{\partial\theta}\right)\Psi_B &= i[(\epsilon-\tau\Delta')\Psi_A - t'\Psi_{A'}],\\
e^{-i\theta}\left(\frac{\partial}{\partial\rho}-\frac{i}{\rho}\frac{\partial}{\partial\theta}\right)\Psi_A &= i[(\epsilon+\tau\Delta')\Psi_B - t'\Psi_{B'}],\\
e^{-i\theta}\left(\frac{\partial}{\partial\rho}-\frac{i}{\rho}\frac{\partial}{\partial\theta}\right)\Psi_{A'} &= i[(\epsilon-\tau\Delta')\Psi_{B'} - t'\Psi_B],\\
e^{i\theta}\left(\frac{\partial}{\partial\rho}+\frac{i}{\rho}\frac{\partial}{\partial\theta}\right)\Psi_{B'} &= i[(\epsilon+\tau\Delta')\Psi_{A'} - t'\Psi_A].
\end{aligned} \tag{2.15}$$

Here, we chose natural units for all quantities. The radial coordinate is given by $\rho = r/R$, where $R$ is radius of the quantum dot. All the energy parameters, $\epsilon$, $\Delta$ an $t$, are scaled with the natural energy parameter $E_0 = \hbar v_F/R$: $\epsilon = E/E_0$, $t' = t/E_0$, $\Delta' = \Delta/E_0$. Since we are treating a system with angular symmetry, we can extract the angular dependence of the system. With simple manipulations, assuming the components have the form $\psi_i(\rho,\theta) = e^{s_i\theta}\phi(\rho)$, we can show the solution is given by

$$\begin{pmatrix}\psi_A(\rho,\theta)\\ \psi_B(\rho,\theta)\\ \psi_{B'}(\rho,\theta)\\ \psi_{A'}(\rho,\theta)\end{pmatrix} = e^{im\theta}\begin{pmatrix}\phi_A(\rho)\\ ie^{-i\theta}\phi_B(\rho)\\ ie^{-i\theta}\phi_{B'}(\rho)\\ \phi_{A'}(\rho)\end{pmatrix}, \tag{2.16}$$

where $m$ can assume any integer value $m = 0, \pm1, \pm2\cdots$. Replacing Eq. 2.16 into the set of differential equations Eq. 2.15, we obtain

$$\begin{aligned}
\left(\frac{d}{d\rho}-\frac{(m-1)}{\rho}\right)\phi_B &= (\epsilon-\tau\Delta')\phi_A - t'\phi_{A'},\\
\left(\frac{d}{d\rho}+\frac{m}{\rho}\right)\phi_A &= -(\epsilon+\tau\Delta')\phi_B + t'\phi_{B'},\\
\left(\frac{d}{d\rho}+\frac{m}{\rho}\right)\phi_{A'} &= -(\epsilon-\tau\Delta')\phi_{B'} + t'\phi_B,\\
\left(\frac{d}{d\rho}-\frac{(m-1)}{\rho}\right)\phi_{B'} &= (\epsilon+\tau\Delta')\phi_{A'} - t'\phi_A.
\end{aligned} \tag{2.17}$$

The solution of this set of differential equations is quite complicated. One of the main reasons is the existence of $1/\rho$ term appearing on the right-hand side of Eq. 2.17. However, taking the limit $\Delta' \gg 1$ it is possible to show that we can disregard this term. The reason is as follow. If $\Delta'$ is a dominant factor, we can expect a solution having the proportionality $\phi_i \propto e^{-\Delta'\rho}$. Therefore, the derivative has one more $\Delta$ factor $d\phi_i/d\rho \propto \Delta' e^{-\Delta'\rho}$ and we can disregard the second factor on the right side of Eq. 2.17. Also, since $\Delta' \gg 1$ we can also

disregard the $\epsilon'$ factor on the left-hand side. Finally, we obtain the following simplified equation

$$\begin{aligned}
\frac{d\phi_B}{d\rho} &= -\tau\Delta'\phi_A - t'\phi_{A'}, \\
\frac{d\phi_A}{d\rho} &= -\tau\Delta'\phi_B + t'\phi_{B'}, \\
\frac{d\phi_{A'}}{d\rho} &= \tau\Delta'\phi_{B'} + t'\phi_B, \\
\frac{d\phi_{B'}}{d\rho} &= \tau\Delta'\phi_{A'} - t'\phi_A.
\end{aligned} \tag{2.18}$$

Now we have a set of linear differential equation that can be easily solved assuming an exponential dependence of the functions: $\phi_i(\rho) = \sum_{j=1}^{4} C_{ij} e^{\alpha_j \rho}$. This results in a set of linear equations for the $C_j$ coefficients. Solving this system we obtain

$$\begin{aligned}
\phi_A &= C_1^+ e^{\alpha_+(\rho-1)} + C_2^+ e^{-\alpha_+(\rho-1)} + C_1^- e^{\alpha_-(\rho-1)} + C_2^- e^{-\alpha_-(\rho-1)}, \\
\phi_B &= -\tau\left[C_1^+ e^{\alpha_+(\rho-1)} - C_2^+ e^{-\alpha_+(\rho-1)} + C_1^- e^{\alpha_-(\rho-1)} - C_2^- e^{-\alpha_-(\rho-1)}\right], \\
\phi_{A'} &= i\tau\left[C_1^+ e^{\alpha_+(\rho-1)} + C_2^+ e^{-\alpha_+(\rho-1)} - C_1^- e^{\alpha_-(\rho-1)} - C_2^- e^{-\alpha_-(\rho-1)}\right] \\
\phi_{B'} &= i\left[C_1^+ e^{\alpha_+(\rho-1)} - C_2^+ e^{-\alpha_+(\rho-1)} - C_1^- e^{\alpha_-(\rho-1)} + C_2^- e^{-\alpha_-(\rho-1)}\right],
\end{aligned} \tag{2.19}$$

where $\alpha_\pm = |\Delta' \pm it'|$. We chose the $C_j^\pm$ to emphasize the region where the potential is defined between $\delta \leq \rho - 1 \leq \delta$. Since the solutions must exist at the boundaries $\rho = 1 \pm \delta$, we can write a set of expression to the frontiers of the ring, $\phi_I = \phi(1-\delta)$ and $\phi_{III} = \phi(1+\delta)$. Now we use the continuity of the wavefunctions by making the match of them in the regions $I$ and $III$ in the limit $\delta \ll 1$. What we obtain is the following set of transcendental equations:

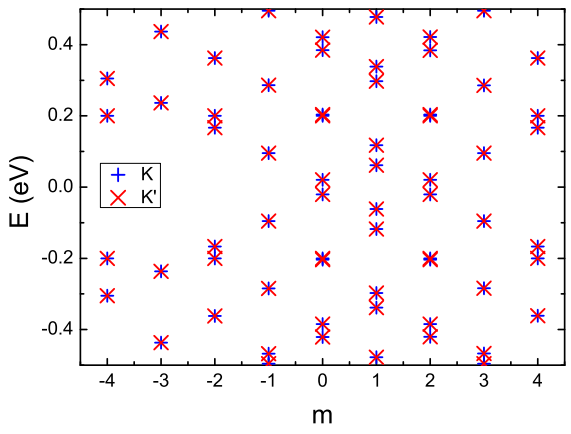


Figure 2.3: (Color online) Energy levels of a circular AA-stacked BLG quantum dot as a function of angular momentum label $m$ for $R = 10$ nm and in the absence of a magnetic field. The energy levels corresponding to the $K$ and $K'$ valleys are shown by the blue + symbols and the red $\times$ symbols, respectively.

$$\phi^{III}_{B'}(1) - \phi^{I}_{B'}(1) = -i\tau\left(\phi^{III}_{B}(1) - \phi^{I}_{B}(1)\right) + \tanh\left(\alpha_{-}\delta\right)$$
$$\times\left[\tau\left(\phi^{III}_{A'}(1) + \phi^{I}_{A'}(1)\right) - i\left(\phi^{III}_{A}(1) + \phi^{I}_{A}(1)\right)\right],$$
$$\phi^{III}_{A'}(1) - \phi^{I}_{A'}(1) = -i\tau\left(\phi^{III}_{A}(1) - \phi^{I}_{A}(1)\right) + \tanh\left(\alpha_{+}\delta\right)$$
$$\times\left[\tau\left(\phi^{III}_{B'}(1) + \phi^{I}_{B'}(1)\right) - i\left(\phi^{III}_{B}(1) + \phi^{I}_{B}(1)\right)\right].$$

Eq. 2.20 is a general boundary condition. We can now specialize for some particular cases. If we consider the ring thickness going to zero and the assuming the potential very large, while we keep the product constant, i.e.

$$\delta \to 0, \quad \Delta' \to \infty \Rightarrow \tanh\left(\alpha_{\pm}\delta\right) = P = \text{const.} \tag{2.20}$$

What we obtain is the boundary condition for the ring barrier environment as ilustraded in 2.2. In the same fashion, we can find the conditions for the quantum dot surounded by the staggered potential. First we notice that the parameter $P$ is related to the magnitude of the barrier with maximum value 1. [37] It is possible to show that the boundary conditions for the quantum dot are obtained by assuming the following requirements

$$\Delta' = \infty, \qquad P = 1,$$
$$\phi^{III}_{A}(1) = \phi^{III}_{B}(1) = \phi^{III}_{A'}(1) = \phi^{III}_{B'}(1) = 0, \tag{2.21}$$

The reason is, since the potential is suficiently large, we can assume the wavefunction goes to zero before reaching the outer edge of the ring. Finally, the expression obtained is the IMBC for the AA-stacked bilayer

$$\begin{aligned} \phi^{I}_{A'}(1) + \tau\phi^{I}_{B'}(1) &= 0, \\ \phi^{I}_{A}(1) - \tau\phi^{I}_{B}(1) &= 0. \end{aligned} \tag{2.22}$$

Note that Eqs. 2.22 are very similar to the IMBC obtained for graphene, vide Eq. 2.14. In fact, they are just like two uncoupled equations with different signs for the different valleys. Despite that, we emphasize that interlayer interactions was not disregarded in any step for the derivation of Eq. 2.22. In the next sections we will solve the quantum dot problem for the bilayer graphene in the precense of a magnetic field.

## 2.5 Quantum Dots

In this section, we apply the boundary conditions derived in Sec. 2.4 to investigate the energy levels of the charge carriers confined in a circular quantum dot of radius $R$. First, we calculate the levels in absence of an external magnetic. The result shall be compared with the one obtained for the graphene case. Latter, we include am uniform perpendicular magnetic field in the dot and we discuss the results in the light of the formation of Landau Levels (LLs). For this problem, the mass term profile has the form

$$\Delta(r) = \begin{cases} 0, & \text{for} \quad r < R \\ \infty, & \text{for} \quad r \geq R \end{cases}. \tag{2.23}$$

In this manner, we calculate the eigenstates of the Hamiltonian for the inner part of QD, since the infinity mass is assumed only outside of the system boundaries.

### 2.5.1 Zero Magnetic Field

We start by defining the two differential operators $\mathcal{L}_1 = d/d\rho + m/\rho$ and $\mathcal{L}_2 = d/d\rho - (m-1)/\rho$. In terms of $\mathcal{L}_1$ and $\mathcal{L}_2$, Eqs. 2.17 inside the dot can be simplified

$$\begin{aligned} \mathcal{L}_1\phi_A &= -\epsilon\phi_B + t'\phi_{B'}, \\ \mathcal{L}_1\phi_{A'} &= -\epsilon\phi_{B'} + t'\phi_B, \\ \mathcal{L}_2\phi_B &= \epsilon\phi_A - t'\phi_{A'}, \\ \mathcal{L}_2\phi_{B'} &= \epsilon\phi_{A'} - t'\phi_A. \end{aligned} \tag{2.24}$$

The system of coupled differential equations can be solved if we apply $\mathcal{L}_2$ to the first pair of equations. Using the second pair, we obtain a set of coupled equations for $\phi_A$ and $\phi_{A'}$

$$\begin{aligned} \mathcal{L}\phi_A &= 2\epsilon t'\phi_{A'}, \\ \mathcal{L}\phi_{A'} &= 2\epsilon t'\phi_A, \end{aligned} \tag{2.25}$$

where $\mathcal{L} = \mathcal{L}_2\mathcal{L}_1 + (\epsilon^2 + t'^2)$. Finally, this differential equations can also be decoupled. If we apply $\mathcal{L}$ on both sides of Eq. 2.25 we obtain

$$\mathcal{L}^2\phi_A = 2\epsilon t'\mathcal{L}\phi_{A'} = (2\epsilon t')^2\phi_A \qquad \leftrightarrow \qquad \mathcal{L}_+\mathcal{L}_-\phi_A = 0, \tag{2.26}$$

Here, $\mathcal{L}_\pm = \mathcal{L} \pm 2\epsilon t'$. Now we observe that the operators $\mathcal{L}_+$ and $\mathcal{L}_-$ commutate, i.e. they satisfy the relation $[\mathcal{L}_+, \mathcal{L}_-] = 0$. Therefore, if $\phi_A$ is an eigenvector of $\mathcal{L}_+$, it is also an $\mathcal{L}_-$ eigenvector

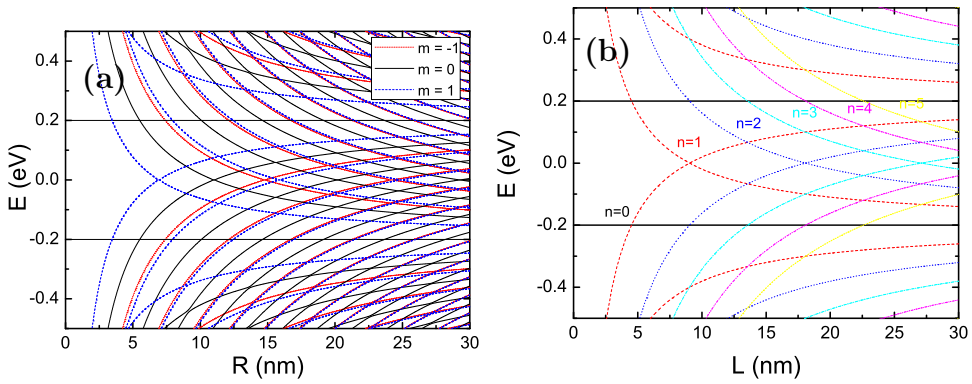


Figure 2.4: Energy Levels of a AA-stacked bilayer graphene dot with no magnetic field as a function of the radius of the system. (a) Results for the analycal model with the mass infinity boundary conditions; (b) Analytical results obtained by diagonalization of the Hamiltonian Eq. 2.7;

$$\begin{aligned} \mathcal{L}_+\phi_A &= \lambda_+\phi_A, \\ \mathcal{L}_-\phi_A &= \lambda_-\phi_A. \end{aligned} \tag{2.27}$$

Combined with Eq. 2.26, equation 2.27 leads to the condition $\lambda_+\lambda_- = 0$. For simplicity, we will assume $\lambda_\pm = 0$. Returning to the definition of $\mathcal{L}_\pm$, we finally obtain the differential equation

$$\left(\frac{d^2}{d\rho^2} + \frac{1}{\rho}\frac{d}{d\rho} + \bar{\epsilon}_\pm^2 - -\frac{m^2}{\rho^2}\right)\phi_A = 0, \tag{2.28}$$

with $\bar{\epsilon}_\pm = \epsilon \pm t'$ and an analagous equation for $\phi_{A'}$. Equation 2.28 is readly acknowledged as the Bessel differenial equation. Its solutions for a quantum dot are linear combinations of the Bessel functions of the first kind, since Bessel functions of the second kind (also possible solutions of the equation!) diverge at the origin. Therefore, we obtain

$$\begin{aligned}\phi_A &= C_1 J_m(\bar{\epsilon}_+\rho) + C_2 J_m(\bar{\epsilon}_-\rho),\\ \phi_{A'} &= \bar{C}_2 J_m(\bar{\epsilon}_+\rho) + \bar{C}_2 J_m(\bar{\epsilon}_-\rho).\end{aligned}$$

Next, we observe that $C_1 = \bar{C}_1$ and $C_2 = \bar{C}_2$. These relations can be derived replacing solutions Eq. 2.29 into Eqs. (2.25) and using the orthogonality of Bessel functions. The sublattices $B$ and $B'$ amplitudes can also be found replacing the solutions Eq. 2.29 in the first pair of Eqs. 2.24. The resulting expression is given by

$$\begin{aligned}\phi_B &= -\frac{C_1}{\bar{\epsilon}_-}J_{m-1}(\bar{\epsilon}_+\rho) - \frac{C_2}{\bar{\epsilon}_+}J_{m-1}(\bar{\epsilon}_-\rho),\\ \phi_{B'} &= \frac{C_1}{\bar{\epsilon}_-}J_{m-1}(\bar{\epsilon}_+\rho) - \frac{C_2}{\bar{\epsilon}_+}J_{m-1}(\bar{\epsilon}_-\rho),\end{aligned} \tag{2.29}$$

Here, we made use of the following recurrence relation satisfied by the Bessel functions: $\mathcal{L}_1 J_m(\bar{\epsilon}_\pm\rho) = \bar{\epsilon}_\pm J_{m-1}(\bar{\epsilon}_\pm\rho)$.

The solutions Eqs. 2.29-2.29 are imcomplete. In order to obtain the quantum dots energy levels, we have to apply the IBMC discussed in the previous section. This results in the following matricial equation

$$\begin{pmatrix} f_1 & f_2 \\ f_3 & f_4 \end{pmatrix}\begin{pmatrix} C_1 \\ C_2 \end{pmatrix} = 0, \tag{2.30}$$

where

$$\begin{aligned} f_1 &= \frac{1}{\bar{\epsilon}_-}J_{m-1}(\bar{\epsilon}_+R) + \tau J_m(\bar{\epsilon}_+R),\\ f_2 &= \frac{1}{\bar{\epsilon}_+}J_{m-1}(\bar{\epsilon}_-R) + \tau J_m(\bar{\epsilon}_-R),\\ f_3 &= \frac{1}{\bar{\epsilon}_-}J_{m-1}(\bar{\epsilon}_+R) - \tau J_m(\bar{\epsilon}_+R),\\ f_4 &= -\left(\frac{1}{\bar{\epsilon}_+}J_{m-1}(\bar{\epsilon}_-R) - \tau J_m(\bar{\epsilon}_-R)\right).\end{aligned} \tag{2.31}$$

Non-trivial solutions for Eq. (2.30) are found only if the determinant of the $2\times2$ matrix vanish. This condition leads to a transcendental equations for the energy levels in the quantum dot, $f_1 f_4 - f_2 f_3 = 0$.

Figure 2.3 shows our first result, namely the energy levels for the QD in the absence of a magnetic field as a function of the angular momentum $m$ for a radius $R = 10$ nm. The results show that the energy for the valleys $\boldsymbol{K}$ and $\boldsymbol{K}'$ are degenerate. This is easily seen as a consequence of the boundary conditions, because, if we make the substitution $A \to A'$ and $B \to B'$, we find the analagous equations as those in Eq. 2.22. By this graphic, we also see that the system has electron-hole symmetry as should be expected. Finally, another interesting symmetry presented by this system is $E^{e(h)}_{\boldsymbol{K},\boldsymbol{K}'}(m) = E^{e(h)}_{\boldsymbol{K},\boldsymbol{K}'}(2-m)$, which indicates that the value m = 1 corresponds to the fundamental state in angular momentum.

The results for the energy levels as a function of the radius of the QD are showed in Fig. 2.4, where we have displayed both the analytical and numerical results. Figure 2.4(a) show the result obtained using the IBMC conditions. Here, we are showing the results for $m = 0, \pm 1$. We can see that the upper set of levels approaches the value $E = 200$ meV for larger $R$, which is the value of the intralayer hopping. This can be seen as a consequence of the fact that these levels are related with the upper band of the bilayer. We also had considered another set of analytical solutions for comparison. These results are represented in Fig. 2.4(b). In order to do such calculations, we simply considered the diagonalization of the Hamiltonian Eq. 2.7 with the wave-vector $\boldsymbol{k}$ quantified in the simplest possible way such that we have $\pi = k_x - ik_y = ke^{-i\theta_{\boldsymbol{k}}} = (n\pi/R)e^{-i\theta_{\boldsymbol{k}}}$. We see that this results are in very good agreement with the ones obtained with the mass infinity boundary conditions. Actually, we can find an analytical expression for the energies:

$$E = \pm\sqrt{\Delta^2 + (\hbar v_{\mathrm{F}} k \pm t)^2}. \tag{2.32}$$

This result help us to see that the dependence of the energy with the radius goes with $1/R$, since the momentum is proportial to $k$. In contraposition, for the AB bilayer case we observe that $E$ exhibits a $1/R^2$ dependence (energy $\propto k^2$)[67].

### 2.5.2 Nonzero Magnetic Field

Now we investigate the case of a circular quantum dot in the presence of a magnetic field perpendicular to its plane. For this case, the operators $\pi$ and $\pi^\dagger$ are now refined using the minimal coupling transformation

$$\begin{aligned} \pi &= v_{\mathrm{F}} e^{i\theta}\left[-i\hbar\left(\frac{\partial}{\partial r} + \frac{i}{r}\frac{\partial}{\partial\theta}\right) + \frac{ieB_0 r}{2}\right], \\ \pi^\dagger &= v_{\mathrm{F}} e^{-i\theta}\left[-i\hbar\left(\frac{\partial}{\partial r} - \frac{i}{r}\frac{\partial}{\partial\theta}\right) - \frac{ieB_0 r}{2}\right]. \end{aligned} \tag{2.33}$$

Here, we have used the radial gauge, given in polar coordinates by $\boldsymbol{A} = (0, B_0 r/2, 0)$. Using this definition in the Hamiltonian (2.7), we arrive in the following equations

$$\begin{aligned}
v_{\mathrm{F}} e^{i\theta}\left[-i\hbar\left(\frac{\partial}{\partial r}+\frac{i}{r}\frac{\partial}{\partial\theta}\right)+\frac{ieB_0 r}{2}\right]\psi_B &= E\psi_A - t\psi_{A'},\\
v_{\mathrm{F}} e^{-i\theta}\left[-i\hbar\left(\frac{\partial}{\partial r}-\frac{i}{r}\frac{\partial}{\partial\theta}\right)-\frac{ieB_0 r}{2}\right]\psi_A &= -E\psi_B + t\psi_{B'},\\
v_{\mathrm{F}} e^{-i\theta}\left[-i\hbar\left(\frac{\partial}{\partial r}-\frac{i}{r}\frac{\partial}{\partial\theta}\right)-\frac{ieB_0 r}{2}\right]\psi_{A'} &= -E\psi_{B'} + t\psi_B,\\
v_{\mathrm{F}} e^{i\theta}\left[-i\hbar\left(\frac{\partial}{\partial r}+\frac{i}{r}\frac{\partial}{\partial\theta}\right)+\frac{ieB_0 r}{2}\right]\psi_{B'} &= E\psi_{A'} - t\psi_A.
\end{aligned} \tag{2.34}$$

We can use the same substitution used in the previous section in order to eliminate the angular dependence of the wave function: $\Psi = e^{im\theta}\left[\phi_A, ie^{-i\theta}\phi_B, ie^{-i\theta}\phi_{B'}, \phi_{A'}\right]$. Therefore, we obtain the set of coupled equations

$$\begin{aligned}
\mathcal{L}_{2\beta}\phi_B &= \epsilon\phi_A - t'\phi_{A'}\\
\mathcal{L}_{1\beta}\phi_A &= \epsilon\phi_B - t'\phi_{B'}\\
\mathcal{L}_{1\beta}\phi_{A'} &= \epsilon\phi_{B'} - t'\phi_B\\
\mathcal{L}_{2\beta}\phi_{B'} &= \epsilon\phi_{A'} - t'\phi_A
\end{aligned} \tag{2.35}$$

in total analogy to what was defined in the previous section for the case $B_0 = 0$. The operators $\mathcal{L}_{1\beta}$ and $\mathcal{L}_{1\beta}$ are defined by

$$\mathcal{L}_{1\beta} = \left(d/d\rho + m/rho + \beta\rho\right), \tag{2.36}$$

$$\mathcal{L}_{2\beta} = \left(d/d\rho - (m-1)/rho - \beta\rho\right). \tag{2.37}$$

Here, we have defined $\beta = eB_0R^2/2\hbar$. Proceeding in the same way as previously done for the case of zero magnetic field, we obtain the differential equation for $\phi_A$

$$\left(\frac{d^2}{d\rho^2}+\frac{1}{\rho}\frac{d}{d\rho}-\frac{m^2}{\rho^2}-2(m-1)\beta-\beta^2\rho^2+\epsilon_\pm\right)\phi_A = 0 \tag{2.38}$$

In order to solve this differential equation, we use the following substitution $\phi_A = \rho^{|m|}e^{-\beta\rho^2/2}\mathcal{E}(\beta\rho^2)$. This leads to the equation

$$\tilde{\rho}\frac{d^2\mathcal{E}}{d\tilde{\rho}^2} + (|m|+1-\tilde{\rho})\frac{d\mathcal{E}}{d\tilde{\rho}} + \left(\frac{\epsilon_\pm}{4\beta}-\frac{m+|m|}{2}\right)\mathcal{E} = 0 \tag{2.39}$$

where we define $\tilde{\rho} = \beta\rho^2$. The solutions for this equation are the generalized confluent hypergeometric functions ${}_1F_1$ and we can write the general solution as

$$\mathcal{E} = C_1 {}_1F_1(A_+, |m|+1, \tilde{\rho}) + C_2 {}_1F_1(A_-, |m|+1, \tilde{\rho}) \tag{2.40}$$

where $A_\pm = (m+|m|)/2 - \epsilon_\pm/4\beta$. We can now derive expressions for $\phi_A$ and equivalently $\phi_{A'}$, $\phi_B$ and $\phi_{B'}$ using the relations Eq. 2.24 (with $\mathcal{L}_{1,2}$ replaced by $\mathcal{L}_{1\beta}$) and using the

property of the hypergeometric functions: $d_1F_1(a,b,x)/dx = a_1F_1(a+1,b+1,x)$. This finally results in the solutions

$$\begin{aligned}
\phi_A &= \rho^{|m|}e^{-\beta\rho^2/2}\left(C_1\ {}_1F_1(A_+,|m|+1,\tilde{\rho}) + C_2\ {}_1F_1(A_-,|m|+1,\tilde{\rho})\right),\\
\phi_B &= -\rho^{|m|-1}e^{-\beta\rho^2/2}\left[\frac{C_1}{\epsilon_+ + t'}\left(2\tilde{\rho}A_{+1}F_1(A_+ + 1,|m|+2,\tilde{\rho})\right.\right.\\
&\quad +(m+|m|)_1F_1(A_+,|m|+1,\tilde{\rho})) + \frac{C_2}{\epsilon_- - t'}\left(2\tilde{\rho}A_{-1}F_1(A_- + 1,|m|+2,\tilde{\rho})+\right.\\
&\quad \left.\left. + (m+|m|)_1F_1(A_-,|m|+1,\tilde{\rho})\right)\right],\\
\phi_{B'} &= -\rho^{|m|-1}e^{-\beta\rho^2/2}\left[-\frac{C_1}{\epsilon_+ + t'}\left(2\tilde{\rho}A_{+1}F_1(A_+ + 1,|m|+2,\tilde{\rho})\right.\right.\\
&\quad +(m+|m|)_1F_1(A_+,|m|+1,\tilde{\rho})) + \frac{C_2}{\epsilon_- - t'}\left(2\tilde{\rho}A_{-1}F_1(A_- + 1,|m|+2,\tilde{\rho})+\right.\\
&\quad \left.\left. + (m+|m|)_1F_1(A_-,|m|+1,\tilde{\rho})\right)\right],\\
\phi_{A'} &= \rho^{|m|}e^{-\beta\rho^2/2}\left(-C_1\ {}_1F_1(A_+,|m|+1,\tilde{\rho}) + C_2\ {}_1F_1(A_-,|m|+1,\tilde{\rho})\right).
\end{aligned} \tag{2.41}$$

Now we can proceed as in the previous section and apply the IMBC conditions. The final

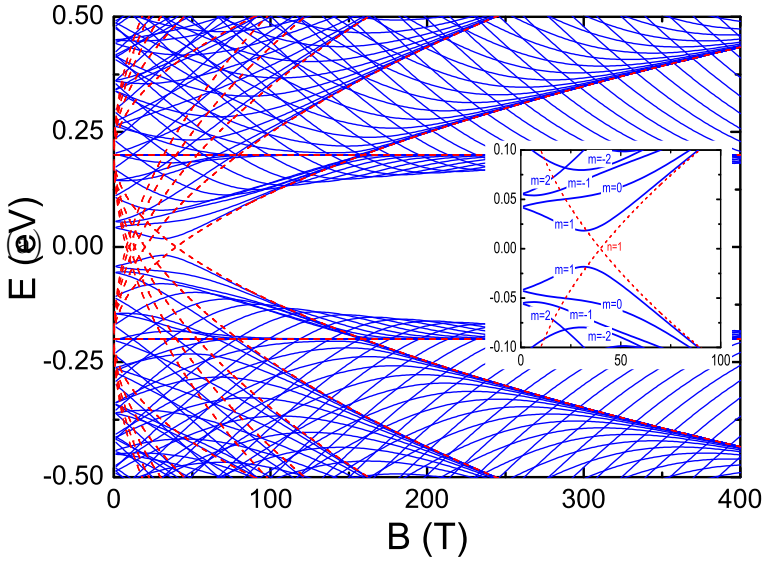


Figure 2.5: Energy spectrum of a circular $AA$ - stacked BLG QD obtained within the continuum model as a function of a perpendicular magnetic field with R = 10 nm and for angular momentum $-40 \leq m \leq 40$.The inset shows an enlargement of the low energy levels at small magnetic field. All levels are double degenerate corresponding to the $\boldsymbol{K}$ and $\boldsymbol{K}'$ points.

condition for the eigenvalues is an equation of the form Eq. 2.30. The numerical results obtained by solving the transcendental equation are represented in Fig. 2.5, which shows the energy levels of the system as a function of the magnetic field $B$. In the same plot are also shown for comparison the Landau levels of the system. The expression for the

Landau Levels in the AA-stacked bilayer is given by[68]-[71]

$$E = \pm\left(\sqrt{\frac{2neB}{\hbar}} \pm \sqrt{t_\perp^2 + \delta^2}\right) \tag{2.42}$$

The first observation that we can extract of the results in figure 2.5 is that the energy levels tends to converge asymptotically for the Landau levels as we consider larger values of the magnetic field $B$. We also see that the system preserves the symmetry between electron and hole states. The eigenvalues are doubly degenerate. The argument follows the one presented in the previous section. It is interesting to point out that this degeneracy depends on the number of layers, i.e., for a $N$-layer system, we have a $N$-degenerate. Besides that, the system presents a large gap. This behaviour is very different from the case of a bilayer with AB-stacking. The reason can be obtained if we observe the spectrum of graphene AA-stacked bilayer (Fig. 2.1). The bandstructure corresponds to two pairs of Dirac cones shifted by $\pm t_\perp$. Therefore, the states for the Landau level $n = 0$ converges for this two separete states and there is no states in between. Also, the inset shows an enlargement of the region for $-0.1 \leq E \leq 0.1$. We can see that the lower states correspond to the value $m = 1$. This can be verified for other values of radius once more reinforcing that $m = 1$ corresponds to the fundamental state of the system. Finally, in order to compare our analytical result obtained using the IMBC we plot in Fig. 2.6 the energy levels using two different tight-binding numerical approximations as function of the magnetic field. In Fig. 2.6(a) we have the plots for a square graphene quantum dot where we applied a staggered potential around a circular central region and Fig. 2.6(b) shows the results for a cut geometry. Both results show very good agreement with our analytical result obtained using the IBMC. There is a however a difference when comparing our results with the numerical ones shown in Fig. 2.6(b). Besides the Landau levels already discussed, we can see from it the appearence of some states localized inside the gap. These states appear due the imperfection on the edges. When the magnetic field is turned one these localized edge state modes align and the resulting effect is the one presented in the figure.

## 2.6 Conclusion

In this chapter, we have derived the infinite mass boundary conditions for an AA-stacked bilayer. Later, we used the IMBC to investigated the eigenergies of an AA dots. Because of its Dirac behaviour, our results present many similarities with the results obtained for a graphene quantum dot. As matter of fact, we show that the spectrum of the quantum dots are equivalent to two monolayer spectrum, one for the Dirac cone shifted by $t$ and the other for the cone shifted by $-t$. This also revealed in the radius dependence of the quantum dot, which, as we have showed goes with $1/R$ (see Eq. 2.32) instead of the $1/R^2$ dependence observed for AB-stacking.

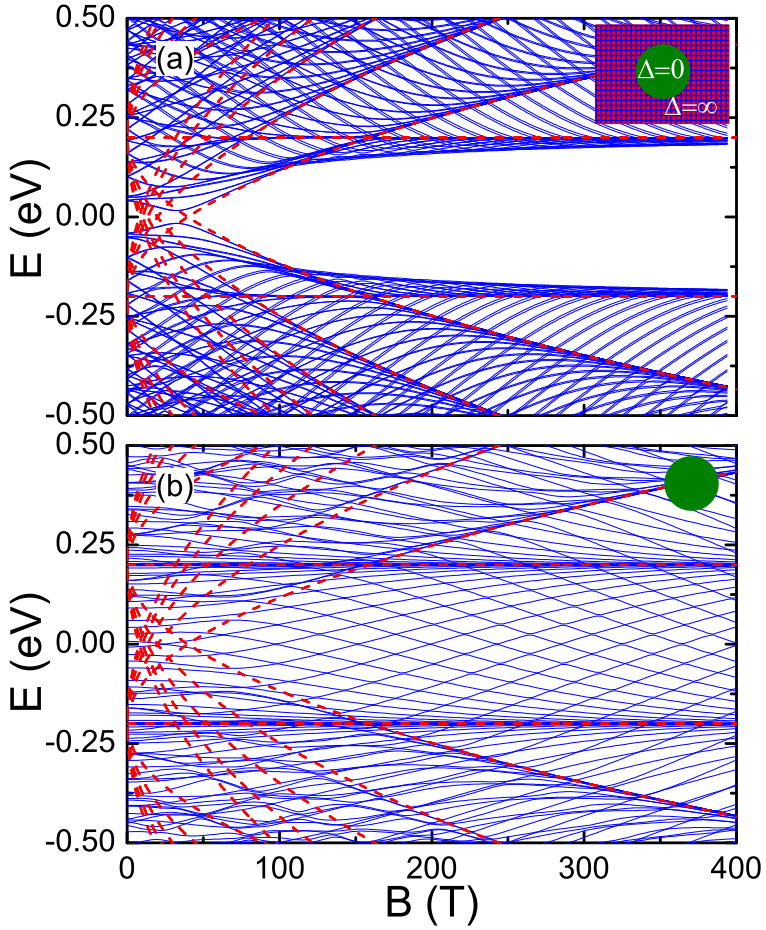


Figure 2.6: Energy levels of a circular $AA$-stacked BLG quantum dot obtained within the tight-binding model as a function of a perpendicular magnetic field for R = 10 nm, considering (a) a QD defined by a circular region of zero potential surrounded by an infinite region of staggered potential. The red dashed lines are the five first LLs of $AA$-stacked BLG, and (b) a circular nanostructure cut out from an infinite BLG sheet.

In the presence of an external magnetic field, our result have show the formation of Landau levels in the AA spectrum with the oppening of a gap and the convergence of this edge Landau states to the $\pm t$ energy. Finally, in order to check the validity of the calculations, our results were compared with numerical tight-binding ones. They have shown very good qualitative agreement with the appereance of localized edge states in the latter due to the presence of imperfections.

It also important mention that AA-stacked bilayer graphene systems have received less attention because of their lake of experimental realization. However, recently AA-bilayer samples have been produced[80]-[82] therefore making possible the observation of the quantum dots investigated here.

# 3 Two-dimensional electron-liquids: acoustic plasmons

## 3.1 Overview

In this chapter we theoretically study acoustic plasmon modes in a two-dimensional (2D) electron liquid. The calculations derived here can be directly related with the near-field optical microscopy in the hydrodynamic regime. Our calculations use a semiclassical kinetic equation of motion and takes into account the effects of (momentum-conserving) electron-electron collisions, (momentum-relaxing) electron-phonon and electron-impurity collisions, and many-body interactions beyond the celebrated Random Phase Approximation (RPA)[11, 12]. We calculate an expression for the non-local conductivity coefficient using this approach. Finally, the resulting expression allow us to calculate the dispersion and, most importantly, the damping of acoustic plasmon modes and their coupling to a near-field probe, identifying key experimental signatures of the crossover between collisionless and hydrodynamic regimes. Later, we can use this to determine how these signatures can efficiently be seen.

The content of this chapter was published in Physical Review B[83].

## 3.2 Acoustic Plasmons

In electron systems a collective charge mode exists at frequency above the threshold for intra-band electron-hole excitations. This mode is called "plasmon" [12, 84] and is particularly useful for technological applications in the case of two-dimensional (2D) electron systems. In this case indeed plasmons are gapless modes typically falling in the mid-infrared [85, 86, 87] or Terahertz (THz) [88, 89, 90] frequency ranges.

In recent years plasmons in 2D materials [91, 92, 93] such as graphene have attracted a great deal of attention because of their ability to confine light on length scales much shorter than the free-space wavelength [90, 94], their long lifetimes [87, 95], and their gate tunability [96, 85, 86, 87].

Due to the long-range nature of the bare electron-electron (e-e) interaction, plasmons in 2D materials on a dielectric substrate have a long-wavelength "unscreened" dispersion

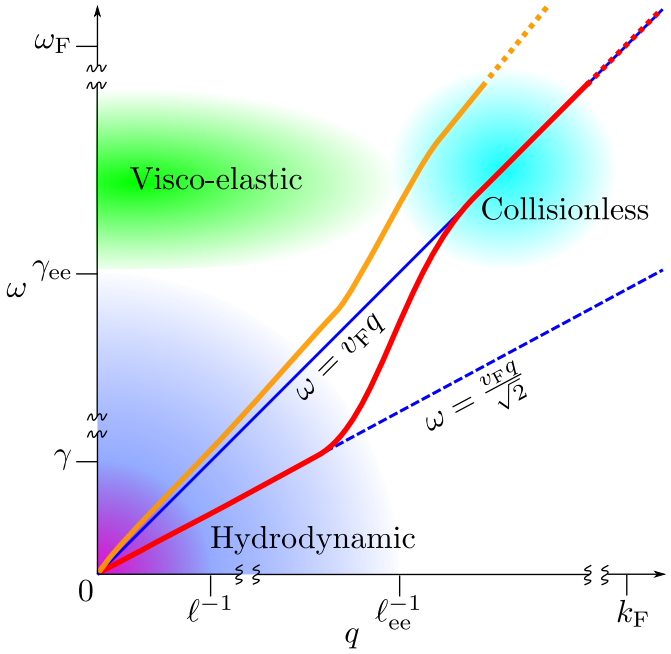


Figure 3.1: Sketch of the $q$-$\omega$ plane showing the relevant frequency and length scales for the problem at hand, and the plasmon dispersion (red and orange lines) for two different values of the screening parameter $\Lambda$ defined in Eq. (3.47). Red line: $\Lambda \gg 1$. Orange line: $\Lambda < 1$. The blue solid line is the electron dispersion $\omega = v_F q$ while the blue dashed line is the sound dispersion $\omega = v_F q/\sqrt{2}$ (ignoring here many-body corrections). Different regimes of linear response are highlighted. In the hydrodynamic regime (blue shaded region) the Navier-Stokes equation (3.1) is applicable. In the overdamped regime (magenta shaded region) Eq. (3.1) is still applicable but plasmons are strongly damped. In the visco-elastic regime (green shaded region) Eq. (3.1) can still be applied considering a frequency-dependent complex viscosity [116, 109].

of the form [12, 84] $\omega \propto \sqrt{q}$, where $\omega$ is the angular frequency and $q$ is the in-plane wave vector. Conversely, if the long-range part of the e-e interaction is screened by e.g. a nearby conducting gate, the plasmon dispersion is modified into an acoustic one (see e.g. Ref. [97]), $\omega \propto q$.

Acoustic plasmons (APs) [89, 90, 97, 98, 99] are particularly interesting because they can achieve larger mode confinement with respect to their unscreened counterpart. This happens for two reasons. First, an AP is more confined in the vertical direction due to the presence of the metallic gate [94], with the largest part of the electromagnetic energy density being localized between the gate and the 2D material. Second, due to the screening of the long-range part of the Coulomb interaction, APs are softer (because the restoring force is reduced) and carry high values of $q$, for a given value of $\omega$. This allows the study of interesting quantum non-local effects [90], which become important when the plasmon dispersion gets close to the boundary of the intra-band electron-hole continuum located at $\omega = v_F^* q$, $v_F^*$ being the quasiparticle velocity. By "quasiparticle" velocity we mean the Fermi velocity as dressed by electron-electron (e-e) interactions [12, 84, 100]. The same jargon and notation will be used below for the Drude weight $\mathcal{D}^*$, the density-of-states at

the Fermi energy $\mathcal{N}^*$, etc. The same quantities without the "$*$" symbol, e.g. $v_\mathrm{F}$, $\mathcal{D}$, $\mathcal{N}$, etc, will denote instead the non-interacting counterparts.

In 2D conducting materials of extremely high electronic quality, such as graphene encapsulated in hexagonal Boron Nitride [101], e-e interactions induce, in the intermediate-to-high-temperature regime, the so-called hydrodynamic transport regime. In this regime, e-e collisions are so frequent that they can establish a local thermal quasi-equilibrium. This happens when the e-e mean-free-path $\ell_\mathrm{ee} \equiv v_\mathrm{F}^* \tau_\mathrm{ee}$ (here $\tau_\mathrm{ee}$ is the e-e scattering time [102, 103, 104, 105, 106]) is much shorter than both the mean-free-path for momentum-relaxing collisions with phonons or impurities $\ell \equiv v_\mathrm{F}^* \tau$ and the characteristic wavelength [107, 108] $1/q$ of external perturbations. In the ac regime, we should also require [107, 108, 109] the angular frequency of the perturbation $\omega$ to be much smaller than the e-e scattering rate $1/\tau_\mathrm{ee}$. Transport signatures of hydrodynamic behaviour have been found in different high-quality materials like single- and bi-layer graphene [108, 110, 112, 111], GaAs/AlGaAs heterostructures [113, 114], and $PdCoO_2$ [115].

The rate $\gamma \equiv 1/\tau$ of momentum non-conserving collisions with impurities and phonons and the e-e scattering rate $\gamma_\mathrm{ee} \equiv 1/\tau_\mathrm{ee}$ define several regimes in the $q$-$\omega$ plane, which are sketched in Fig. 3.1.

In the hydrodynamic regime [117] and at the level of linear-response theory, the electron liquid can be described by the continuity equation $i\omega n(\boldsymbol{r},\omega) = \nabla \cdot \boldsymbol{J}(\boldsymbol{r},\omega)$, $n(\boldsymbol{r},\omega)$ being the deviation of the particle density from its equilibrium value $\bar{n}$ and $\boldsymbol{J}(\boldsymbol{r},\omega)$ the particle current, and the Navier-Stokes equation [107, 108, 109]

$$\begin{aligned} - \quad & i\omega \boldsymbol{J}(\boldsymbol{r},\omega) = -\gamma \boldsymbol{J}(\boldsymbol{r},\omega) + \nu^* \nabla^2 \boldsymbol{J}(\boldsymbol{r},\omega) + \\ - \quad & \frac{\mathcal{D}^*}{\mathcal{D}} \left[ \frac{e\bar{n}}{m} \boldsymbol{E}(\boldsymbol{r},\omega) + \frac{1}{\bar{n} m K^*} \nabla n(\boldsymbol{r},\omega) \right] . \end{aligned} \tag{3.1}$$

Here, $\boldsymbol{E}(\boldsymbol{r},\omega)$ is the electric field, $e$ is the elementary charge, $m \equiv \hbar k_\mathrm{F}/v_\mathrm{F}$ is the bare effective mass, $k_\mathrm{F}$ being the Fermi wave vector, $K^* = [\bar{n}\partial P/\partial \bar{n}]^{-1}$ is the compressibility [84, 12, 118], $P = P(\bar{n})$ being the pressure, $\nu^*$ is the kinematic viscosity [107, 108, 109, 117], $\mathcal{D}^*$ ($\mathcal{D}$) is the Drude weight of the interacting [119, 120] (non-interacting) electron system. A derivation of Eq. (3.1) is given in sec. 3.4.

In this work we identify signatures of the transition between the hydrodynamic ($\omega \ll \gamma_\mathrm{ee}$) and collisionless ($\omega \gg \gamma_\mathrm{ee}$) regimes in the dispersion and, most importantly, the damping of AP modes. In the case of single-layer graphene (SLG) at room temperature, for example, $\tau_\mathrm{ee} \approx 0.15$ ps at typical carrier densities [106] ($\bar{n} = 1.0 \times 10^{12}$ cm$^{-2}$, say) and the crossover is expected to occur in the THz range.

## 3.3 Kinetic equation

For sufficiently long-wavelengths (long compared with the inverse of the Fermi wavevector $k_\mathrm{F}$) and low-frequencies (low with respect to the Fermi energy $E_\mathrm{F}$ and to the energy

$E_g$ of the lowest inter-band excitation), an interacting 2D electron system can be described as a gas of weakly-interacting quasiparticles [84, 12]. If the system is in the paramagnetic state and there is no external perturbation coupling to the spin degrees of freedom, the dynamics of quasiparticles is governed by the *classical*, spin-independent, Hamiltonian [84, 12]

$$\mathcal{H}(\boldsymbol{r},\boldsymbol{p},t)=\frac{1}{2m^{\star}}\left(\boldsymbol{p}-\frac{e}{c}\boldsymbol{A}(\boldsymbol{r},t)\right)^{2}-e\phi(\boldsymbol{r},t)+U_{\mathrm{L}}(\boldsymbol{r},\boldsymbol{p},t). \tag{3.2}$$

Here, $m^{\star}_{\boldsymbol{p}}$ is the effective mass renormalized by e-e interactions, $U_{\mathrm{L}}$ is the spin-averaged electron-electron interaction, and $\phi(\boldsymbol{r},t)$ and $\boldsymbol{A}(\boldsymbol{r},t)$ are the electric scalar and vector potentials respectively. In this chapter, we also assume $\boldsymbol{A}(\boldsymbol{r},t)=0$. The specific case of magneto-plasmons, for which $\boldsymbol{A}(\boldsymbol{r},t)\neq 0$ will be addressed in the next chapter. The total electric potential is summed contribution of two terms $\phi(\boldsymbol{r},t)=\phi_{\mathrm{ex}}(\boldsymbol{r},t)+\phi_{\mathrm{ee}}(\boldsymbol{r},t)$, where $\phi_{\mathrm{ex}}$ is the external electric potential and $\phi_{\mathrm{ee}}$ is the long-range part of the electron-electron interaction. Short-range interactions, on the other hand, are described by the $\mathrm{U_L(r,t)}$ potential. We can have a better understanding of the factors in the hamiltonian (3.2) if we look into the quasi-particle energy functional $\mathcal{E}$. In general, $\mathcal{E}$ can be expressed as a function of the phase space position $(\boldsymbol{r},\boldsymbol{p})$ and the distribution function of the electrons $f^{(1)}(\boldsymbol{r},\boldsymbol{p},t)$. Since we are assuming small deviations around the equilibrium distribution we have $f^{(1)}(\boldsymbol{r},\boldsymbol{p},t)=f_0(\epsilon_{\boldsymbol{p}})+\delta f^{(1)}(\boldsymbol{r},\boldsymbol{p},t)$ and this allow us to writte $\mathcal{E}$ in the following form

$$\mathcal{E}(\boldsymbol{r},\boldsymbol{p},f^{(1)})=\mathcal{E}(\boldsymbol{r},\boldsymbol{p},f_0)+\sum_{\sigma,\sigma'}\int\frac{d\boldsymbol{r}'d\boldsymbol{p}'}{(2\pi\hbar)^2}g_{\boldsymbol{p},\sigma,\boldsymbol{p}',\sigma'}(\boldsymbol{r},\boldsymbol{r}')\delta f^{(1)}(\boldsymbol{r}',\boldsymbol{p}') \tag{3.3}$$

The first term corresponds to the bare quasi-particle energy $\epsilon^{\star}_{\boldsymbol{p}}=p^2/2m^{\star}-e\phi(\boldsymbol{r},t)$, while the second term gives the spin average Hartree electron-electron interaction $U_{\mathrm{L}}$. Since the contributions on the last term of Eq. 3.3 are short-ranged, only variations around $\boldsymbol{r}$ are appreciable. Therefore, this allow us to define the so-called Landau interaction function

$$f_{\boldsymbol{p}\sigma,\boldsymbol{p}'\sigma'}=\frac{1}{L^2}\int d\boldsymbol{r}\,g_{\boldsymbol{p},\sigma,\boldsymbol{p}',\sigma'}(\boldsymbol{r},\boldsymbol{r}'), \tag{3.4}$$

where $L^2$ is the surface of the 2D electron system. Another way to put it is Eq, 3.4 allow us to write the non-local contributions, in a mean-field way, dynamical exchange and correlation effects arising from the deviation of the occupation numbers of the electronic states from their equilibrium values.

The relevance of the short-range interactions can be understand by remembering the Pauli exclusion principle. Since most of the states are occupied close the Fermi surface, particles experience a strong blocking effect for scattering from a state to another if the exchange energy is small. This blocking effect is carried through $f_{\boldsymbol{p}\sigma,\boldsymbol{p}'\sigma'}$. Therefore, $f_{\boldsymbol{p}\sigma,\boldsymbol{p}'\sigma'}$ allow us write $U_{\mathrm{L}}$ as following

$$U_{\mathrm{L}}(\boldsymbol{r},\boldsymbol{p},t)=\frac{L^2}{2\hbar^2}\sum_{\sigma\sigma'}\int\frac{d\boldsymbol{p}'}{(2\pi)^2}f_{\boldsymbol{p}\sigma,\boldsymbol{p}'\sigma'}\delta f^{(1)}(\boldsymbol{r},\boldsymbol{p}',t). \tag{3.5}$$

The classical Hamiltonian (3.2) determines the response of quasiparticles. If we remember the classical Lioville theorem of statistical mechanics, the time evolution of the equilibrium distribution of the collective of particles should be given by $\partial f^{(1)}/\partial t = \{f^{(1)}, \mathcal{H}\}$, where $\{\ ,\ \}$ denotes the Poisson brackets. However because of collisions the system undergo process that can deviate the distribution from equilibrium in the phase space. We add collision terms $S\{f^{(1)}(\boldsymbol{r},\boldsymbol{p}',t)\}(\boldsymbol{r},\boldsymbol{p},t)$ in order to capture these effects. Finally, including all these contributions [84, 12], we obtain the equation of motion

$$\begin{aligned}[\partial_t + \boldsymbol{v}(\boldsymbol{r},\boldsymbol{p},t)\cdot\nabla_{\boldsymbol{r}} + \boldsymbol{F}(\boldsymbol{r},\boldsymbol{p},t)\cdot\nabla_{\boldsymbol{p}}]\, f^{(1)}(\boldsymbol{r},\boldsymbol{p},t) = \\ S^{\mathrm{el}}\{f^{(1)}(\boldsymbol{r},\boldsymbol{p}',t)\}(\boldsymbol{r},\boldsymbol{p},t) + S^{\mathrm{ee}}\{f^{(1)}(\boldsymbol{r},\boldsymbol{p}',t)\}(\boldsymbol{r},\boldsymbol{p},t),\end{aligned} \tag{3.6}$$

where $\boldsymbol{v}(\boldsymbol{r},\boldsymbol{p},t) \equiv \nabla_{\boldsymbol{p}}\mathcal{H}(\boldsymbol{r},\boldsymbol{p},t)$ is the quasiparticle velocity, $\boldsymbol{F}(\boldsymbol{r},\boldsymbol{p},t) \equiv -\nabla_{\boldsymbol{r}}\mathcal{H}(\boldsymbol{r},\boldsymbol{p},t) = -e\boldsymbol{E}(\boldsymbol{r},t) - \nabla_{\boldsymbol{r}}U_{\mathrm{L}}(\boldsymbol{r},\boldsymbol{p},t)$ is the total force acting on quasiparticles with $\boldsymbol{E}(\boldsymbol{r},t) = -\nabla_{\boldsymbol{r}}\phi(\boldsymbol{r},t)$ being the electric field, $S^{\mathrm{el}}\{f^{(1)}(\boldsymbol{r},\boldsymbol{p}',t)\}(\boldsymbol{r},\boldsymbol{p},t)$ is the collision integral that takes into account collisions with the lattice (i.e. electron-phonon scattering) and electron-impurity collisions, while $S^{\mathrm{ee}}\{f^{(1)}(\boldsymbol{r},\boldsymbol{p}',t)\}(\boldsymbol{r},\boldsymbol{p},t)$ is the collision integral for e-e scattering.

We dedicate the next following subsections to describe three of the main ingredients necessary to solve the kinetic equation Eq. 3.6, namely, the Landau interaction function, the normal modes expansion and the collision integrals. This will be relevant for obtaining the non-local conductivity coefficients from the kinetic equation.

### 3.3.1 Landau interaction function

In order to proceed, it is necessary to find a handful expression for calculating $f_{\boldsymbol{p}\sigma,\boldsymbol{p}'\sigma}$. Because of the isotropicity of the system, it is possible to infer that the interactions between two-particles with momentum $\boldsymbol{p}$ and $\boldsymbol{p}'$ only depends on the difference $\boldsymbol{p}-\boldsymbol{p}'$ between them. Moreover, since we are assuming small deviations close the Fermi surface, both particles have $|\boldsymbol{p}| \approx |\boldsymbol{p}'| \approx p_{\mathrm{F}}$. Therefore, the Landau interaction function Eq. 3.4 can only depend on the angular difference $\theta - \theta'$ between the trajectories of the particles in momentum space. This naturally allow us to make a Fourier decomposition of the interaction function in this angle, resulting in the expression

$$\frac{f_{\boldsymbol{p}\uparrow,\boldsymbol{p}'\uparrow} + f_{\boldsymbol{p}\uparrow,\boldsymbol{p}'\downarrow}}{2} = \frac{1}{L^2\mathcal{N}^\star}\sum_{l=-\infty}^{\infty} F^{\mathrm{s}}_{|l|} e^{il(\theta_{\boldsymbol{p}}-\theta_{\boldsymbol{p}'})}. \tag{3.7}$$

The set of parameters $F^{\mathrm{s}}_l$ are the so-called dimensionless symmetric Landau parameters [12, 121]. The several coefficients are directly related with the change of some physical quantities due to the presence of interactions. In order to illustrate, we consider the lowest order coefficient, which is related with the compressibility of the system $K$. We define compressibility as a measure of the change in the volume of the system due to the application of pressure. Its inverse is named bulk modulos $\mathcal{B}$. By definition we have

$$\mathcal{B} = \frac{1}{K} = -V\frac{\partial P}{\partial V} = n^2\frac{\partial \mu}{\partial n} = \frac{nq_{\mathrm{F}}}{2}\frac{\partial \mu}{\partial q_{\mathrm{F}}}, \tag{3.8}$$

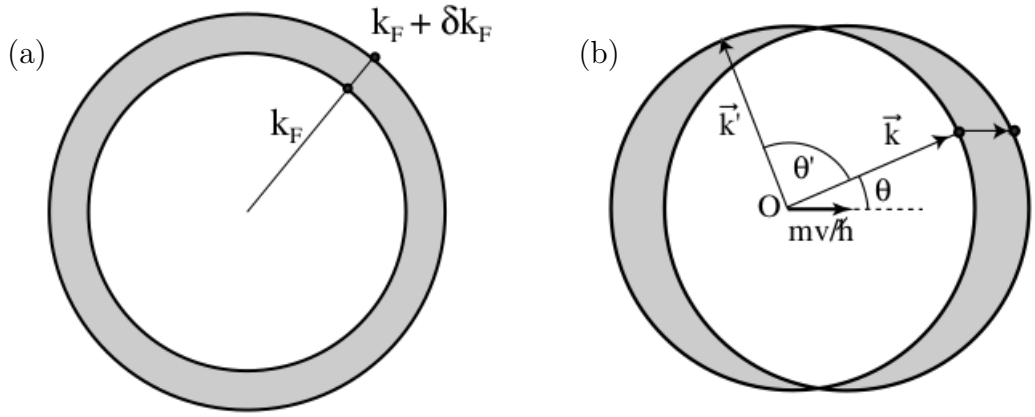


Figure 3.2: (a) Calculation of the compressibility in Landau theory. The energy of quasi particles change due the dilatation of the Fermi surface and the interaction of quasi particles in the shaded area. (b) Calculation of the mass in the Landau theory. We consider a boost of the Fermi surface and the energy is modified due to the horizontal boost and the interaction in the shaded area. Figure adapted from [12].

where $V$ is the volume of the system, $P$ is the pressure, n is the particle density, $\mu$ is the chemical potential and $q_F$ is Fermi wavevector. Here, $\mathcal{B}$, and consequently $K$, is defined with negative sign since a positive pressure is associated with a shrinking of the system. The last two steps were obtained using the fact that pressure is defined as the change of energy with respect to volume and $\mu$ is defined as the energy per particle. Therefore, we can see that $K$ is related with the variation of $\mu$ with respect to $q_F$ which in turn correspond to either an increase or decrease of the Fermi surface. Consider the quasiparticle energy Eq. 3.3. In the non-interacting equilibrium case $\mu$ is simply the Fermi energy. Under the influence of interactions, the Fermi surface is deformatted in order to accommodate more electron. Assuming $q_F$ is slightly changed by $\delta q$. This is directly followed by a change in the quasiparticles energy

$$\delta\mu = \mathcal{E}(q_F + \delta q) - \mathcal{E}(q_F) = \hbar v_F^\star \delta q + \frac{L^2}{\hbar^2} \sum_{\sigma,\sigma'} \int_{q_F \le q' \le q_F + \delta q} \frac{\hbar d\boldsymbol{q}'}{(2\pi)^2} f_{\boldsymbol{p},\sigma,\boldsymbol{p}',\sigma'} \delta f^{(1)}(\boldsymbol{r}', \boldsymbol{p}') \tag{3.9}$$

This two terms have simple interpretations. The first one correspond to the increase in energy due to the expansion of the Fermi surface from $\delta q$. The second one is the change in energy due to the interaction between electrons in the narrow region of thickness $\delta q$ and the other electrons. Using the result Eq. 3.7 and solving the integral we finally obtain

$$\delta\mu = (1 + F_0^S)\hbar v_F^\star \delta q \tag{3.10}$$

Identifying $\delta\mu = \hbar v_F \delta q$ as the equivalent expression for the non-interacting system we obtain the following relation for the compressibility

$$\frac{K^\star}{K} = \frac{\frac{v_F}{v_F^\star}}{(1 + F_0^S)}. \tag{3.11}$$

A similar relation can be obtained for the quasi particle mass. In order to see how the quasi particles mass $m$ is changed due to interactions, we appy a transformation similar to the one considered above and look to the changes in the energy. Instead of looking to contraction/dilation of the Fermi surface, we now apply a rigid translation for the sytem. The boost performed generates an out of equilibrium region for the electron system (Fig. 3.2) and if we consider that the electron in these region interact we finally obtain the following expression for the interaction mass

$$m^* = m(1 + F_1^{\mathrm{S}}). \tag{3.12}$$

Generally, we have $F_1^{\mathrm{S}} < 0$ which means that the electron-electron interaction decrease the mass of the system. It is possible to show[12] that other Landau parameters are related with the change in other physical quantities. Here we only consider modification in the Landau parameters until $m = 1$, i.e, we only look to modificatation in the compressibility and mass.

## 3.4 Solution of the Kinetic Equation

### 3.4.1 Fourier decomposition and hydrodynamic quantities

As we have discussed previously, the quasi-particle distribution $f^{(1)}(\boldsymbol{r}, \boldsymbol{p}, t)$ corresponds to a first order deviation towards the equilibrium distribution. Since $|\boldsymbol{p}| \approx p_{\mathrm{F}}$, to simplify we can introduce the following Ansatz[109]

$$f^{(1)}(\boldsymbol{r}, \boldsymbol{p}, t) = f_0(\epsilon^\star_{\boldsymbol{p}}) - f_0'(\epsilon^\star_{\boldsymbol{p}})\mathcal{F}(\boldsymbol{r}, \theta_{\boldsymbol{p}}, t), \tag{3.13}$$

where $f_0(\epsilon) = \{\exp[(\epsilon - \bar{\mu})/(k_{\mathrm{B}}T)] + 1\}^{-1}$ is the equilibrium Fermi-Dirac distribution function at chemical potential $\bar{\mu}$ and temperature $T$, $f_0'(\epsilon)$ is its derivative with respect to the energy $\epsilon$ and $\mathcal{F}(\boldsymbol{r}, \theta_{\boldsymbol{p}}, t)$ is a function proportional to the pertubation. Before replacing the ansatz Eq. 3.13 in Eq. 3.6, we take some time for analysing the distribuion $\mathcal{F}(\boldsymbol{r}, \theta_{\boldsymbol{p}}, t)$. First, consider the Fourier decomposition

$$\mathcal{F}_m(\boldsymbol{r}, \theta_{\boldsymbol{p}}, t) = \sum_{m=-\infty}^{\infty} \mathcal{F}_m(\boldsymbol{r}, t) e^{im\theta_{\boldsymbol{p}}}, \tag{3.14}$$

with the inverse transforamtion given by

$$\mathcal{F}(\boldsymbol{r}, t) = \int_0^{2\pi} \frac{d\theta_{\boldsymbol{p}}}{2\pi} \mathcal{F}_m(\boldsymbol{r}, \theta_{\boldsymbol{p}}, t) e^{-im\theta_{\boldsymbol{p}}}. \tag{3.15}$$

Different modes of the distribution are responsible for the different ways in which we can deform the Fermi surface. Furthermore, the first few modes are related with simple physical quantities. Consider the first order deviation of the particle density $n(\boldsymbol{r}, t)$ for

instance. We can show this is directly related with the $\mathcal{F}_0$ coefficient. By taking the definition we have

$$n(\boldsymbol{r},t)=\frac{1}{\hbar^2}\int\frac{d\boldsymbol{p}}{(2\pi)^2}\delta f^{(1)}(\boldsymbol{r},\boldsymbol{p},t)=\frac{1}{\hbar^2}\int\frac{d\boldsymbol{p}}{(2\pi)^2}\left[-f_0'(\epsilon^\star_{\boldsymbol{p}})\mathcal{F}(\boldsymbol{r},\theta_{\boldsymbol{p}},t)\right]=\mathcal{N}^\star\mathcal{F}_0 \tag{3.16}$$

We can directly see the geometric definition of $\mathcal{F}_0(\boldsymbol{r},t)$ as a contraction/dilatation of the Fermi surface. Analagously, the $\mathcal{F}_{\pm1}$ coefficients are related with a geometrical transformation of the system. They are related with rigid translation of the Fermi surface for which results a net current. This can be shown by taking the definition of the particle current

$$\boldsymbol{J}(\boldsymbol{r},t)=\frac{1}{\hbar^2}\int\frac{d\theta_{\boldsymbol{p}}}{(2\pi)^2}\boldsymbol{v}^\star_{\boldsymbol{p}}\delta f^{(1)}(\boldsymbol{r},\boldsymbol{p},t)=\frac{(1+F_1^{\mathrm{S}})\mathcal{N}^\star v_{\mathrm{F}}^\star}{2}\begin{pmatrix}\mathcal{F}_1(\boldsymbol{r},t)+\mathcal{F}_{-1}(\boldsymbol{r},t)\\ i\left(\mathcal{F}_1(\boldsymbol{r},t)-\mathcal{F}_{-1}(\boldsymbol{r},t)\right)\end{pmatrix}. \tag{3.17}$$

As an last example, we can show that the $\mathcal{F}_{\pm2}$ are related with the stress tensor. The stress tensor describes how the forces deforming the liquid are in a given point of space. It is defined by

$$\begin{aligned}T(\boldsymbol{r},t)=\int d\boldsymbol{p}\boldsymbol{p}\otimes\boldsymbol{v}_p\delta f^{(1)}(\boldsymbol{r},\boldsymbol{p},t)=\\ \frac{(1+F_0^{\mathrm{S}})\mathcal{N}^*m(v_{\mathrm{F}}^*)^2}{2}\left[\mathcal{F}_0(\boldsymbol{r},t)\mathbb{I}+(1+F_1^{\mathrm{S}})\left(\frac{\mathcal{F}_{-2}+\mathcal{F}_2}{2}\tau_z+\frac{\mathcal{F}_2-\mathcal{F}_{-2}}{2}\tau_x\right)\right],\end{aligned} \tag{3.18}$$

where $\tau_i$ denotes the Pauli matrices. Later, these expressions will be used to relate the $\mathcal{F}_m$ coefficients with the response to the external electric field.

Finally, a more tractable expression for the Landau kinetic equation ca be obtained if we insert the ansatz Eq. 3.13 in Eq. 3.6. Retaining only terms that are linear in the coefficients $\mathcal{F}_m(\boldsymbol{r},\theta_{\boldsymbol{p}},t)$, integrating over the energy $\epsilon^\star_{\boldsymbol{p}}$, Fourier transforming with respect to time we obtain:

$$\begin{aligned}-i\omega\sum_{m=-\infty}^{+\infty}\mathcal{F}_m(\boldsymbol{r},\omega)e^{im\theta_{\boldsymbol{p}}}+v_{\mathrm{F}}^\star\hat{\boldsymbol{p}}\cdot\left[\sum_{m=-\infty}^{+\infty}(1+F^{\mathrm{s}}_{|m|})\nabla\mathcal{F}_m(\boldsymbol{r},\omega)e^{im\theta_{\boldsymbol{p}}}+e\boldsymbol{E}(\boldsymbol{r},\omega)\right]=\\ -\sum_{m=-\infty}^{+\infty}\left[S_m^{\mathrm{el}}+S_m^{\mathrm{ee}}\right](\boldsymbol{r},\omega)e^{im\theta_{\boldsymbol{p}}}.\end{aligned} \tag{3.19}$$

Here, we have defined the Fourier transformation of the collision integrals $S_m^{\mathrm{ee/el}}$

$$S_m^\lambda=\int_{-\infty}^{\infty}d\epsilon_{\boldsymbol{p}}\int\frac{d\theta_{\boldsymbol{p}}}{2\pi}e^{-im\theta_{\boldsymbol{p}}}S_1^\lambda\{-f'(\epsilon_{\boldsymbol{p}'})\mathcal{F}(\boldsymbol{r},\theta_{\boldsymbol{p}'},\omega)\}(\boldsymbol{p}), \tag{3.20}$$

where $\lambda=\mathrm{ee},\mathrm{el}$ identifies the scattering mechanism.

### 3.4.2 Relaxation time approximation

Up to now our model has been completely general. However, in most cases the collision integral is very difficult of obtained. As a matter of fact, for electron-lattice interactions

the collision integral is given by

$$S^{\mathrm{el}} = \int W_{\boldsymbol{p},\boldsymbol{p}'} \left[ f_{\boldsymbol{p}}(1 - f_{\boldsymbol{p}'}) - (1 - f_{\boldsymbol{p}}) f_{\boldsymbol{p}'} \right], \tag{3.21}$$

which is very difficult of solving in general ($W$ is the transition probability between the $\boldsymbol{p}$ and $\boldsymbol{p}'$ states). Here, we are going to make use of the relaxation time approximation. This approximation assumes there is a characteristic rate for which collisions can change the distribution function. This can be expressed mathematically as $S = \Gamma \delta f^{(1)}$, where $\Gamma$ is the collisions rate. If we consider this substitution in our modal decomposition of the distribution we obtain

$$S_m^{\lambda} = \Gamma_m^{\lambda} \mathcal{F}_m \tag{3.22}$$

$$\Gamma_m^{\lambda} = \int_{-\infty}^{\infty} d\epsilon_{\boldsymbol{p}} \int \frac{d\theta_{\boldsymbol{p}}}{2\pi} e^{-im\theta_{\boldsymbol{p}}} S_1^{\lambda} \{ -f'(\epsilon_{\boldsymbol{p}'}) e^{im\theta_{\boldsymbol{p}'}} \}(\boldsymbol{p}), \tag{3.23}$$

For the purpose of obtaining a simple expression for the response function we make the following assumptions:

1. The electron-lattice and electron-impurity processes are characterized by only one parameter, i.e. $\gamma$. This process has to conserve the number of particles in the system, while other characteristics can change. This is guaranteed if we set $\Gamma_0^{\mathrm{el}} = 0$ and $\Gamma_m^{\mathrm{el}} = \gamma$ for $|m| > 1$.

2. The e-e collisions are described by only one parameter, i.e. $\gamma_{\mathrm{ee}}$. Besides the number of particles, this process has to conserve the total momentum of the electrons. This imply as we will see in $\Gamma_0^{\mathrm{ee}}$, $\Gamma_{\pm 1}^{\mathrm{ee}} = 0$, and $\Gamma_m^{\mathrm{ee}} = \gamma_{\mathrm{ee}}$ for $|m| > 1$.

With the aforementioned approximations, we are now in the position of analytically solving the kinetic equation.

### 3.4.3 Matricial Representation

Now we have all the necessary information for solving the Landau Kinetic equation. Since our major interest here is to characterize the quasi-particle state, we specialize our discussion for a translationally invariant system. Therefore we can Fourier transform the spacial variable of Eq. 3.19. Next, we multiply (3.19) by $\exp[-in\theta_{\boldsymbol{p}}]$, and average over the angle $\theta_{\boldsymbol{p}}$ obtaining the set of differential equations

$$\begin{aligned}
&-i\omega \mathcal{F}_m(\boldsymbol{q},\omega) + \frac{iv_{\mathrm{F}}^*}{2} \left[ (1 + F_{|m-1|}^{\mathrm{S}})(q_x - iq_y) \mathcal{F}_{m-1}(\boldsymbol{q},\omega) + \right. \\
&\left. (1 + F_{|m+1|}^{\mathrm{S}})(q_x + iq_y) \mathcal{F}_{|m+1|}(\boldsymbol{q},\omega) \right] + \frac{ev_{\mathrm{F}}^*}{2} \left[ E_x(\boldsymbol{q},\omega)(\delta_{n,1} + \delta_{n,-1}) - \right. \\
&\left. iE_y(\boldsymbol{q},\omega)(\delta_{n,1} - \delta_{n,-1}) \right] = -\gamma_{\mathrm{ee}} \left[ \mathcal{F}_m(\boldsymbol{q},\omega) - \mathcal{F}_0(\boldsymbol{q},\omega)\delta_{m,0} - \mathcal{F}_1(\boldsymbol{q},\omega)\delta_{m,1} - \mathcal{F}_{-1}(\boldsymbol{q},\omega)\delta_{m,-1} \right] \\
&\gamma \left[ \mathcal{F}_m(\boldsymbol{q},\omega) - \mathcal{F}_0(\boldsymbol{q},\omega)\delta_{m,0} \right]
\end{aligned} \tag{3.24}$$

From Eq. 3.24 we can see that for $m = 0$, both the $\gamma$ and $\gamma_{\rm ee}$ term cancel. This is a consequence of the conservation of the number of particles. Indeed, for $m = 0$ Eq. 3.19 is just the continuity equation

$$-i\omega\mathcal{F}_0 + \frac{iv_{\rm F}^*}{2}(1+F_1^{\rm S})\left[q_x(\mathcal{F}_1+\mathcal{F}_{-1}) - iq_y(\mathcal{F}_1-\mathcal{F}_{-1})\right] = 0 \tag{3.25}$$

or if we use the definitions of $n$ and $\boldsymbol{J}$

$$-i\omega n(\boldsymbol{q},\omega) + i\boldsymbol{q}\cdot\boldsymbol{J}(\boldsymbol{q},\omega) = 0 \tag{3.26}$$

Similarly, the equations for $m = \pm 1$ the contribution of $\gamma_{\rm ee}$ cancel and since the current is related with momentum density of the system, this is related with the conservation of momentum of the system.

Because of the angular decomposition, we have an infinite set of equations relating the coefficients $\mathcal{F}_m$ with the electric field. One way of solving this is by writing Eq as matricial equation. In this case, we have an infinite tridiagonal equation

$$\begin{pmatrix} \ddots & \vdots & \vdots & \vdots & \vdots & \vdots & \iddots \\ \cdots & a_{-2} & b_{-1} & 0 & 0 & 0 & \cdots \\ \cdots & b_{-2}^* & a_{-1} & b_0 & 0 & 0 & \cdots \\ \cdots & 0 & b_{-1}^* & a_0 & b_1 & 0 & \cdots \\ \cdots & 0 & 0 & b_0^* & a_1 & b_2 & \cdots \\ \cdots & 0 & 0 & 0 & b_1^* & a_2 & \cdots \\ \iddots & \vdots & \vdots & \vdots & \vdots & \vdots & \ddots \end{pmatrix} \begin{pmatrix} \vdots \\ \mathcal{F}_{-2}(\boldsymbol{q},\omega) \\ \mathcal{F}_{-1}(\boldsymbol{q},\omega) \\ \mathcal{F}_0(\boldsymbol{q},\omega) \\ \mathcal{F}_1(\boldsymbol{q},\omega) \\ \mathcal{F}_2(\boldsymbol{q},\omega) \\ \vdots \end{pmatrix} = -\frac{iev_{\rm F}^*}{2} \begin{pmatrix} \vdots \\ 0 \\ E^{(+)}(\boldsymbol{q},\omega) \\ 0 \\ E^{(-)}(\boldsymbol{q},\omega) \\ 0 \\ \vdots \end{pmatrix}, \tag{3.27}$$

where

$$a_n = \omega + i\Gamma_n^{\rm ee} + i\Gamma_n^{\rm el}\ , \tag{3.28}$$

and

$$b_n = b(1+F_{|n|}^{\rm S})\ . \tag{3.29}$$

Here, $b = -v_{\rm F}^* q^{(+)}/2$, with $q^{(\pm)} = q_x \pm iq_y$, and $E^{(\pm)}(\boldsymbol{q},\omega) = E_x(\boldsymbol{q},\omega) \pm iE_y(\boldsymbol{q},\omega)$.

The solution of Eq. (3.27) requires the inversion of the tridiagonal matrix $M$ appearing on the left hand side of this equation. In what follows we will evaluate the relevant elements of $M^{-1}$, using the continued fraction method [124], with the aim of calculating the response of the electron density to a longitudinal electric field.

## 3.5 The non-local conductivity from Landau kinetic theory

We have all necessary ingredients for solving the Landau kinetic equation and therefore obtain the response of a 2D electron liquid to an external scalar potential. Again, we reinforce this approach is only valid if we consider slow-varying electromagnetic fields [116,

109]. Its use is justified when the excitation wavelength is sufficiently long compared to the inverse of the Fermi wave vector $k_{\mathrm{F}}$, and when the excitation energy $\hbar\omega$ is sufficiently small compared to the Fermi energy $E_{\mathrm{F}}$, and to the energy of the lowest inter-band excitation $E_{\mathrm{g}}$.

Now, we focus on the calculation of the non-local conductivity. As we already know, this expression will be necessary later for describing the excitations spectrum. For a longitudinal electric field applied, Ohm's law gives the following relation between the current and E

$$e^2 J(\boldsymbol{q},\omega) = \sigma_{\mathrm{L}}(\boldsymbol{q},\omega) E(\boldsymbol{q},\omega), \tag{3.30}$$

where $\sigma_{\mathrm{L}}$ is the longitudinal conductivity. In this case, we also have $\boldsymbol{E}(\boldsymbol{q},\omega) = -i\boldsymbol{q}\phi(\boldsymbol{q},\omega)$, where $\phi$ is the electrostic potential. Also, the continuity equation allows us to write the current density as $J = (\omega/q)n$. Using this results on Eq. 3.30 we obtain

$$\sigma_{\mathrm{L}}(\boldsymbol{q},\omega) = i\frac{e^2\omega}{q^2}\tilde{\chi}_{nn}(\boldsymbol{q},\omega). \tag{3.31}$$

Here, we have used the definition of $\tilde{\chi}_{nn}$ from Eq. 1.32. From Eq. 3.27 and inverting the infinite matrix $M$ we obtain the value $\tilde{\chi}_{nn}$ is given by

$$\begin{aligned}\tilde{\chi}_{nn}(\boldsymbol{q},\omega) &= \frac{\mathcal{N}^*\mathcal{F}_0(\boldsymbol{q},\omega)}{-e\phi(\boldsymbol{q},\omega)} = -\mathcal{N}^*\left\{b\left[M^{-1}\right]_{0,-1} + b^*\left[M^{-1}\right]_{0,1}\right\} \\ &= \mathcal{N}^*\frac{a_0[M^{-1}]_{00} - 1}{1+F_0^{\mathrm{s}}}.\end{aligned} \tag{3.32}$$

In writing the last equality we had to invert the matrix $M$ in Eq. (3.27). We also used: i) the Kramers rule expression for the inverse matrix elements $[M^{-1}]_{0,\pm1} = -D_{\pm1,0}/D$, $[M^{-1}]_{00} = D_{0,0}/D$, where $D_{i,j}$ is the determinant of the matrix obtained from $M$ by suppressing the $i$-th row and the $j$-th column and $D = \det[M]$. ii) The Laplace expansion on the 0-th column of the determinant $D$, which yields $D = a_0 D_{0,0} - b_0 D_{-1,0} - b_0^* D_{1,0}$. iii) $b_0 = b(1+F_0^{\mathrm{s}})$.

For a tridiagonal matrix $M$ in the form (3.27), a diagonal element of the inverse matrix $M^{-1}$ can be expressed as a continued fraction[124]

$$[M^{-1}]_{ii} = \cfrac{1}{a_i - \cfrac{b_{i+1}b_i^*}{a_{i+1} - \cfrac{b_{i+2}b_{i+1}^*}{a_{i+2} - \cdots}} - \cfrac{b_i b_{i-1}^*}{a_{i-1} - \cfrac{b_{i-1}b_{i-2}^*}{a_{i-2} - \cdots}}}. \tag{3.33}$$

Therefore this results in the expression

$$[M^{-1}]_{00} = \cfrac{1}{a_i - \cfrac{2|b|^2(1+F_0^{\mathrm{s}})(1+F_1^{\mathrm{s}})}{a_1 + (1+F_1^{\mathrm{s}})\xi(q,\omega)}}, \tag{3.34}$$

where $\xi(q,\omega)$ respects the self-consistent equation

$$\xi(q,\omega) = \cfrac{-|b|^2}{a_2 - \cfrac{|b|^2}{a_2 - \cfrac{|b|^2}{\cdots}}} = -\frac{|b|^2}{a_2 + \xi(q,\omega)}. \tag{3.35}$$

Solving for $\xi(q,\omega)$ and substituting the values of $a_2$ and $b$ we obtain

$$\xi(q,\omega) = \frac{\omega + i\gamma_{\rm tot}}{2}\left[\sqrt{1 - \frac{(v_{\rm F}^*)^2 q^2}{(\omega + i\gamma_{\rm tot})^2}} - 1\right]. \tag{3.36}$$

Here, we chose the solution of Eq. (3.35) with the positive sign of the square root to make sure that the first-order expansion of $\xi$ in powers of $|b|^2$ in Eq. (3.36) coincides with the truncation of the continued fraction up to first order in Eq. (3.35).

Making use of Eqs. (3.32)-(3.33), and (3.36), we obtain the final result

$$\tilde{\chi}_{nn}(\boldsymbol{q},\omega) = \frac{(1+F_1^{\rm s})(v_{\rm F}^*)^2\mathcal{N}^* q^2}{\omega(\omega+i\gamma)(1-F_1^{\rm s}) - (1+F_1^{\rm s})\left[i\gamma_{\rm ee}\omega - \omega\sqrt{(\omega+i\gamma_{\rm tot})^2 - (v_{\rm F}^*)^2q^2} + (v_{\rm F}^*)^2q^2(1+F_0^{\rm s})\right]}. \tag{3.37}$$

Eq. (3.37) is the semi-classical density-density response function of a 2D electron liquid, taking into account momentum-conserving and momentum-non-conserving collisions, and many-body effects through the renormalization of $v_{\rm F}$ and $\mathcal{N}$, and the Landau parameters $F_0^{\rm s}$ and $F_1^{\rm s}$. If we turn the interactions off by making the Landau parameters $F_0^{\rm S} = 0$ and the collisions rate $\gamma_{\rm ee} = 0$, we obtain the expression

$$\tilde{\chi}_{nn}(\boldsymbol{q},\omega) = -\mathcal{N}\left(1 - \frac{\omega}{\sqrt{\omega^2 - v_{\rm F}^2 q^2}}\right), \tag{3.38}$$

which is just the Lindhard formula from chapter 1.

This result can be easily converted into the longitudinal conductivity using the identity Eq. (3.31). Next, we discuss the properties of this non local conductivity.

### 3.5.1 The Non-local conductivity

Replacing the final result of Eq. 3.37 in Eq. 3.31, we obtain

$$\sigma_{\rm L}(q,\omega) = \frac{i\mathcal{D}^*/\pi}{\omega + i\gamma + \frac{\omega + i\gamma + i\gamma_{\rm ee}}{2}\frac{\mathcal{D}^*}{\mathcal{D}}\frac{v_{\rm F}}{v_{\rm F}^*}\left[\sqrt{1 - \left(\frac{v_{\rm F}^* q}{\omega + i\gamma + i\gamma_{\rm ee}}\right)^2} - 1\right] - \frac{1}{2}\frac{\mathcal{D}^*}{\mathcal{D}}\frac{K}{K^*}\frac{v_{\rm F}^2 q^2}{\omega}}. \tag{3.39}$$

Here, we chose to present the $\sigma$ coefficient as a function of physical quantities, better than the Landau parameters. In order to do that, we define the Drude weigh $\mathcal{D} = \pi e^2 \mathcal{N} E_{\rm F}/m$ of the non-interacting system. In Landau theory of Fermi liquids, we have renormalizations of $\mathcal{D}$ as well as $K$ therefore resulting in the expressions $\mathcal{D}^*/\mathcal{D} = (v_{\rm F}^*/v_{\rm F})(1+F_1^{\rm s})$ and $K/K^* = (v_{\rm F}^*/v_{\rm F})(1+F_0^{\rm s})$. It is important to highlight that the many-body corrections $v_{\rm F}^*/v_{\rm F}$, $K^*/K$, and $\mathcal{D}^*/\mathcal{D}$ can be calculated from approximate theories [100, 118, 119, 90]

and are fundamental for a quantitative interpretation of experimental data since, for example, $v_{\rm F}^*/v_{\rm F} \approx 1.3$ [100], $K^*/K \approx 0.8$ [90], and $\mathcal{D}^*/\mathcal{D} \approx 1.5$ [119] in SLG at densities on the order of $10^{12}$ cm$^{-2}$.

We again reinforce that, while deriving Eq. (3.39) we made the assumptions that the momentum-conserving and the momentum-relaxing collisions are described by one parameter each, i.e. differences between the relaxation times of the different angular components of the distribution function [122, 123] and the difference between $\tau_{\rm ee}$ and the viscosity time $\tau_{\rm v}$ [106] are neglected as explained in Sec. **??**. Also, we are only considering Landau paramters corrections until $l = 1$. Higher-angular-momentum Landau parameters $F_l^{\rm s}$ with $l \geq 2$ are typically smaller, unless the system is highly correlated. We used these assumptions to derive the simplest yet highly-non-trivial model for the non-local longitudinal conductivity. However, the technique we used in our derivation, based on analytical inversion of tridiagonal matrices [124], easily allows the introduction of different scattering rates for the different harmonics of the distribution function [122, 123] as well as higher-order Landau parameters.

Eq. (3.39) is the first important result of this work because, despite its simplicity, it i) embodies a wealth of physical effects, including many-body effects beyond the Random Phase Approximation (RPA), ii) allows us to span the whole frequency range, from the hydrodynamic to the collisionless regime, and iii) is valid with no assumptions on the relative values of the parameters, other than the ones mentioned previously for the applicability of Landau kinetic equation. In what follows we will anyway assume that $\gamma_{\rm ee} \gg \gamma$ because the hydrodynamic regime is relevant only in this case.

We now look at four special limits of Eq. (3.39).

1. We first set $q = 0$, i.e. we consider the local conductivity. In this case, Eq. (3.39) reduces to a Drude-like formula with a renormalized Drude weight $\mathcal{D}^*$ and a damping rate $\gamma$ induced solely by momentum-non-conserving collisions

$$\sigma_{\rm L}(\boldsymbol{q} = 0, \omega) = \frac{i\mathcal{D}^*/\pi}{\omega + i\gamma}. \tag{3.40}$$

   The e-e collision rate $\gamma_{\rm ee}$ appears at order $q^2$. Note that e-e interactions fully disappear from $\sigma_{\rm L}(0,\omega)$ in a Galilean invariant electron system where $\mathcal{D}^* = \mathcal{D}$ because in this case [84, 12] $v_{\rm F}^*/v_{\rm F} = 1/(1 + F_1^{\rm s})$.

2. Second, expanding to second order in $|v_{\rm F}^* q/(\omega + i\gamma + i\gamma_{\rm ee})|$ the square root in the denominator of Eq. (3.39) and taking the limit $\omega \ll \gamma_{\rm ee}$, we obtain the hydrodynamic non-local conductivity [106]

$$\sigma_{\rm L}^{\rm h}(q,\omega) = \frac{i\mathcal{D}^*/\pi}{\omega + i\gamma + q^2\left(i\nu^* - \dfrac{\mathcal{D}^*}{\bar{n}m\mathcal{D}K^*\omega}\right)}, \tag{3.41}$$

   where $\nu^* \equiv \mathcal{D}^* v_{\rm F}^* v_{\rm F}/[4\mathcal{D}(\gamma_{\rm ee} + \gamma)]$. Ignoring many-body renormalizations, our result for $\nu^*$ reduces to the "classical" formula for the viscosity of an electron gas [125, 109],

while for Galileian invariant systems it reduces to the expression given in Ref. [116] with $F_2^{\rm s} = 0$. The quantity $\sigma_{\rm L}^{\rm h}(q,\omega)$ can be obtained directly by using Eq. (3.1) coupled to the continuity equation.

3. Third, if both many-body renormalizations and e-e collisions are neglected we recover the response function used in Ref. [126] to discuss the effect of diffusion (i.e. electron-impurity collisions) on 2D unscreened plasmons.

4. Finally, if the scattering rates $\gamma$ and $\gamma_{\rm ee}$ are both sent to zero, the long-wavelength ($q \ll k_{\rm F}$) limit of the collisionless conductivity of a 2D electron system [127] with parameters renormalized by e-e interactions is recovered.

## 3.6 The screened electron-electron interaction

The dispersion of plasmons in a material depends also on the interaction potential $v_{q,\omega}$ between charges in the material itself. This quantity relates the Fourier transform of $n(\boldsymbol{q},\omega)$ to the Fourier transform of the induced (i.e. Hartree) scalar potential $V_{\rm ind}(\boldsymbol{q},\omega)$, i.e. $V_{\rm ind}(\boldsymbol{q},\omega) = v_{q,\omega} n(\boldsymbol{q},\omega)$. In 2D materials the interaction potential is strongly affected by the presence of nearby dielectrics or conductors. The interaction potential for generic

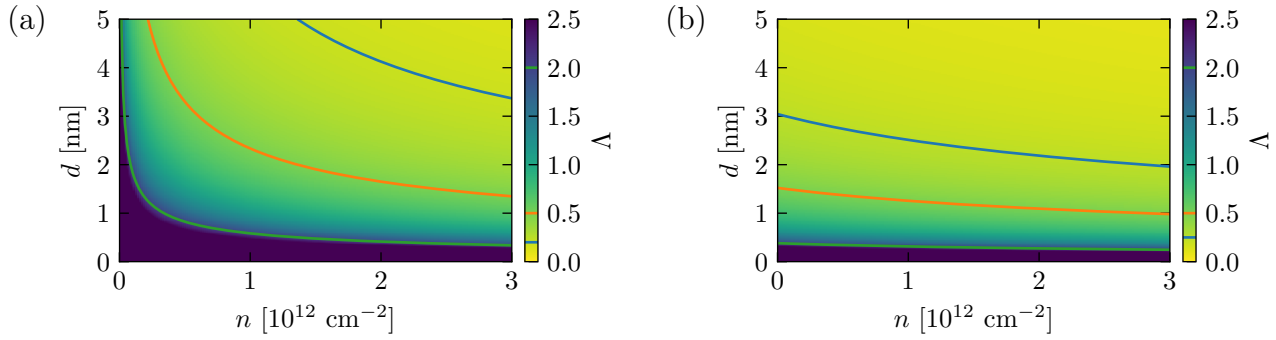


Figure 3.3: (a) Screening parameter $\Lambda$ as a function of electronic density $n$ and spacer thickness $d$ for a single-layer graphene/hBN/metal heterostructure like the one used in Ref. [90]. Results in this figure have been obtained by setting $\bar{\epsilon}_{zz} = 3.5$ and $\mathcal{Z} = 0$. Contour lines have been drawn for $\Lambda = 0.25$ (blue), $\Lambda = 0.5$ (orange), and $\Lambda = 0.25$ (green). (b) Same as in panel (a) but for bilayer graphene.

layered structures can be easily calculated [128, 89]. For example, for a graphene sheet encapsulated between hBN slabs of different thickness and in the presence of a metallic gate has been calculated in Ref. [89]. For low frequencies (i.e. low compared to all, e.g. phonon, features in the dielectric functions of the nearby dielectrics) and long wavelengths (i.e. for $q$ much smaller than the inverse of the dielectric thickness) $v_{q,\omega}$ can be safely replaced by its limit $v_{q,\omega} \approx \lim_{q,\omega\to 0} v_{q,\omega} \equiv e^2/C$, $C$ being the capacitance per unit area of the structure. The reasoning behind this approximation is as follows. The interaction potential between two electrons in a 2D system is

$$v_q = e^2 G(q,0,0), \tag{3.42}$$

where $G(q,z,z')$ is the electrostatic Green function satisfying

$$q^2\epsilon_{\parallel}(z)G(q,z,z') - \partial_z[\epsilon_{\perp}(z)\partial_z G(q,z,z')] = 4\pi\delta(z-z'), \tag{3.43}$$

where $z=0$ is the plane where electrons roam, and $\epsilon_{\parallel}$ ($\epsilon_{\perp}$) is the in-plane (out-of plane) dielectric constant of the dielectric environment. This equation must be supplemented by the boundary conditions at the metallic gate, i.e.

$$\frac{qG(q,z=-d^+,z')}{\epsilon_{\perp}(z=-d^+)\partial_z G(q,z=-d^+,z')} = \mathcal{Z}. \tag{3.44}$$

Here, $\mathcal{Z}$ is the dimensionless impedance of the metallic gate ($\mathcal{Z}=0$ for a perfect conductor). In presence of screening by nearby conductors, the electrostatic Green function converges to a finite limit in the long-wavelength limit. It is therefore meaningful to define a capacitance per unit area

$$C \equiv \lim_{q\to 0}\frac{1}{G(q,0,0)}. \tag{3.45}$$

If we consider a structure made of a perfectly conducting gate parallel to the 2D electron system and separated along the $\hat{\boldsymbol{z}}$-direction by a dielectric spacer of thickness $d$ and dielectric tensor $\bar{\boldsymbol{\epsilon}}$, the capacitance per unit area is $C=\bar{\epsilon}_{zz}/(4\pi d)$, where $\bar{\epsilon}_{zz}$ denotes the tensor component along the $\hat{\boldsymbol{z}}$ direction. For all realistic experimental geometries [89, 90] using e.g. graphene encapsulated in hBN, the plasmon wavelength is much longer than the thickness of the whole device and, therefore, the replacement $v_{q,\omega}\to e^2/C$, i.e. the so-called local capacitance approximation (LCA), is fully justified in the THz regime where the hydrodynamic-ballistic crossover takes place. All results reported in Figs. 3.4-3.5 refer to SLG encapsulated in hBN.

## 3.7 Acoustic plasmons velocity and damping

Following the discussion presented in Sec. 1.2.3, plasmons are zeroes of the longitudinal dielectric function $\epsilon_{\rm L}(q,\omega)$ and they are related to the conductivity coefficient through the relation $\epsilon_{\rm L}(q,\omega)=1-v_{q,\omega}\tilde{\chi}_{nn}(q,\omega)/(e^2\omega)$. Using the LCA and Eq. 3.31 latter becomes

$$\epsilon_{\rm L}(q,\omega) = 1-\Lambda^{-1}\frac{(-i)\pi q^2 v_{\rm F}^2\sigma_{\rm L}(q,\omega)}{2\omega\mathcal{D}}. \tag{3.46}$$

Here, we have defined a new parameter

$$\Lambda = \frac{C}{e^2\mathcal{N}}, \tag{3.47}$$

that characterizes how much the e-e interaction is screened by the nearby dielectric environment. This is the most important parameter of our theory since its value determines whether or not the crossover between the collisionless and hydrodynamic regimes is clearly discernible. In Fig. 3.3 we show its value as a function of density and gate distance for an

heterostructure made of graphene separated from a metal gate by an hBN slab of thickness $d$. It is evident that SLG allows to reach larger values of $\Lambda$ with respect to bilayer graphene thanks to its smaller effective mass, especially at low densities.

In what come next, we evaluate Eq. 3.46 to obtain the values of the velocity and damping of plasmon excitations.

### 3.7.1 Exact solution of plasmon equation

By rearranging the various terms, the equation $\epsilon_{\rm L}(q,\omega)=0$ is equivalent to

$$\sqrt{(\omega+i\gamma+i\gamma_{\rm ee})^2-(qv_{\rm F}^*)^2}=\frac{(\Lambda^{-1}+\frac{K}{K^*})v_{\rm F}^*}{\omega v_{\rm F}}(qv_{\rm F})^2-\frac{2\mathcal{D}v_{\rm F}^*(\omega+i\gamma)}{\mathcal{D}^*v_{\rm F}}+(\omega+i\gamma+i\gamma_{\rm ee}). \tag{3.48}$$

We solve this equation under the condition

$$\mathrm{Re}\left[\frac{(\Lambda^{-1}+\frac{K}{K^*})v_{\rm F}^*}{\omega v_{\rm F}}(qv_{\rm F})^2-\frac{2\mathcal{D}v_{\rm F}^*(\omega+i\gamma)}{\mathcal{D}^*v_{\rm F}}+(\omega+i\gamma+i\gamma_{\rm ee})\right]\geq 0, \tag{3.49}$$

in order to guarantee that the solutions have real values of $\omega$ and $q$. Rearranging this terms becomes

$$\left(\frac{qv_{\rm F}}{\omega}\right)^4+Q\left(\frac{qv_{\rm F}}{\omega}\right)^2+R=0, \tag{3.50}$$

with

$$Q=\frac{\omega\frac{\mathcal{D}^*}{\mathcal{D}}\frac{v_{\rm F}^*}{v_{\rm F}}-2\left[(2\frac{v_{\rm F}^*}{v_{\rm F}}-\frac{\mathcal{D}^*}{\mathcal{D}})(\omega+i\gamma)-i\frac{\mathcal{D}^*}{\mathcal{D}}\gamma_{\rm ee}\right](\Lambda^{-1}+\frac{K}{K^*})}{\omega(\Lambda^{-1}+\frac{K}{K^*})^2\frac{\mathcal{D}^*}{\mathcal{D}}\frac{v_{\rm F}^*}{v_{\rm F}}}, \tag{3.51}$$

and

$$R=-\frac{4(\omega+i\gamma)[\frac{\mathcal{D}^*}{\mathcal{D}}(\omega+i\gamma+i\gamma_{\rm ee})-\frac{v_{\rm F}^*}{v_{\rm F}}(\omega+i\gamma)]}{\omega^2\frac{v_{\rm F}^*}{v_{\rm F}}(\frac{\mathcal{D}^*}{\mathcal{D}})^2(\Lambda^{-1}+\frac{K}{K^*})^2}. \tag{3.52}$$

Eq. (3.50) is a quadratic equation for $(qv_{\rm F}^*/\omega)^2$ with solutions

$$\left(\frac{qv_{\rm F}}{\omega}\right)^2=-\frac{Q}{2}-\frac{\sqrt{Q^2-4R}}{2}=-Q\frac{1+\sqrt{1+4RQ^{-2}}}{2}, \tag{3.53}$$

where we discarded the second solution since it gives $\mathrm{Im}(q)<0$, which has no physical meaning. Finally, from the value of $qv^*/\omega$ of Eq. (3.53) we define the following quantities as the velocity and damping

$$S_\omega=\frac{v_{\rm F}}{\sqrt{\mathrm{Re}\left[\left(\frac{qv_{\rm F}}{\omega}\right)^2\right]}}, \tag{3.54}$$

and

$$\Gamma_\omega=\frac{\omega}{2}\frac{\mathrm{Im}\left[\left(\frac{qv_{\rm F}}{\omega}\right)^2\right]}{\mathrm{Re}\left[\left(\frac{qv_{\rm F}}{\omega}\right)^2\right]}. \tag{3.55}$$

The plasmon equation $\epsilon_{\rm L}(q,\omega)=0$ with $\epsilon_{\rm L}(q,\omega)$ as in Eq. (3.46) can be solved for the plasmon wave vector $q_{\rm p}$. We find $q_{\rm p}(\omega)=(\omega/S_\omega)\sqrt{1+2i\Gamma_\omega/\omega}$, where $S_\omega$ and $\Gamma_\omega$ are real functions of the frequency representing the velocity and the damping of the mode respectively. These two functions can be calculated analytically and the result is shown in Fig. 3.4. We are now interested in the asymptotic behavior of $S_\omega$ and $\Gamma_\omega$ for $\omega\gg\gamma_{\rm ee}$ (collisionless limit) and $\omega\ll\gamma_{\rm ee}$ (hydrodynamic limit). In order to obtain expressions for $S_\omega$ and $\Gamma_\omega$ in the collisionless limit, we expand up to linear order in $\gamma/\omega$ and $\gamma_{\rm ee}/\omega$. We find $Q\approx Q_0+i\gamma/\omega Q_\gamma+i\gamma_{\rm ee}/\omega Q_{\rm ee}$ and $R\approx R_0+i\gamma/\omega R_\gamma+i\gamma_{\rm ee}/\omega R_{\rm ee}$, where

$$Q_0=-\frac{2(2\frac{v_{\rm F}^*}{v_{\rm F}}-\frac{\mathcal{D}^*}{\mathcal{D}})(\Lambda^{-1}+\frac{K}{K^*})-\frac{\mathcal{D}^*}{\mathcal{D}}\frac{v_{\rm F}^*}{v_{\rm F}}}{(\Lambda^{-1}+\frac{K}{K^*})^2\frac{\mathcal{D}^*}{\mathcal{D}}\frac{v_{\rm F}^*}{v_{\rm F}}}, \tag{3.56}$$

$$Q_\gamma=-\frac{2(2\frac{v_{\rm F}^*}{v_{\rm F}}-\frac{\mathcal{D}^*}{\mathcal{D}})}{(\Lambda^{-1}+\frac{K}{K^*})\frac{\mathcal{D}^*}{\mathcal{D}}\frac{v_{\rm F}^*}{v_{\rm F}}}, \tag{3.57}$$

$$Q_{\rm ee}=\frac{2\frac{\mathcal{D}^*}{\mathcal{D}}}{(\Lambda^{-1}+\frac{K}{K^*})\frac{\mathcal{D}^*}{\mathcal{D}}\frac{v_{\rm F}^*}{v_{\rm F}}}, \tag{3.58}$$

and,

$$R_0=-\frac{4(\frac{\mathcal{D}^*}{\mathcal{D}}-\frac{v_{\rm F}^*}{v_{\rm F}})}{\frac{v_{\rm F}^*}{v_{\rm F}}(\frac{\mathcal{D}^*}{\mathcal{D}})^2(\Lambda^{-1}+\frac{K}{K^*})^2}, \tag{3.59}$$

$$R_\gamma=-\frac{8(\frac{\mathcal{D}^*}{\mathcal{D}}-\frac{v_{\rm F}^*}{v_{\rm F}})}{\frac{v_{\rm F}^*}{v_{\rm F}}(\frac{\mathcal{D}^*}{\mathcal{D}})^2(\Lambda^{-1}+\frac{K}{K^*})^2}, \tag{3.60}$$

$$R_{\rm ee}=-\frac{4}{\frac{v_{\rm F}^*}{v_{\rm F}}\frac{\mathcal{D}^*}{\mathcal{D}}(\Lambda^{-1}+\frac{K}{K^*})^2}. \tag{3.61}$$

The replacement of the approximate expressions for $Q$ and $R$, with the coefficients above, into Eq. (3.53) results in the following expression

$$\begin{aligned}\left(\frac{qv_{\rm F}}{\omega}\right)^2\approx\left[-Q_0\frac{1+\sqrt{1+4R_0Q_0^{-2}}}{2}\right]+\frac{i\gamma}{\omega}\frac{Q_\gamma\left[-Q_0\frac{1+\sqrt{1+4R_0Q_0^{-2}}}{2}\right]+R_\gamma}{Q_0\sqrt{1+4R_0Q_0^{-2}}}\\+\frac{i\gamma_{\rm ee}}{\omega}\frac{Q_{\rm ee}\left[-Q_0\frac{1+\sqrt{1+4R_0Q_0^{-2}}}{2}\right]+R_{\rm ee}}{Q_0\sqrt{1+4R_0Q_0^{-2}}}.\end{aligned} \tag{3.62}$$

Finally, the replacement of Eq. (3.62) into Eqs. (3.54) and (3.55) yields Eqs. (3.63) and (3.64) results

$$S_{\rm c}=\frac{v_{\rm F}(\Lambda^{-1}+\frac{K}{K^*})}{\sqrt{\frac{(4\mathcal{D}v_{\rm F}^*-2\mathcal{D}^*v_{\rm F})(\Lambda^{-1}+\frac{K}{K^*})-\mathcal{D}^*v_{\rm F}^*}{2\mathcal{D}^*v_{\rm F}^*}\left[1+\sqrt{1-\frac{16v_{\rm F}^*\mathcal{D}(v_{\rm F}^*\mathcal{D}-v_{\rm F}\mathcal{D}^*)(\Lambda^{-1}+\frac{K}{K^*})^2}{[(2\mathcal{D}v_{\rm F}+4\mathcal{D}v_{\rm F}^*-2\mathcal{D}^*v_{\rm F})(\Lambda^{-1}+\frac{K}{K^*})-\mathcal{D}^*v_{\rm F}^*]^2}}\right]}}, \tag{3.63}$$

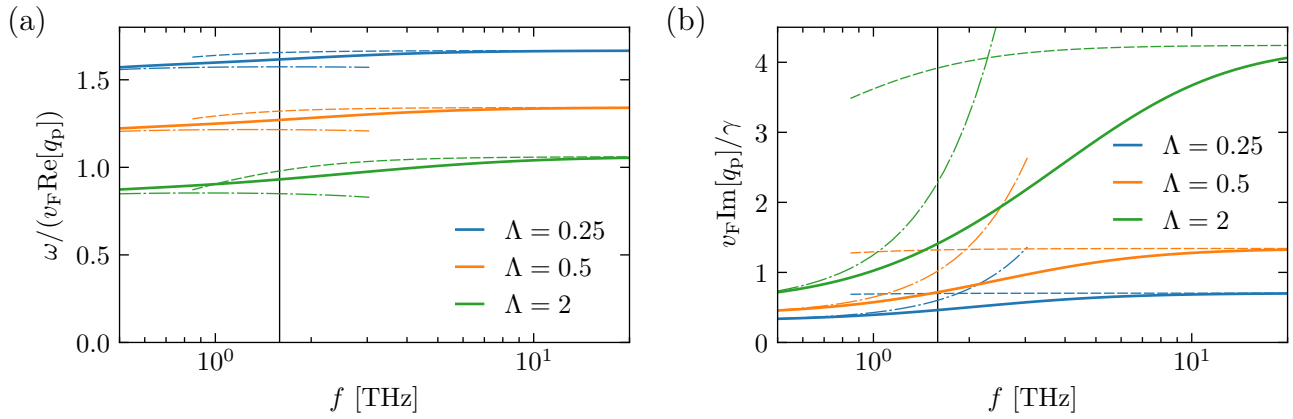


Figure 3.4: (Color online) AP phase velocity normalized to the Fermi velocity (a), and AP damping, normalized to the extrinsic damping $\gamma$, (b), as functions of the frequency $f = \omega/(2\pi)$, for different values of the screening parameter: $\Lambda = 0.25$ (blue), $\Lambda = 0.5$ (orange), and $\Lambda = 2$ (green). Results in this figure have been obtained by setting $\gamma = 10^{12}$ s$^{-1}$, $\gamma_{ee} = 10^{13}$ s$^{-1}$, and neglecting, for the sake of simplicity, many-body renormalizations by setting $v_F^*/v_F = K^*/K = \mathcal{D}^*/\mathcal{D} = 1$. For each value of $\Lambda$, the solid line denotes the result of the solution of $\epsilon_L(q,\omega) = 0$, while the dashed (dash-dotted) line represents the asymptotic collisionless (hydrodynamic) result. The vertical black lines mark the frequency $2\pi f = \gamma_{ee}$ around which the crossover occurs.

$$\Gamma_c = \frac{\gamma\dfrac{(\mathcal{D}v_F + 2\mathcal{D}v_F^* - \mathcal{D}^*v_F)S_h^2 - 2(\mathcal{D}v_F^* - \mathcal{D}^*v_F)S_c^2}{v_F^3\mathcal{D}^*} + \gamma_{ee}\dfrac{S_c^2 - S_h^2}{v_F^2}}{\dfrac{(4\mathcal{D}v_F^* - 2\mathcal{D}^*v_F)(\Lambda^{-1} + \frac{K}{K^*}) - \mathcal{D}^*v_F^*}{2\mathcal{D}v_F}\sqrt{1 - \dfrac{16v_F^*\mathcal{D}(v_F^*\mathcal{D} - v_F\mathcal{D}^*)(\Lambda^{-1} + \frac{K}{K^*})^2}{[(2\mathcal{D}v_F + 4\mathcal{D}v_F^* - 2\mathcal{D}^*v_F)(\Lambda^{-1} + \frac{K}{K^*}) - \mathcal{D}^*v_F^*]^2}}}, \tag{3.64}$$

On the other hand, we can obtain the corresponding results in the hydrodynamic limit by expanding (3.53) for $\gamma_{ee} \gg \omega$. This leads to

$$\left(\frac{qv_F}{\omega}\right)^2 + R^h = 0, \tag{3.65}$$

with

$$R^h = \frac{-2(\omega + i\gamma)}{\frac{\mathcal{D}^*}{\mathcal{D}}\omega\left[(\Lambda^{-1} + \frac{K}{K^*}) - i\frac{v_F^*\omega}{2v_F(\gamma+\gamma_{ee})}\right]}. \tag{3.66}$$

Replacing Eq. (3.65) into Eqs. (3.54) and (3.55) results

$$S_h = v_F\sqrt{\frac{\mathcal{D}^*(\Lambda^{-1} + \frac{K}{K^*})}{2\mathcal{D}}}, \tag{3.67}$$

$$\Gamma_h = \frac{\gamma}{2} + \frac{\mathcal{D}^*v_Fv_F^*\omega^2}{8\mathcal{D}(\gamma + \gamma_{ee})S_h^2}. \tag{3.68}$$

### 3.7.2 Discussion

Eqs. (3.63)-(3.68) are the second important result of this work. In particular, Eqs. (3.67)-(3.68) can be obtained by directly solving Eq. (3.46) with the conductivity given in Eq. (3.41) and ignoring terms of order higher than one in $\omega/\gamma_{ee}$.

From these results one can easily understand why achieving high values of the screening parameter $\Lambda$ is of pivotal importance to observe the crossover from the collisionless to the hydrodynamic regime. Indeed, in the limit $\Lambda \to 0$ we have $S_{\rm h} = S_{\rm c} = v_{\rm F}\sqrt{\mathcal{D}^*/(2\mathcal{D}\Lambda)}$ and $\Gamma_{\rm h} = \Gamma_{\rm c} = \gamma/2$. Therefore, for small values of $\Lambda$ no crossover can be observed as $S_{\rm h} = S_{\rm c}$ and $\Gamma_{\rm h} = \Gamma_{\rm c}$, and the damping of the AP mode is completely controlled by momentum-relaxing collision, with $\gamma_{\rm ee}$ dropping out of the problem.

On the other hand, for $\Lambda \gg 1$ the velocities in the two regimes converge to distinct values. The velocity of the AP mode in the collisionless regime tends to a value which is close (ignoring here, for the sake of simplicity, many-body corrections) to the Fermi velocity, $S_{\rm c} \to v_{\rm F}$, while in the hydrodynamic regime it converges to the speed of sound in a neutral Fermi liquid [129, 137], i.e. $S_{\rm h} \to v_{\rm F}\sqrt{(\mathcal{D}^*K)/(2\mathcal{D}K^*)} \approx v_{\rm F}/\sqrt{2}$. The situation is even more dramatic for the damping $\Gamma_\omega$. In the hydrodynamic regime, and for $\Lambda \gg 1$, we have $\Gamma_{\rm h} \approx \gamma/2 + \omega^2/[4(\gamma+\gamma_{\rm ee})]$, while $\Gamma_{\rm c} \approx \gamma + \gamma_{\rm ee}$, implying that the extrinsic dissipation controlled by $\gamma$ becomes twice more efficient with respect to the $\Lambda \ll 1$ case and a new damping mechanism controlled by $\gamma_{\rm ee}$ kicks in. In Fig. 3.4 we show the impact of $\Lambda$ on the real and imaginary parts of $q_{\rm p}$. When frequency increases, the damping starts to acquire a significant contribution from e-e collisions. This shows up as viscous dissipation in the hydrodynamic regime—see the second term in Eq. (3.68). In this regime, indeed, the contribution to the damping is proportional to $q^2$ and therefore to $\omega^2$, since we are probing the damping along the AP dispersion. When frequency is further increased above $\gamma_{\rm ee}$, the e-e contribution to the damping saturates to a finite value. Note that since in hydrodynamic electron liquids $\gamma_{\rm ee} \gg \gamma$, this contribution can be the dominant one even with moderate values of $\Lambda$ and lead to a significant increase of the imaginary part of $q$, as shown in Fig. 3.4(b).

## 3.8 Coupling efficiency to a near-field probe

In order to excite plasmons in a 2D nanostructure, it is necessary to provide light with the same frequency as the plasmon energy in the material. One way of performing such observation is through a scanning near-field optical microscope (s-SNOM). In this technique, photons from an AFM tip excite plasmon modes in a graphene sample. The propagating photon-plasmon is lately reflected on the edges and the information of the back-scattered radiation can later be used for the determination of plasmons velocity and damping. Another near field way of observing plasmons is by the deposition of gold nanorods in a graphene flake. The system composed in this way generates a dipole by the coupling of the gold nanorod with an electromagnetic field. The dipole field excites the plasmon modes in the graphene flake.

Motivated by this near field experiments, here we describe a way of measure signatures of plasmons. how to measure In order to design experiments that are able to probe the collisionless to hydrodynamic crossover with light, it is important also to consider the

coupling strength of APs to an external field[130]. We characterize the coupling to an external near-field probe using the quantity $\eta_z(\omega)$ defined by the ratio between the power $\langle W\rangle_{\rm AP}(z)$ fed into the AP mode by a dipole source of strength $p$ and frequency $\omega$, located at an height $z$, with its axis perpendicular to the 2D liquid, and the power radiated by the same source in vacuum, given by Larmor's formula

$$W_{\rm Larmor} = \frac{p^2\omega^4}{3c^3}. \tag{3.69}$$

We characterize the effect of the dipole by an oscillating charge density

$$\rho_{\rm ext}(\boldsymbol{q}, z', \omega) = -p\delta'(z'-z), \tag{3.70}$$

where $\delta'(z)$ is the derivative of $\delta(z)$ with respect to its argument. The field it generates is $\boldsymbol{E}_{\rm d}(\boldsymbol{r}, z, \omega) = -\nabla\phi_{\rm d}(\boldsymbol{r}, z, \omega)$, with

$$\begin{aligned}\phi_{\rm d}(\boldsymbol{r}, z, \omega) &= \int \frac{d^2\boldsymbol{q}}{(2\pi)^2} e^{i\boldsymbol{q}\cdot\boldsymbol{r}} \int dz' G(q, z, z')\rho_{\rm ext}(\boldsymbol{q}, z', \omega) \\ &= \int \frac{d^2\boldsymbol{q}}{(2\pi)^2} e^{i\boldsymbol{q}\cdot\boldsymbol{r}} pG'(q, z_d, z),\end{aligned} \tag{3.71}$$

where $G(q, z, z')$ is the electrostatic Green function defined in Sect. 3.6 and $G'(q, z, z') \equiv \partial_z G(q, z, z')$.

The field $\boldsymbol{E}_{\rm d}(\boldsymbol{r}, z, \omega)$ induces a charge oscillation in the electron liquid, which absorbs an average power

$$\begin{aligned}\langle W\rangle(z) &= \int d^2\boldsymbol{r} \frac{1}{2}{\rm Re}[-e\boldsymbol{J}^*(\boldsymbol{r}, \omega)\cdot\boldsymbol{E}_{\rm d}(\boldsymbol{r}, 0, \omega)] \\ &= \frac{\omega e^2 p^2}{2} \int \frac{dqq}{2\pi} \frac{|G'(q, z, 0)|^2}{G(q, 0, 0)} \mathcal{L}(q, \omega).\end{aligned} \tag{3.72}$$

The details of this derivation are presented in App. A.

Since we are interested only in the power fed into the AP, which will be denoted by the symbol $\langle W\rangle_{\rm AP}(z)$, we consider only the contribution to the above integral coming from wave vectors smaller than the edge $q_{\rm eh}$ of the intra-band electron-hole continuum, $q_{\rm eh}(\omega) \equiv \lim_{\Lambda\to\infty} {\rm Re}[q_{\rm p}(\omega)]$.

Finally, using the definition of the coupling efficiency as the ratio $\eta_z(\omega) \equiv \langle W\rangle_{\rm AP}(z)/W_{\rm Larmor}$, we obtain the expression

$$\eta_z(\omega) = \frac{3c^3}{4\pi\omega^3} \int_0^{q_{\rm eh}(\omega)} dqq \frac{|G'(q, z, 0)|^2}{G(q, 0, 0)} \mathcal{L}(q, \omega). \tag{3.73}$$

In Fig. 3.5 we show the numerically-calculated dependence of $\eta_z(\omega)$ on frequency for different vertical positions $z$ of the dipole for the aforementioned case of a 2D material separated from a perfect metal located at $z = -d$ by a dielectric spacer. In this case, for long wavelengths, $G(q, z, 0) \approx e^{-qz}/C$ if $z > 0$ and $G(q, z, 0) \approx (z + d)/(dC)$ $0 > z > -d$. Furthermore, if dissipation is small, we can approximate the loss function, in the relevant

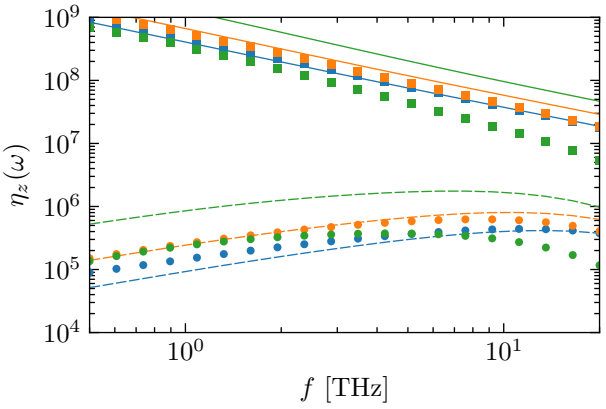


Figure 3.5: (Color online) Coupling efficiency $\eta_z(\omega)$ as a function of frequency. Results in this figure refer to SLG separated from a metal gate by an hBN spacer of thickness $d = 4$ nm, having $\bar{\epsilon}_{xx} = \bar{\epsilon}_{yy} = 6.68$ and $\bar{\epsilon}_{zz} = 3.56$. Squares correspond to excitation in the center of the spacer $z = -2$ nm, while circles correspond to $z = 10$ nm, above SLG. Solid (dashed) lines represent the approximate result of Eq. (3.74) for excitation at $z = -2$ nm ($z = 10$ nm), setting $Z = -0.5$. Different colors refer to different values of the screening parameter: $\Lambda = 0.25$ (blue), $\Lambda = 0.5$ (orange), and $\Lambda = 2$ (green). All other parameters are as in Fig 3.4.

range of wave vectors, as a delta function peak $\mathcal{L}(q,\omega) \approx \pi|Z|\mathrm{Re}(q_\mathrm{p})\delta(q - \mathrm{Re}(q_\mathrm{p}))$ with $Z \equiv [\mathrm{Re}(q_\mathrm{p})\partial_q\epsilon_\mathrm{L}(q,\omega)|_{q=q_\mathrm{p}}]^{-1} = -[2+q_P\partial_q\sigma_\mathrm{L}(q,\omega)|_{q=q_\mathrm{p}}/\sigma_\mathrm{L}(q_\mathrm{p},\omega)]^{-1} \approx -1/2$. Using these approximations in Eq. (3.73) we get the approximate result for $\eta_z(\omega)$:

$$\eta_z(\omega) \approx \frac{3\pi|Z|c^3[\mathrm{Re}(q_\mathrm{p})]^3}{\bar{\epsilon}\omega^3} \times \begin{cases} d\mathrm{Re}(q_\mathrm{p})e^{-2\mathrm{Re}(q_\mathrm{p})z} & z > 0 \\ [d\mathrm{Re}(q_\mathrm{p})]^{-1} & 0 > z > -d, \end{cases} \tag{3.74}$$

where $Z \equiv [\mathrm{Re}(q_\mathrm{p})\partial_q\epsilon_\mathrm{L}(q,\omega)|_{q=q_\mathrm{p}}]^{-1} = -\{2 + q_\mathrm{p}\partial_q \log[\sigma_\mathrm{L}(q_\mathrm{p},\omega)]\}^{-1} \approx -1/2$. Since $q_\mathrm{p}d$ is a small number, we see that the AP modes are much more coupled to a dipole located between the material and the gate. This happens because the electric field of AP modes is mainly concentrated in the spacer region [131]. This suggest that to couple efficiently to these modes, structures specially designed for launching plasmons should be put in the region where the field is concentrated.

## 3.9 Conclusion

In summary, we have studied the dispersion and damping of APs in a 2D electron liquid at the crossover between the hydrodynamic and collisionless regimes. We have found that, in the presence of strong screening by an external gate, both the velocity and the damping of AP modes are enhanced in the collisionless regime, with the enhancement being more dramatic for the damping. If the screening is strong enough, i.e. if $\Lambda > 1$, well defined APs with a phase velocity smaller than the Fermi velocity $v_\mathrm{F}$ (but larger than the sound velocity $\approx v_\mathrm{F}/\sqrt{2}$) are allowed in the hydrodynamic regime.

Our theory relies on the presence of only one electron band close to the Fermi level and, therefore, cannot be directly applied to graphene close to charge neutrality. Interestingly,

we notice that the hydrodynamic theory for graphene (see e.g. Ref. [129]) also predicts (after taking into account the screening of the electric potential by a metal gate) that the plasmon velocity converges to $\approx v_F/\sqrt{2}$ for low electron densities. A more general kinetic theory approach for single-layer graphene was developed in Refs. [132, 133], neglecting Landau parameters.

The crossover between the collisional and the hydrodynamic regime can be considered the 2D electronic analogue of the transition between the first and zero sound in neutral Fermi liquid. This was predicted by Abrikosov and Khalatnikov [134, 135] and experimentally verified[136], for example, in liquid $He^3$.

Notice that some properties of plasmons in 2D Fermi liquids have been discussed in two recent publications, Refs. [137] and [133]. However, the former mainly focusses on the difference between long-range and short-range interactions, and considers only the many-body compressibility renormalization. In the latter work, effects beyond RPA are neglected, and so are momentum non-conserving processes. We have, however, demonstrated that the latter processes are important to correctly describe the plasmon damping and introduce the possibility of having overdamped excitations at low frequencies and long wavelengths, as shown in Eqs. (3.64) and (3.68). The non-linear electromagnetic response of a Dirac electron fluid at the crossover between the collisionless and hydrodynamic regimes has been discussed in Ref. [138].

# 4 Dynamical and nonlocal magnetoconductivity tensor of a two-dimensional Fermi liquid

## 4.1 Overview

In this chapter, we explore the effects of interaction of an uniform external magnetic field to the spectrum of plasmon in a 2D Fermi liquid. Using the same formalism of Chapter 3, we derive analytical expressions for the conductivity tensor $\sigma_{ij}$. Latter, we calculate the dispersion of collective modes of the system by fully taking into account the effect of retardation that leads to the appearance of transversal modes and hybridization of the latter with the longitudinal magnetoplasmon modes.

About the work presented in this chapter a small paper is being written.

## 4.2 Magnetoplasmon experimental observation

The introduction of an external magnetic field can change appreciable the dynamics of two-dimensional materials. One of the most basic examples is the Hall effect for which it is observed the emergence of a transverse resistivity in the material because of an external magnetic field[13, 8, 143]. Another example of magnetic field applications in condensed matter physics is the de Haas–van Alphen effect in which the magnetic susceptibility of a pure metal crystal oscillates with the magnitude of the magnetic field $B$[13, 143].

Classicaly, the moviment of electrons under the influence of an external magnetic field are circular orbits. If we excite this system with an external electric field in order to generate a collective motion, a hybrid mode of these circular orbits and plasmons emerge. We call this collective excitation magnetoplasmons. First experiments were performed on GaAs/AlGaAs disks epitaxialy fabricated [144]. In convetional 2D materials, many experimental observations have been made since then[146]-[148]. Several experimental have been performed in quantum wells. One of relevance was the observation of magnetoplasmon resonances on grid-gated samples and quantum point contacts using THz radiation[149]. They used high quality CdTe/CdMgTe quantum wells and reported hy-

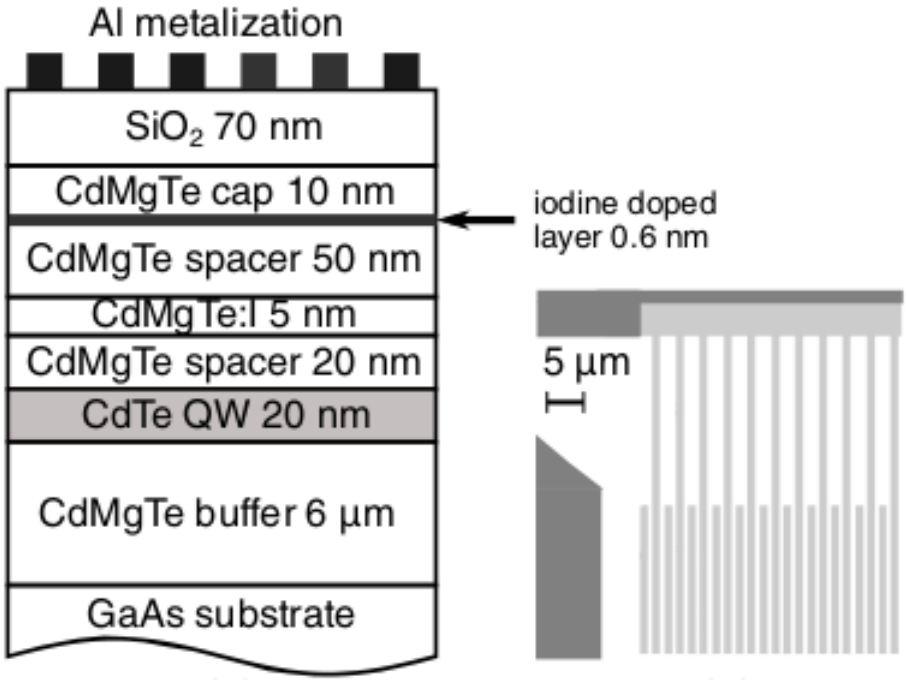


Figure 4.1: layout of wafers used for the fabrication of the grid-gated samples and a sketch of a metallic grid pattern, lithographically defined on the wafer surface. This type of geometry allows the observation of hybridization of cyclotronic resonances and plasmons. Figure adapted from [149].

bridization between the cyclotronic orbits and plasmons in the system.

In graphene, Dirac magnetoplasmon have been observed in arrays of graphene disks using infrared spectroscopy[150]. In this work, graphene single layers grown copper foil through chemical vapor deposition. They report the observation of bulk and edge magnetoplasmons using infrared excitation of the sample. Surprisingly, the edge magnetoplasmon present a longer lifetime when compared with bulk.

Finally, we would like to enphasize the importance of nonlocality for describing properties on 2D systems. Some experimental observations have shown the presence of higher order cyclotronic resonance in photocurrent experiments[146]. This can only be explained with the inclusion of nonlocal contribution for the conductivity of the excitations. As we are going to see it is possible to tune their response considering a more correlated system.

## 4.3 Conductivity tensor

Using the same approach of the previous chapter, in this section we solve Eq. (3.27) to find the current and density response to longitudinal and transverse electric fields. This is encoded in the conductivity tensor $\sigma_{ij}(\boldsymbol{q},\omega)$, defined by

$$J_i(\boldsymbol{q},\omega) = \sigma_{ij}(\boldsymbol{q},\omega)E_j(\boldsymbol{q},\omega). \tag{4.1}$$

The introduction of an external magnetic field along the $\boldsymbol{z}$ direction modifies the total force $\boldsymbol{F}(\boldsymbol{r},\boldsymbol{p},t)$ of Eq. 3.6, which is now given by

$$\boldsymbol{F}(\boldsymbol{r},\boldsymbol{p},t) = -e\left[\boldsymbol{E}(\boldsymbol{r},t) + \frac{\boldsymbol{v}_{\boldsymbol{p}}^{\star}}{c}\times\boldsymbol{B}(\boldsymbol{r},t)\right] - \nabla_{\boldsymbol{r}}U_{\mathrm{L}}(\boldsymbol{r},\boldsymbol{p},t), \tag{4.2}$$

The term involving the magnetic can be easily calculated. First, we notice the momentum derivative can be rewritten in the following way

$$\nabla_{\boldsymbol{p}} = \frac{\partial\epsilon_{\boldsymbol{p}}}{\partial\boldsymbol{p}}\frac{\partial}{\partial\epsilon_{\boldsymbol{p}}} + \frac{\partial\theta_{\boldsymbol{p}}}{\partial\boldsymbol{p}}\frac{\partial}{\partial\theta_{\boldsymbol{p}}} = \boldsymbol{v}_{\boldsymbol{p}}\frac{\partial}{\partial\epsilon_{\boldsymbol{p}}} + \frac{\hat{\boldsymbol{z}}\times\boldsymbol{p}}{p^2}\frac{\partial}{\partial\theta_{\boldsymbol{p}}}. \tag{4.3}$$

Using this relation, the magnetic force contribution is given by

$$\frac{e\boldsymbol{v}_{\boldsymbol{p}}\times\boldsymbol{B}}{c}\cdot\nabla_{\boldsymbol{p}}f^{(1)}(\boldsymbol{r},\boldsymbol{p},t) = -\omega_c\frac{\partial}{\partial\theta_{\boldsymbol{p}}}f^{(1)}(\boldsymbol{r},\boldsymbol{p},t), \tag{4.4}$$

where we have defined the classical cyclotronic frequency $\omega_c = eB/mc$.

The key point of our method is to treat exactly the submatrix of the infinite matrix appearing (3.27) containing the coefficients $a_n$ and $b_n$ with $|n| < N$, with $N$ a given positive integer, and then resumming analytically the two tails of the matrix, under the assumption that the coefficients $a_n$ and $b_n$ already converged to their asymptotic values, i.e.

$$a_n = \omega + i\Gamma_\infty - n\omega_{\mathrm{c}}^{\star} = a - n\omega_{\mathrm{c}}^{\star}, \tag{4.5}$$

$$b_n = b, \tag{4.6}$$

for $|n| \geq N$.

This procedure allows to obtain general expressions for the three independent elements of the conductivity tensor, i.e. the longitudinal, transverse, and Hall conductivity that can take into account any finite number of Landau parameters or different relaxation rates.

Explicit expressions for two important case $N = 0$ and $N = 2$ are provided.

### 4.3.1 Infinite matrix inversion using continued fractions

The infinite matrix appearing in Eq. (3.27) is a tridiagonal matrix. As we already explained in Sec. 3.5, such matrices admit closed-form expressions of their inverses in terms of continued fractions [124]. In particular, any diagonal element of the inverse matrix $M^{-1}$ can be expressed as [124]

$$\begin{aligned}
&\left[M^{-1}\right]_{n,n} = \\
&= \cfrac{1}{a_n - \cfrac{b_{n+1}b_n^*}{a_{n+1} - \cfrac{b_{n+2}b_{n+1}^*}{a_{n+2}+\cdots}} - \cfrac{b_n b_{n-1}^*}{a_{n-1} - \cfrac{b_{n-1}b_{n-2}^*}{a_{n-2}+\cdots}}} = \\
&= \frac{1}{a_n + \xi_n^{(+)} + \xi_n^{(-)}},
\end{aligned} \tag{4.7}$$

where we defined

$$\xi_n^{(+)} \equiv -\cfrac{b_{n+1}b_n^*}{a_{n+1} - \cfrac{b_{n+2}b_{n+1}^*}{a_{n+2}+\cdots}} = -\frac{b_{n+1}b_n^*}{a_{n+1}+\xi_{n+1}^{(+)}}, \tag{4.8}$$

$$\xi_n^{(-)} \equiv -\cfrac{b_n b_{n-1}^*}{a_{n-1} - \cfrac{b_{n-1}b_{n-2}^*}{a_{n-2}+\cdots}} = -\frac{b_n b_{n-1}^*}{a_{n-1}+\xi_{n-1}^{(-)}}. \tag{4.9}$$

The calculation of the off-diagonal elements can be recursively reduced to the calculation of diagonal elements using the identity [124]

$$\left[M^{-1}\right]_{n,m} = \begin{cases} -b_n d_n^{(-)} \left[M^{-1}\right]_{n+1,m} & \text{if} \quad n < m \\ -b_n^* d_n^{(+)} \left[M^{-1}\right]_{n-1,m} & \text{if} \quad n > m. \end{cases} \tag{4.10}$$

where the $d_n^{(\pm)}$ coefficients satisfy the recurrence relations

$$d_{n+1}^{(+)} = \frac{1}{b_{n+1}b_n^*}\left(a_n - \frac{1}{d_n^{(+)}}\right), \tag{4.11}$$

$$d_{n-1}^{(-)} = \frac{1}{b_n b_{n-1}^*}\left(a_n - \frac{1}{d_n^{(-)}}\right). \tag{4.12}$$

Using the recursive relations (4.11-4.12) we obtain

$$\begin{aligned} d_n^{(+)} &= \frac{1}{a_n - b_{n+1}b_n^* d_{n+1}^{(+)}} = \cfrac{1}{a_n - \cfrac{b_{n+1}b_n^*}{a_{n+1} - \cfrac{b_{n+2}b_{n+1}^*}{a_{n+2}+\ldots}}} = \\ &= \frac{1}{a_n + \xi_n^{(+)}}, \end{aligned} \tag{4.13}$$

and similarly

$$d_n^{(-)} = \frac{1}{a_n + \xi_n^{(-)}}. \tag{4.14}$$

Making use of (4.7-4.14) we can find the following expressions for the relevant matrix elements

$$[M^{-1}]_{0,0}(q,\omega) = \frac{1}{a_0 + \xi_0^{(+)}(q,\omega) + \xi_0^{(-)}(q,\omega)}, \tag{4.15}$$

$$\begin{aligned} &[M^{-1}]_{\pm1,\pm1}(q,\omega) = \\ &= -\frac{\xi_0^{(\pm)}(q,\omega)(a_0 + \xi_0^{(\mp)}(q,\omega))[M^{-1}]_{0,0}(q,\omega)}{|b|^2(1+F_0^{\mathrm{S}})(1+F_1^{\mathrm{S}})}, \end{aligned} \tag{4.16}$$

$$\begin{aligned} &[M^{-1}]_{1,-1}(\boldsymbol{q},\omega) = \\ &= \frac{(b^*)^2\xi_0^{(+)}(q,\omega)\xi_0^{(-)}(q,\omega)[M^{-1}]_{0,0}(q,\omega)}{|b|^4(1+F_0^{\mathrm{S}})(1+F_1^{\mathrm{S}})}, \end{aligned} \tag{4.17}$$

$$\begin{aligned} &[M^{-1}]_{-1,1}(\boldsymbol{q},\omega) = \\ &= \frac{b^2\xi_0^{(+)}(q,\omega)\xi_0^{(-)}(q,\omega)[M^{-1}]_{0,0}(q,\omega)}{|b|^4(1+F_0^{\mathrm{S}})(1+F_1^{\mathrm{S}})}. \end{aligned} \tag{4.18}$$

The conductivity tensor can be decomposed according to

$$\sigma_{ij}(\boldsymbol{q},\omega) = \hat{P}^{\mathrm{L}}_{ij}(\boldsymbol{q})\sigma_{\mathrm{L}}(q,\omega) + \hat{P}^{\mathrm{T}}_{ij}(\boldsymbol{q})\sigma_{\mathrm{T}}(q,\omega) + \hat{\epsilon}_{ij}\sigma_{\mathrm{H}}(q,\omega), \tag{4.19}$$

where $\hat{P}^{\mathrm{L}}_{ij}(\boldsymbol{q}) = q_i q_j/q^2$, $\hat{P}^{\mathrm{T}}_{ij}(\boldsymbol{q}) = \delta_{ij} - q_i q_j/q^2$ are the projectors on the longitudinal and transverse direction respectively, and $\hat{\epsilon}_{ij}$ is the 2D Levi-Civita tensor.

Using (3.17-3.27-4.1) and the results for the matrix element (4.15-4.18), remembering that $a_0 = \omega$, and comparing with (4.19) we obtain (comparison can be made easily by setting $\boldsymbol{q} = \hat{\boldsymbol{x}}q$)

$$\sigma_{\mathrm{L}}(q,\omega) = \frac{-ie^2\mathcal{N}^\star}{(1+F_0^{\mathrm{S}})\,q^2}\frac{\omega\left[\xi_0^{(+)}(q,\omega)+\xi_0^{(-)}(q,\omega)\right]}{\omega+\xi_0^{(+)}(q,\omega)+\xi_0^{(-)}(q,\omega)}, \tag{4.20}$$

$$\begin{aligned}\sigma_{\mathrm{T}}(q,\omega) &= \sigma_{\mathrm{L}}(q,\omega) + \\ &+ \frac{-ie^2\mathcal{N}^\star}{(1+F_0^{\mathrm{S}})\,q^2}\frac{4\xi_0^{(+)}(q,\omega)\xi_0^{(-)}(q,\omega)}{\omega+\xi_0^{(+)}(q,\omega)+\xi_0^{(-)}(q,\omega)},\end{aligned} \tag{4.21}$$

$$\sigma_{\mathrm{H}}(q,\omega) = \frac{-ie^2\mathcal{N}^\star}{(1+F_0^{\mathrm{S}})\,q^2}\frac{i\omega\left[\xi_0^{(+)}(q,\omega)-\xi_0^{(-)}(q,\omega)\right]}{\omega+\xi_0^{(+)}(q,\omega)+\xi_0^{(-)}(q,\omega)}. \tag{4.22}$$

The longitudinal part of the conductivity is closely related to the proper density-density response function $\tilde{\chi}_{nn}(q,\omega) = q^2\sigma_{\mathrm{L}}(q,\omega)/(i\omega e^2)$.

The above expressions are completely general and hold for any number of different scattering rates and Landau parameters. Since for $|n| \geq N$ (4.5) hold, for $n \geq N$ $\xi_n^{(+)} = \bar{\xi}_n^{(+)}$ while for $n \leq N$, $\xi_n^{(-)} = \bar{\xi}_n^{(-)}$, where

$$\begin{aligned}\bar{\xi}_n^{(\pm)}(q,\omega) &\equiv -\cfrac{|b|^2}{a-\omega_{\mathrm{c}}^\star(n\pm1)-\cfrac{|b|^2}{a-\omega_{\mathrm{c}}^\star(n\pm2)+\cdots}} \\ &= -\frac{|b|^2}{a-(n\pm1)\omega_{\mathrm{c}}}\frac{{}_0F_1\left(\mp\frac{a}{\omega_{\mathrm{c}}}\pm n+2,-\frac{|b|^2}{\omega_{\mathrm{c}}^2}\right)}{{}_0F_1\left(\mp\frac{a}{\omega_{\mathrm{c}}}\pm n+1,-\frac{|b|^2}{\omega_{\mathrm{c}}^2}\right)} \\ &= \pm\frac{qv_{\mathrm{F}}^\star}{2}\frac{J_{\mp\frac{\omega+i\Gamma_\infty}{\omega_{\mathrm{c}}}\pm n+1}\left(\frac{qv_{\mathrm{F}}^\star}{\omega_{\mathrm{c}}}\right)}{J_{\mp\frac{\omega+i\Gamma_\infty}{\omega_{\mathrm{c}}}\pm n}\left(\frac{qv_{\mathrm{F}}^\star}{\omega_{\mathrm{c}}}\right)}\end{aligned} \tag{4.23}$$

In the second step of Eq. 4.23 we identify our result with the continued fraction representation of the ratio between two hypergeometric functions[124], while in the last step we used the relation

$$J_\nu(z) = \left(\frac{z}{2}\right)^\nu\frac{1}{\Gamma(\nu+1)}{}_0F_1\left(-;\nu+1;\frac{-z^2}{4}\right) \tag{4.24}$$

Repeatedly using $N$ times (4.8-4.9) we can calculate $\xi_0^{(\pm)}$.

Next we evaluate explicitly the conductivity coefficients for some special cases.

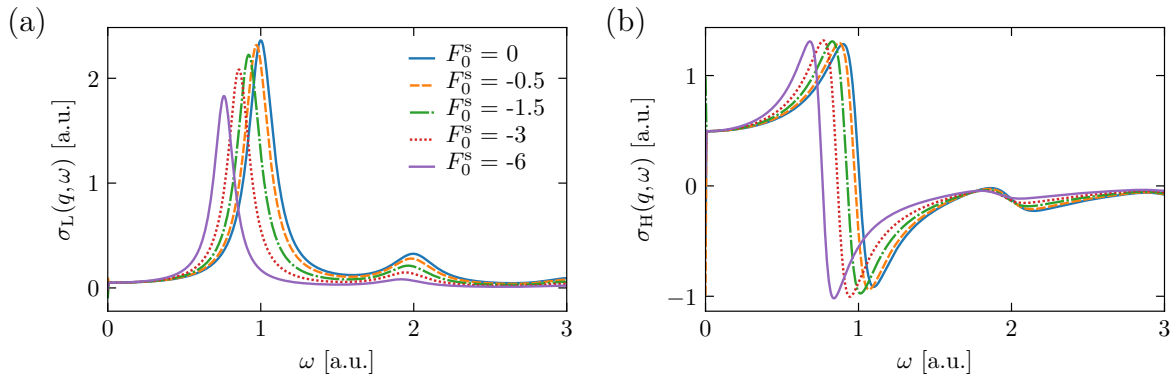


Figure 4.2: Conductivity coefficients for different values of $F_0^S$ as function of $\omega/\omega_c$: (a) $\sigma_{=L}$ and (b) $\sigma_H(q,\omega)$. Other parameters are $\gamma = 0.01\omega_c$, $\gamma_{ee} = 0.01\omega_c$ and $F_1^S = 0$.

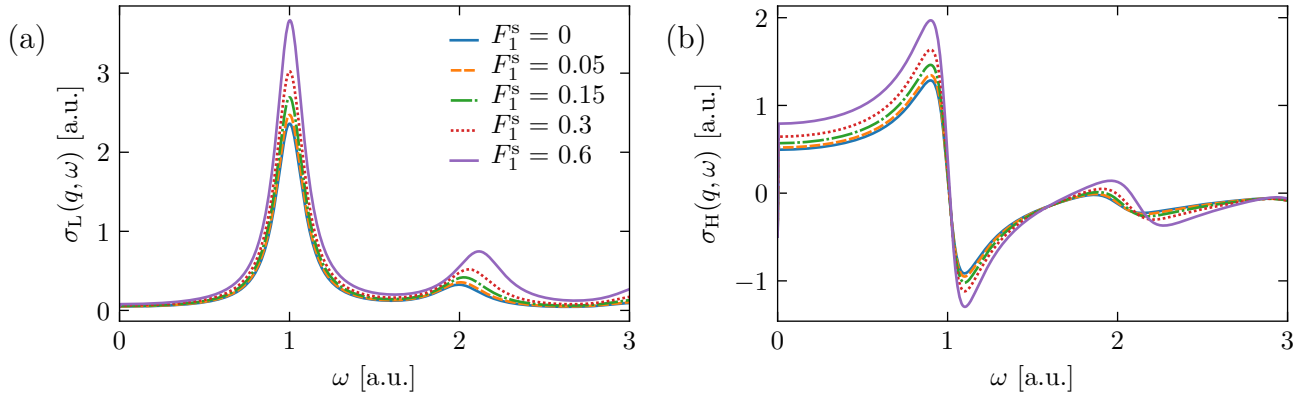


Figure 4.3: Conductivity coefficients for different values of $F_1^S$ as function of $\omega/\omega_c$: (a) $\sigma_{=L}$ and (b) $\sigma_H(q,\omega)$. Other parameters are $\gamma = 0.01\omega_c$, $\gamma_{ee} = 0.01\omega_c$ and $F_0^S = 0$.

### 4.3.2 Local limit

We now look to the local limit, i.e, the $q \to 0$ limit of Eq. 4.20. Equivalently to Chap. 3 (Eq. 3.40) we obtained a Drude like expression for the conductivity coefficients

$$\sigma_L(\omega) = \left(\frac{i\mathcal{D}^\star}{\pi}\right) \frac{\omega + i\gamma}{(\omega + i\gamma)^2 - \omega_c^2} \tag{4.25}$$

$$\sigma_T(\omega) = \sigma_L(\omega) \tag{4.26}$$

$$\sigma_H(\omega) = \left(\frac{\mathcal{D}^\star}{\pi}\right) \frac{\omega_c}{(\omega + i\gamma)^2 - \omega_c^2} \tag{4.27}$$

We see from this expression that electron-electron collisions $\gamma_{ee}$ again only appear at $q^2$ order and the damping is induced solely by $\gamma$ scattering. This result show agreement with the values found in literature for Hall conductivity in the local regime. Also, we see from Eqs. 4.25-4.27 that the conductivities present resonances only for the first cyclotronic frequency $\omega = \omega_c$, while other resonances are suppresed.

### 4.3.3 Conductivity tensor in absence of collisions

In the absence of collisions and also turning the Landau interaction parameters off, the tail of the continued fraction is obtained for $N = 0$. Therefore this results in the expression

$$\bar{\xi}_0^{\pm}(q,\omega) = \bar{\xi}_0^{(\pm)}(q,\omega) = \pm\frac{qv_{\mathrm{F}}^{\star}}{2}\frac{J_{\mp\frac{\omega}{\omega_{\mathrm{c}}}+1}\left(\frac{qv_{\mathrm{F}}^{\star}}{\omega_{\mathrm{c}}}\right)}{J_{\mp\frac{\omega}{\omega_{\mathrm{c}}}}\left(\frac{qv_{\mathrm{F}}^{\star}}{\omega_{\mathrm{c}}}\right)}. \tag{4.28}$$

Now we have $\xi_0 = \bar{\xi}_0$ and the substitution on Eq's. 4.20 give

$$\sigma_{\mathrm{L}}^0(q,\omega) = \frac{-ie^2\mathcal{N}^{\star}}{q^2}\omega\left[1-\left(\frac{\pi\omega}{\omega_{\mathrm{c}}}\right)\frac{J_{\frac{\omega}{\omega_{\mathrm{c}}}}\left(\frac{qv_{\mathrm{F}}^{\star}}{\omega_{\mathrm{c}}}\right)J_{-\frac{\omega}{\omega_{\mathrm{c}}}}\left(\frac{qv_{\mathrm{F}}^{\star}}{\omega_{\mathrm{c}}}\right)}{\sin\left(\frac{\pi\omega}{\omega_{\mathrm{c}}}\right)}\right] \tag{4.29}$$

$$\begin{aligned}\sigma_{\mathrm{T}}^0(q,\omega) &= \sigma_{\mathrm{L}}^0(q,\omega)+\\ &+\frac{ie^2\mathcal{N}^{\star}}{q^2}\left(\frac{\pi(qv_{\mathrm{F}}^{\star})^2}{\omega_{\mathrm{c}}}\right)\frac{J_{\frac{\omega}{\omega_{\mathrm{c}}}+1}\left(\frac{qv_{\mathrm{F}}^{\star}}{\omega_{\mathrm{c}}}\right)J_{-\frac{\omega}{\omega_{\mathrm{c}}}+1}\left(\frac{qv_{\mathrm{F}}^{\star}}{\omega_{\mathrm{c}}}\right)}{\sin\left(\frac{\pi\omega}{\omega_{\mathrm{c}}}\right)},\end{aligned} \tag{4.30}$$

$$\sigma_{\mathrm{H}}^0(q,\omega) = \frac{ie^2\mathcal{N}^{\star}}{q^2}i\omega\left[1+\left(\frac{\pi qv_{\mathrm{F}}^{\star}}{\omega_{\mathrm{c}}}\right)\frac{J_{\frac{\omega}{\omega_{\mathrm{c}}}}\left(\frac{qv_{\mathrm{F}}^{\star}}{\omega_{\mathrm{c}}}\right)J'_{-\frac{\omega}{\omega_{\mathrm{c}}}}\left(\frac{qv_{\mathrm{F}}^{\star}}{\omega_{\mathrm{c}}}\right)}{\sin\left(\frac{\pi\omega}{\omega_{\mathrm{c}}}\right)}\right]. \tag{4.31}$$

Here, we used "′" to denote derivative with respect to $qv_{\mathrm{F}}/\omega_{\mathrm{c}}$. Differently of the local limit, we see from Eq's. 4.29-4.31 that the conductivity coefficients present several resonance $\omega = n\omega_{\mathrm{c}}$ modes generated by the oscillatory behavior of the functions.

### 4.3.4 Conductivity in presence of momentum conserving and momentum relaxing collisions

Now a more complex situation for which we assume both electron-electron and electron-lattice collision coefficients non zero. Therefore, this results in $\Gamma_0 = 0$, $\Gamma_1 = \gamma$, $\Gamma_\infty = \gamma + \gamma_{\mathrm{ee}}$. Also, we keep the Landau parameters until $m = 1$. When doing this, the tail of the continued fraction is obtained for $N = 1$. Therefore, $\xi_0^{\pm}(q,\omega)$ becomes

$$\xi_0^{\pm}(q,\omega) = -\frac{(1+F_0^{\mathrm{S}})(1+F_1^{\mathrm{S}})\frac{(v_{\mathrm{F}}^{\star}q)^2}{4}}{\omega+i\gamma-\omega_{\mathrm{c}}+(1+F_1^{\mathrm{S}})\bar{\xi}_{\pm1}^{\pm}(q,\omega)} \tag{4.32}$$

$$\sigma_{\mathrm{L}}(q,\omega) = \frac{i\mathcal{N}^{\star}e^2}{q^2}\times$$

$$\frac{\omega(1+F_1^{\mathrm{S}})\frac{(v_F^{\star}q)^2}{4}\left[2\omega+2i\gamma+(1+F_1^{\mathrm{S}})(\bar{\xi}_1^{+}+\bar{\xi}_{-1}^{-})\right]}{\omega\left[\omega-\omega_c+i\gamma+(1+F_1^{\mathrm{S}})\bar{\xi}_1^{+}\right]\left[\omega+\omega_c+i\gamma+(1+F_1^{\mathrm{S}})\bar{\xi}_{-1}^{-}\right]-(1+F_0^{\mathrm{S}})(1+F_1^{\mathrm{S}})\frac{(v_F^{\star}q)^2}{4}\left[2\omega+2i\gamma+(1+F_1^{\mathrm{S}})(\bar{\xi}_1^{+}+\bar{\xi}_{-1}^{-})\right]}, \tag{4.33}$$

$$\sigma_{\mathrm{T}}(q,\omega)=\frac{i\mathcal{N}^{\star}e^{2}}{q^{2}}\times \frac{\omega(1+F_1^{\mathrm{S}})\frac{(v_F^{\star}q)^2}{4}\left[2\omega+2i\gamma+(1+F_1^{\mathrm{S}})(\bar{\xi}_1^{+}+\bar{\xi}_{-1}^{-})\right]-(1+F_0^{\mathrm{S}})\left[(1+F_1^{\mathrm{S}})\frac{(v_F^{\star}q)^2}{4}\right]^2}{\omega\left[\omega-\omega_c+i\gamma+(1+F_1^{\mathrm{S}})\bar{\xi}_1^{+}\right]\left[\omega+\omega_c+i\gamma+(1+F_1^{\mathrm{S}})\bar{\xi}_{-1}^{-}\right]-(1+F_0^{\mathrm{S}})(1+F_1^{\mathrm{S}})\frac{(v_F^{\star}q)^2}{4}\left[2\omega+2i\gamma+(1+F_1^{\mathrm{S}})(\bar{\xi}_1^{+}+\bar{\xi}_{-1}^{-})\right]}, \tag{4.34}$$

$$\sigma_{\mathrm{H}}(q,\omega)=\frac{\mathcal{N}^{\star}e^{2}}{q^{2}}\times \frac{\omega(1+F_1^{\mathrm{S}})\frac{(v_F^{\star}q)^2}{4}\left[2\omega_{\mathrm{c}}+(1+F_1^{\mathrm{S}})(\bar{\xi}_1^{+}-\bar{\xi}_{-1}^{-})\right]}{\omega\left[\omega-\omega_c+i\gamma+(1+F_1^{\mathrm{S}})\bar{\xi}_1^{+}\right]\left[\omega+\omega_c+i\gamma+(1+F_1^{\mathrm{S}})\bar{\xi}_{-1}^{-}\right]-(1+F_0^{\mathrm{S}})(1+F_1^{\mathrm{S}})\frac{(v_F^{\star}q)^2}{4}\left[2\omega+2i\gamma+(1+F_1^{\mathrm{S}})(\bar{\xi}_1^{+}+\bar{\xi}_{-1}^{-})\right]}. \tag{4.35}$$

In fig's. 4.2 and 4.3 we show the longitudinal and Hall conductivities as function of $\omega$ with $q$ satisfying $qv_{\mathrm{F}}/\omega = 0.5$ and for different values of the Landau $F_0^{\mathrm{S}}$ and $F_1^{\mathrm{S}}$ respectively. Other parameters are set $\gamma = \gamma_{\mathrm{ee}} = 0.01\omega_{\mathrm{c}}$. We see from these results that electron electron interactions can tune the resonances in the system. This can latter be used for coupling the system with second and higher harmonics.

## 4.4 Spectrum derivation

The electric current induced in a 2D electron liquid is related to the total applied electric field by (4.1), where the conductivity tensor has been calculated in the previous section. Since an electric current acts as a source of electromagnetic field, the electric field itself is in turn related to the current flowing in the electron liquid. This relation can be written in terms of a matrix Green function

$$E_i(\boldsymbol{q},\omega) = g_{ij}(\boldsymbol{q},\omega)J_j(\boldsymbol{q},\omega) + E_i^{\mathrm{ext}}(\boldsymbol{q},\omega), \tag{4.36}$$

where $g_{ij}(\boldsymbol{q},\omega)$ gives the Green function matrix coefficients and is derived from Maxwell equations. Last chapter we did not have to worry with the calculation of $g_{ij}$. Since the electron field was exciting plasmons along the propagation direction, we only had to worry with the density response function (or, equivalently, with the longitudinal conductivity). Note that here $\boldsymbol{E}(\boldsymbol{q},\omega)$ denotes the in-plane electric field evaluated at $z = 0$ where the 2D electron system is located. We perform a complete analytical derivation of the Green function in App. A. By doing this, the Green function can be decomposed in a longitudinal and transverse component according to

$$g_{ij}(\boldsymbol{q},\omega) = g_{\mathrm{L}}(q,\omega)\hat{P}_{ij}^{\mathrm{L}}(\boldsymbol{q}) + g_{\mathrm{T}}(q,\omega)\hat{P}_{ij}^{\mathrm{T}}(\boldsymbol{q}). \tag{4.37}$$

The $g_{\mathrm{L}}$ and $g_{\mathrm{T}}$ expression are derived in App. A for a material located at $z = 0$ with two different enviroments $\epsilon_1$ and $\epsilon_2$ at $z > 0$ and $z < 0$ and a metal gate located at $z = -d$.

Here, we are going to assume $\epsilon_1 = \epsilon_2 = \epsilon$. By doing expression for $g_{\rm L}$ and $g_{\rm T}$ become

$$g_{\rm L}(q,\omega) = -\frac{4\pi i\beta}{\omega\epsilon} e^{-\beta d}\sinh(\beta d) \tag{4.38}$$

$$g_{\rm T}(q,\omega) = -\frac{4\pi i\omega}{\beta c^2} e^{-\beta d}\sinh(\beta d), \tag{4.39}$$

where $\beta = \sqrt{q^2 - \omega^2/c^2}$ is the retarded wavevector for the electromagnetic wave outside the plane[152]. Substituting (4.1) into (4.36) we obtain

$$\epsilon_{ij}(\boldsymbol{q},\omega)E_j(\boldsymbol{q},\omega) = E_i^{\rm ext}(\boldsymbol{q},\omega), \tag{4.40}$$

where

$$\epsilon_{ij}(\boldsymbol{q},\omega) = \delta_{ij} - g_{ik}(\boldsymbol{q},\omega)\sigma_{kj}(\boldsymbol{q},\omega). \tag{4.41}$$

Taking $\boldsymbol{q}$ in the $\hat{\boldsymbol{x}}$ direction, the matrix $\epsilon(\boldsymbol{q},\omega)$ reads

$$\epsilon(q\hat{\boldsymbol{x}},\omega) = \begin{pmatrix} 1-\sigma_{\rm L}(q,\omega)g_{\rm L}(q,\omega) & -\sigma_{\rm H}(q,\omega)g_{\rm L}(q,\omega) \\ \sigma_{\rm H}(q,\omega)g_{\rm T}(q,\omega) & 1-\sigma_{\rm T}(q,\omega)g_{\rm T}(q,\omega) \end{pmatrix}. \tag{4.42}$$

Self-sustained modes in the absence of external sources can therefore be supported when

$$\begin{aligned} &\det[\epsilon(\boldsymbol{q},\omega)] = \\ &= \epsilon_{\rm L}(q,\omega)\epsilon_{\rm T}(q,\omega) + g_{\rm L}(q,\omega)g_{\rm T}(q,\omega)\left[\sigma_{\rm H}(q,\omega)\right]^2 = 0, \end{aligned} \tag{4.43}$$

were we defined the longitudinal and transverse part of the dielectric function as

$$\epsilon_{\rm L/T}(q,\omega) \equiv 1 - g_{\rm L/T}(q,\omega)\sigma_{\rm L/T}(q,\omega). \tag{4.44}$$

The expression obtained here was already derived by other authors [151, 152]. In absence of an Hall conductivity the collective modes of the system are simply given by the zeros of $\epsilon_{\rm L/T}(q,\omega)$. Also, in the limit $d \ll 1$ we recover the expression for $\epsilon_{\rm L}$ from the previous chapter. The Hall conductivity introduces hybridization between the two modes that are no longer purely longitudinal or transverse.

## 4.5 Discussion

In the electrostatic limit, i.e. $q \gg \omega/c$ the transverse part of the Green function vanishes. In this limit only longitudinal modes are allowed that are described by the zeros of the longitudinal dielectric function. To study these confined modes we introduce longitudinal loss function

$$\mathcal{L}_{\rm L}(q,\omega) = -{\rm Im}\left[\frac{1}{\epsilon_{\rm L}(q,\omega)}\right]. \tag{4.45}$$

Peaks of the loss function correspond to zeros of the dielectric function. In Fig. 4.4 we show the the longitudinal loss function for different values of the gate distance $d$. Figure 4.4(a) represent the case of an ungated system. For this case we have $g_{\rm L} = -4\pi i q^2/\omega\epsilon$.

Two features can be observed in the figure. First, we have the plasmon branch. For small values of $q$ the spectrum of the plasmon branch can be approximatly given

$$\omega(q) = \sqrt{\omega_{pl}^2 + \omega_c^2}, \tag{4.46}$$

where $\omega_{pl}$ is the spectrum in the absence of magnetic field. Second, the figure also shows the appearence of several resonance branches. Those are associated with the cyclotronic resonances in the presence of a magnetic field. Because plasmons in an ungated 2D material have a $q$-dependence of the form $\omega_{pl} \propto \sqrt{q}$, we have a separation between plasmons modes and cyclotronic orbits, i.e, there is no hybridisation. The presence of a gate however changes the dispersion dependence. Now we have acoustic plasmons for which $\omega_{pl} \propto q$. Because now the inclination on the $q - \omega$ plane is larger, we have a stronger hybridisation between plasmons and cyclotronic resonances. Those hybridisations are responsable for the formation of the several subbands int the spectrum showed in Fig's. 4.4. This is the semiclassical analogue of the Bernstein modes[153]. In this case the hybrisation between the Landau levels of the quantum system and the plasmon that generate the several subbands.

Next, we discuss the role of the electron-electron interactions for the formation of the hybridisations in the spectrum. Fig. 4.5 show the loss function spectrum for two distinct cases $\gamma_{\mathrm{i}} \ll \omega_c$ and $\gamma_{\mathrm{i}} \gg \omega_c$, where $\gamma_{\mathrm{i}}$ is either $\gamma_{\mathrm{ee}}$ or $\gamma$. Our results show that the hybridisation between plasmon modes is damped when collisions become stronger than the cyclotronic motion. Classicaly, our understanding this result by the fact that if the collision time is larger than the time necessary for an electron to make a revolution in a cyclotronic orbit, the cyclotronic modes are supressed and we only have the plasmon branch Eq. 4.46.

## 4.6 Conclusion

In summary, we have investigated the properties of plasmons in a 2D electron liquid in the presence of an uniform magnetic field. Using the Landau theory of the electron liquid, we provide expressions for the conductivity coefficients of the system. Our theory capture both electron-electron and electron-lattice collisions and also allows the implementation of higher order interactions in the system. We describe the collective excitations in the non-retarded limit, i.e, assuming $c \gg \omega/q$. Furher investigations should also include the effect of finite $c$. We have found that the presence of a metallic gate allows stronger hybridisation between plasmons and cyclotronic motion. Also, this effect is heavily influenced by the presence of collisions in the system.

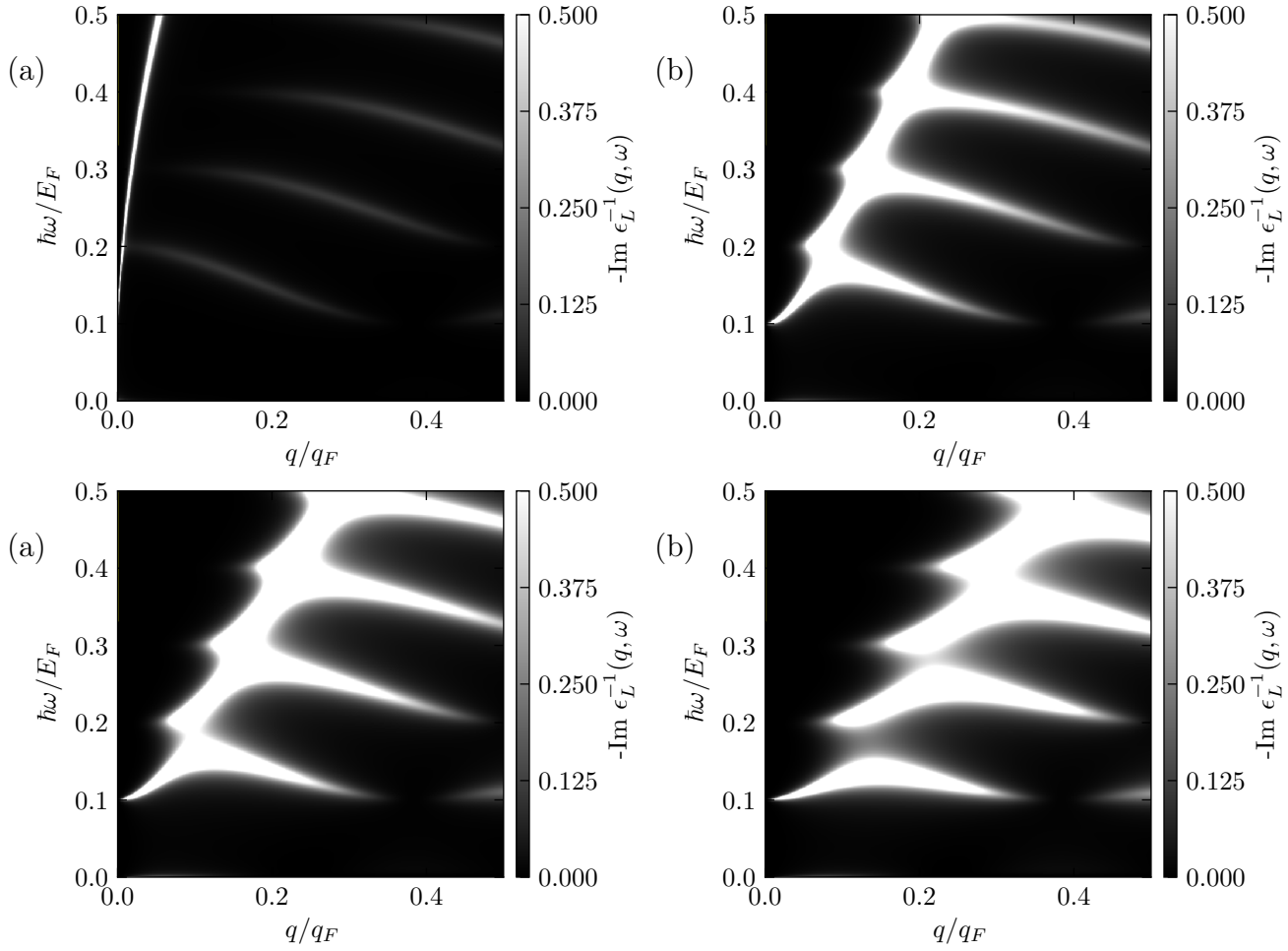


Figure 4.4: Loss function $L(q,\omega) = -\mathrm{Im}(\epsilon_L^{-1})$ for different configuration of gate distance d = (a) $\infty$, (b) 27, (c) 14.5 and (d) 5.5 nm. All Landau parameters are set to zero. Other parameters are $\omega_c = 0.1\omega_\mathrm{F}$, $\gamma = \gamma_{\mathrm{ee}} = 0.01 E_\mathrm{F}/\hbar$.

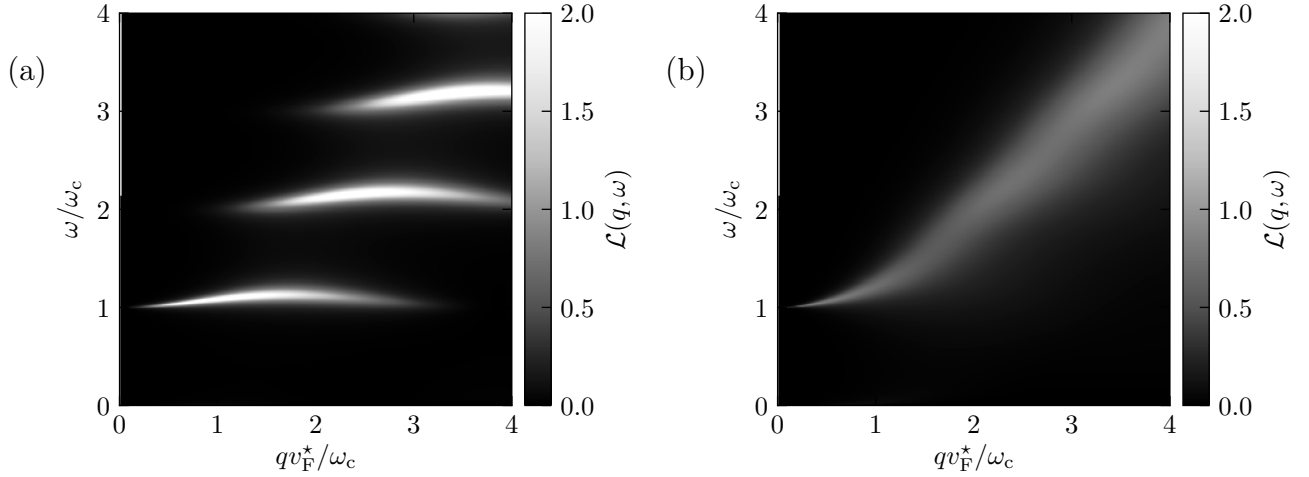


Figure 4.5: Loss function $L(q,\omega) = -\mathrm{Im}(\epsilon_L^{-1})$ for different values of the collision parameters $\gamma = 0.01\omega_c$, (a) $\gamma_{\mathrm{ee}} = 0.01\omega_c$ and (b) $\gamma_{ee} = \omega_c$. All Landau parameters are set to zero and $d = 1$ nm.

# 5

# Concluding remarks and perspectives

In this thesis, we have investigated the properties of different electron systems describing their behaviour as quasi particles. Here, we present the major conclusions of our work and how they fit in the bigger picture of condensed matter theory

**In chapter 2** we studied the properties of quasi electrons confined in graphene bilayers with AA stacking. On the subject of particle confinement, the graphene bilayer presents similar problem as the one observed in monolayer (Klein tunneling). Here, we derived general boundary conditions, videlicet the IMBC, which protects electrons from scaping the region of confinement, i.e, the quantum dot. The biggest advantage of this type of condition is the broader applicability, i.e, once the IMBC is known, we can calculate the energy levels of quantum dots under several external effects. Here, as an application, we have calculated the quantum dot energy levels in the presence of an external uniform magnetic field. A direct extension of our work is the calculation of the energy levels for the quantum dot in the presence of an external electric field. Studies have shown [154] the existence of an antiferromagnetic order in those systems which can be supressed by the application of a perpendicular electric field. The boundary conditions found here also allow us to obtain the energy spectrum of other types of quasi particles, such as excitons and plasmons. Another direct extension of work is the calculation of the excitons spectrum for the bilayer. Exciton are excitations of the electron-hole pair. The calculation of the excitonic levels require the solution of the two-particle AA-stacking bilayer Hamiltonian. However, once we have calculated the solutions of the equation, we can apply the IMBC and obtain the excitonic spectrum. Finally, it is also worth mention that the formalism used here for AA-stacked graphene bilayers can be extended for other two-dimensional materials. These can result in a whole number of different properties to be explored.

**In chapter 3** we have investigated the properties of acoustic plasmons in a 2D electron liquid. This is achievied by the application of a metallic gate which confines the system in the vertical direction. Also, due to screening of the long-range electron-electron interactions, the system becomes softer. In other words, it responds strongly for larger values of momentum and nonlocality effects become more relevant. In order to describe this system we used the Landau theory of the electron liquid. In this theory we assume

there is a one to one correspondence between a noninteracting and a interacting electron system and therefore the implementation of nonlocal interactions come from the renormalization of the quasi particles parameters (such as effective mass, velocity, etc). We use a kinetic equation for describing the collective motion of the quasi particles on this system. This approach is valid when the excitation wavelength is sufficiently long compared to the inverse of the Fermi wave vector $k_F$ , and when the excitation energy $\hbar\omega$ is sufficiently small compared with the Fermi energy and the gap. Collisions were described in the relaxation time approximation, where we separate the momentum conserving and non-conserving interactions. By solving to first order the kinetic equation we obtained expressions for the nonlocal conductivity and therefore the excitations spectrum of the acoustic plasmon in the system. Finally, further investigation of the role of the collision parameters allowed fully understand signatures of the transition between hydrodynamic and ballistic modes.

As we have explained, our theory takes into account only one parameter to characterize collisions between electrons and other quasi particles. Since we are only considering small excitations around the Fermi surface, this assumption presents no problem. If we consider however situations for which the different angular distributions relax in different ways, we have to consider more than one relaxation time parameter. This can be easily implemented using the model presented here since our method of solving the kinetic equation can be implemented in this type of situation. Another possible extension of this work is to investigate the thermoelectric transport in the Fermi liquid. This can generate additional regimes of electron propagation besides the hydrodynamic and ballistic investigated here.

Finally, plasmons on a perpendicular magnetic field were investigated in **chapter 5**. We have used the same formalism presented on the previous chapter to obtain analytical expressions for the conductivity tensor. Collective modes were also investigated and our calculation demonstraded that the application of an external magnetic field generates an hybridization between longitudinal and transversal plasmon excitations in the 2D electron liquid. We expect that the work developed here can be used for the investigation of photocurrent experiments in the hydrodynamic regime. Another extension of this work should be on the already mentioned thermoelectric response, where now we should investigate this in the thermo magnetic transport regime. Finally, we assumed a paramagnetic state of the electron during all our calculations. If this is no longer true, we have to consider that the magnetic field can also couple with the spin of the electrons. Therefore, we can no longer assume a one fluid approximation for the electron liquid.

# Appendices

# A

# Derivation of the condition for observation of Plasmon modes

## A.1 Derivation of the Green's function equation

Using Maxwell equations as the starting point we have

$$\begin{aligned} \nabla \times \boldsymbol{H}(\boldsymbol{r},t) &= \frac{1}{c}\partial_t D(\boldsymbol{r},t) + \frac{4\pi}{c}\boldsymbol{J}(\boldsymbol{r},t), \\ -\nabla \times \boldsymbol{E}(\boldsymbol{r},t) &= \frac{1}{c}\partial_t B(\boldsymbol{r},t), \\ \nabla \cdot \boldsymbol{D}(\boldsymbol{r},t) &= 4\pi\boldsymbol{\rho}(\boldsymbol{r},t), \\ \nabla \cdot \boldsymbol{B}(\boldsymbol{r},t) &= 0. \end{aligned} \tag{A.1}$$

Here, the electric displacement and magnetic field are given by $\boldsymbol{D}(\boldsymbol{r},t) = \epsilon\boldsymbol{E}(\boldsymbol{r},t)$ and $\boldsymbol{B}(\boldsymbol{r},t) = \mu\boldsymbol{H}(\boldsymbol{r},t)$ assuming a dispersive linear medium. The scalar equations are dependent of the vector set of equations. So, we fix our attention in the first set of differential equations.

$$\nabla \times \left(\frac{1}{\mu}\nabla \times \boldsymbol{E}(\boldsymbol{r},\omega)\right) = \frac{\omega^2}{c^2}\epsilon\boldsymbol{E}(\boldsymbol{r},\omega) + \frac{4\pi i\omega}{c^2}\boldsymbol{J}(\boldsymbol{r},\omega) \tag{A.2}$$

$$\nabla = i\boldsymbol{q} + \hat{z}\partial_z \tag{A.3}$$

$$(i\boldsymbol{q} + \hat{z}\partial_z) \times \left[\frac{1}{\mu}(i\boldsymbol{q} + \hat{z}\partial_z) \times \boldsymbol{E}(\boldsymbol{r},\omega)\right] = \frac{\omega^2}{c^2}\epsilon\boldsymbol{E}(\boldsymbol{r},\omega) + \frac{4\pi i\omega}{c^2}\boldsymbol{J}(\boldsymbol{r},\omega) \tag{A.4}$$

$z$-component:

$$\frac{q^2}{\mu}E_z(q,z,\omega) + i\left(\frac{\boldsymbol{q}}{\mu}\cdot\partial_z\boldsymbol{E}_{x-y}(q,z,\omega)\right) = \frac{\omega^2}{c^2}\epsilon E_z(q,z,\omega) \tag{A.5}$$

$x-y$ component:

$$\left(\frac{q^2}{\mu} - \frac{\boldsymbol{q}\boldsymbol{q}}{\mu}\cdot -\partial_z\frac{1}{\mu}\partial_z\right)\boldsymbol{E}_{x-y}(q,z,\omega) + i\boldsymbol{q}\partial_z\frac{E_z(q,z,\omega)}{\mu} = \frac{\omega^2}{c^2}\epsilon\boldsymbol{E}_{x-y}(\boldsymbol{r},t) + \frac{4\pi i\omega}{c^2}\boldsymbol{J}(\boldsymbol{r},\omega) \tag{A.6}$$

We can uncouple Eqs. A.5 and A.6, therefore resulting in the following matricial equation

$$\begin{pmatrix} \hat{\mathcal{L}}_z & 0 & 0 \\ 0 & \hat{\mathcal{L}}_{xx} & \hat{\mathcal{L}}_{xy} \\ 0 & \hat{\mathcal{L}}_{yx} & \hat{\mathcal{L}}_{yy} \end{pmatrix} \begin{pmatrix} E_z(q,z,\omega) \\ E_x(q,z,\omega) \\ E_y(q,z,\omega) \end{pmatrix} = \frac{4\pi i\omega}{c^2} \begin{pmatrix} 0 \\ J_x(q,z,\omega) \\ J_y(q,z,\omega) \end{pmatrix} \tag{A.7}$$

Therefore since we can separate the z-component plane component we can focus only int the calculations of the plane components

$$\begin{pmatrix} \hat{\mathcal{L}}_{xx} & \hat{\mathcal{L}}_{xy} \\ \hat{\mathcal{L}}_{yx} & \hat{\mathcal{L}}_{yy} \end{pmatrix} \begin{pmatrix} E_x(q,z,\omega) \\ E_y(q,z,\omega) \end{pmatrix} = \frac{4\pi i\omega}{c^2} \begin{pmatrix} J_x(q,z,\omega) \\ J_y(q,z,\omega) \end{pmatrix}, \tag{A.8}$$

where the components of the operator $\hat{\mathcal{L}}$ satisfies the relation

$$\hat{\mathcal{L}}_{ij} = \left[\frac{\beta^2}{\mu}\delta_{ij} - q_i q_j \left(\frac{1}{\mu} - \partial_z \frac{1}{\mu\beta^2}\partial_z\right) - \partial_z \frac{1}{\mu}\partial_z\right] \tag{A.9}$$

with $\beta = \sqrt{q^2 - (\omega^2/c^2)\mu\epsilon}$. Instead of trying to solve directly Eq. A.8 we look the Green's function, defined through the equation

$$\begin{pmatrix} \hat{\mathcal{L}}_{xx} & \hat{\mathcal{L}}_{xy} \\ \hat{\mathcal{L}}_{yx} & \hat{\mathcal{L}}_{yy} \end{pmatrix} \begin{pmatrix} G_{xx}(q,z,z',\omega) & G_{xy}(q,z,z',\omega) \\ G_{yx}(q,z,z',\omega) & G_{yy}(q,z,z',\omega) \end{pmatrix} = \frac{4\pi i\omega}{c^2} \begin{pmatrix} 1 & 0 \\ 0 & 1 \end{pmatrix} \delta(z-z') \tag{A.10}$$

The components of the eletric field are obtained from the Green function through

$$E_i(q,z,\omega) = \int dz' G_{ij}(q,z,z',\omega) J_j(q,z',\omega). \tag{A.11}$$

Finally, a great simplication in our equations can be obtained if we look in the components along and perpendicular the wave-vector $\boldsymbol{q}$ instead of $x$ and $y$ components, i.e. $\propto \boldsymbol{q}$ and $\propto \boldsymbol{q} \times \hat{z}$ respectively. This is equivalent to rotate our frame of reference along $\boldsymbol{q}$, By doing this we diagonalize both the operator $\hat{\mathcal{L}}$ and the Green's function $G$ therefore resulting in the expression

$$\begin{pmatrix} \hat{\mathcal{L}}_{\mathrm{L}} & 0 \\ 0 & \hat{\mathcal{L}}_{\mathrm{T}} \end{pmatrix} \begin{pmatrix} G_{\mathrm{L}}(q,z,z',\omega) & 0 \\ 0 & G_{\mathrm{T}}(q,z,z',\omega) \end{pmatrix} = \frac{4\pi i\omega}{c^2} \begin{pmatrix} 1 & 0 \\ 0 & 1 \end{pmatrix} \delta(z-z') \tag{A.12}$$

where the operators $\hat{\mathcal{L}}_{\mathrm{L}}$ and $\hat{\mathcal{L}}_{\mathrm{T}}$ are given by

$$\hat{\mathcal{L}}_{\mathrm{L}} = \frac{\omega^2}{c^2}\left[\partial_z \frac{\epsilon}{\beta^2}\partial_z - \epsilon\right] \tag{A.13}$$

$$\hat{\mathcal{L}}_{\mathrm{T}} = -\partial_z \frac{1}{\mu}\partial_z + \frac{\beta^2}{\mu} \tag{A.14}$$

and $G_{\mathrm{L}}(q,z,z',\omega)$ and $G_{\mathrm{T}}(q,z,z',\omega)$ are related to the $G_{ij}$ components through

$$G_{ij}(q,z,z',\omega) = \frac{q_i q_j}{q^2} G_{\mathrm{L}}(q,z,z',\omega) + \left(\delta_{ij} - \frac{q_i q_j}{q^2}\right) G_{\mathrm{T}}(q,z,z',\omega). \tag{A.15}$$

## A.2 Solution of the Green's function equation

We can now specialize the discussion for the case in which we have inhomogeneity along the z-direction. We assume two different environments and the precense of a gate. This can be done by defining the $\epsilon(z)$ and $\mu(z)$ by

$$\epsilon(z), \mu(z) = \begin{cases} \epsilon_2, \mu_2 & \text{if} \quad z > z' \\ \epsilon_1, \mu_1 & \text{if} \quad -d < z < z' \\ \epsilon_m, \mu_m & \text{if} \quad z < -d \end{cases}, \tag{A.16}$$

where we assume the position of unitary current response given by $z = z'$. Here, the $\epsilon_m$ and $\mu_m$ corresponds to the precense of the gate located at $z = -d$. By the end of the calculation we shall assume $\epsilon_m \to \infty$ and $\mu_m \to 0$. Now, equation A.12 can be separeted in two different equations for the components

$$\begin{aligned} \frac{\partial}{\partial z}\left[\frac{\epsilon}{\beta^2}\frac{\partial G_{\mathrm{L}}}{\partial z}\right] - \epsilon G_{\mathrm{L}} &= \frac{4\pi i}{\omega}\delta(z - z'), \\ \frac{\partial}{\partial z}\left[\frac{1}{\mu}\frac{\partial G_{\mathrm{T}}}{\partial z}\right] - \frac{\beta^2}{\mu}G_{\mathrm{T}} &= -\frac{4\pi i\omega}{c^2}\delta(z - z'). \end{aligned} \tag{A.17}$$

These equations must be supplemented by the boundary conditions at $z = z'$ and $z = -d$, which are given by

$$\begin{aligned} G_{\mathrm{L}}(z' + 0) &= G_{\mathrm{L}}(z' - 0), \\ \frac{\epsilon_2}{\beta_2^2}\frac{\partial}{\partial z}G_{\mathrm{L}}(z' + 0) - \frac{\epsilon_1}{\beta_1^2}\frac{\partial}{\partial z}G_{\mathrm{L}}(z' - 0) &= \frac{4\pi i}{\omega}, \\ G_{\mathrm{L}}(-d + 0) &= G_{\mathrm{L}}(-d - 0), \\ \frac{\epsilon_1}{\beta_1^2}\frac{\partial}{\partial z}G_{\mathrm{L}}(-d + 0) &= \frac{\epsilon_m}{\beta_m^2}\frac{\partial}{\partial z}G_{\mathrm{L}}(-d - 0), \end{aligned} \tag{A.18}$$

for the longitudinal component and

$$\begin{aligned} G_{\mathrm{T}}(z' + 0) &= G_{\mathrm{T}}(z' - 0), \\ \frac{1}{\mu_2}\frac{\partial}{\partial z}G_{\mathrm{T}}(z' + 0) - \frac{1}{\mu_1}\frac{\partial}{\partial z}G_{\mathrm{T}}(z' - 0) &= -\frac{4\pi i\omega}{c^2}, \\ G_{\mathrm{T}}(-d + 0) &= G_{\mathrm{T}}(-d - 0), \\ \frac{1}{\mu_1}\frac{\partial}{\partial z}G_{\mathrm{T}}(-d + 0) &= \frac{1}{\mu_m}\frac{\partial}{\partial z}G_{\mathrm{T}}(-d - 0), \end{aligned} \tag{A.19}$$

for the transversal component. The solution of Eqs. (A.17) is straightforward resulting in the following expressions

$$G_{\mathrm{L(T)}} = \begin{cases} A_{\mathrm{L(T)}}e^{-\beta_2 z} & \text{for} \quad z > z' \\ B_{\mathrm{L(T)}}e^{-\beta_1 z} + C_{\mathrm{L(T)}}e^{\beta_1 z} & \text{for} \quad -d < z < z' \\ D_{\mathrm{L(T)}}e^{\beta_m z} & \text{for} \quad z < -d \end{cases}. \tag{A.20}$$

where $\beta_j = \sqrt{q^2 - (\omega^2/c^2)\mu_j\epsilon_j}$ is related with the propagation along the $z$ direction and $\mathrm{Re}\beta_j > 0$ in order to have solution confined along the $z$-direction. Finally, using the boundary conditions Eqs. A.18 and A.19 we obtain the coefficients

$$
\begin{aligned}
\mathrm{A_L} &= -\frac{4\pi i}{\omega}\left(\frac{\beta_2}{\epsilon_2}\right)\frac{\epsilon_2\beta_1\left(\epsilon_1\beta_m\cosh[\beta_1(z'+d)] + \epsilon_m\beta_1\sinh[\beta_1(z'+d)]\right)}{(\epsilon_2\beta_1\epsilon_1\beta_m + \epsilon_1\beta_2\epsilon_m\beta_1)\cosh[\beta_1(z'+d)] + (\epsilon_2\beta_1\epsilon_m\beta_1 + \epsilon_1\beta_2\epsilon_1\beta_m)\sinh\beta_1(z'+d)]},\\
\mathrm{B_L} &= -\frac{4\pi i}{\omega}\left(\frac{\beta_2}{2\epsilon_2}\right)\frac{(\epsilon_1\beta_m - \epsilon_m\beta_1)\,\epsilon_2\beta_1 e^{-\beta_1 d}}{(\epsilon_2\beta_1\epsilon_1\beta_m + \epsilon_1\beta_2\epsilon_m\beta_1)\cosh[\beta_1(z'+d)] + (\epsilon_2\beta_1\epsilon_m\beta_1 + \epsilon_1\beta_2\epsilon_1\beta_m)\sinh\beta_1(z'+d)]},\\
\mathrm{C_L} &= -\frac{4\pi i}{\omega}\left(\frac{\beta_2}{2\epsilon_2}\right)\frac{(\epsilon_1\beta_m + \epsilon_m\beta_1)\,\epsilon_2\beta_1 e^{\beta_1 d}}{(\epsilon_2\beta_1\epsilon_1\beta_m + \epsilon_1\beta_2\epsilon_m\beta_1)\cosh[\beta_1(z'+d)] + (\epsilon_2\beta_1\epsilon_m\beta_1 + \epsilon_1\beta_2\epsilon_1\beta_m)\sinh\beta_1(z'+d)]},\\
\mathrm{D_L} &= -\frac{4\pi i}{\omega}\left(\frac{\beta_2}{\epsilon_2}\right)\frac{\epsilon_1\beta_m\epsilon_2\beta_1}{(\epsilon_2\beta_1\epsilon_1\beta_m + \epsilon_1\beta_2\epsilon_m\beta_1)\cosh[\beta_1(z'+d)] + (\epsilon_2\beta_1\epsilon_m\beta_1 + \epsilon_1\beta_2\epsilon_1\beta_m)\sinh\beta_1(z'+d)]},\\
\mathrm{A_T} &= \frac{4\pi i\omega}{c^2}\left(\frac{\mu_2}{\beta_2}\right)\frac{\beta_2\mu_1\left(\beta_1\mu_m\cosh[\beta_1(z'+d)] + \beta_m\mu_1\sinh[\beta_1(z'+d)]\right)}{(\beta_2\mu_1\beta_1\mu_m + \beta_1\mu_2\beta_m\mu_1)\cosh[\beta_1(z'+d)] + (\beta_2\mu_1\beta_m\mu_1 + \beta_1\mu_2\beta_1\mu_m)\sinh\beta_1(z'+d)}\\
\mathrm{B_T} &= \frac{4\pi i\omega}{c^2}\left(\frac{\mu_2}{2\beta_2}\right)\frac{(\beta_1\mu_m - \beta_m\mu_1)\,\beta_2\mu_1 e^{-\beta_1 d}}{(\beta_2\mu_1\beta_1\mu_m + \beta_1\mu_2\beta_m\mu_1)\cosh[\beta_1(z'+d)] + (\beta_2\mu_1\beta_m\mu_1 + \beta_1\mu_2\beta_1\mu_m)\sinh\beta_1(z'+d}\\
\mathrm{C_T} &= \frac{4\pi i\omega}{c^2}\left(\frac{\mu_2}{2\beta_2}\right)\frac{(\beta_1\mu_m + \beta_0\mu_1)\,\beta_2\mu_1 e^{\beta_1 d}}{(\beta_2\mu_1\beta_1\mu_m + \beta_1\mu_2\beta_m\mu_1)\cosh[\beta_1(z'+d)] + (\beta_2\mu_1\beta_m\mu_1 + \beta_1\mu_2\beta_1\mu_m)\sinh\beta_1(z'+d}\\
\mathrm{D_T} &= \frac{4\pi i\omega}{c^2}\left(\frac{\mu_2}{\beta_2}\right)\frac{\beta_1\mu_m\beta_2\mu_1}{(\beta_2\mu_1\beta_1\mu_m + \beta_1\mu_2\beta_m\mu_1)\cosh[\beta_1(z'+d)] + (\beta_2\mu_1\beta_m\mu_1 + \beta_1\mu_2\beta_1\mu_m)\sinh\beta_1(z'+d)}
\end{aligned}
\tag{A.21}
$$

Now we perform the limit, $\epsilon_m \to \infty$ and $\mu_m \to 0$, in order to simulate the precense of an ideal gate. For this particular case, the coefficients in Eq. (A.21) become simpler and we obtain

$$
\begin{aligned}
\mathrm{A_\parallel} &= -\frac{4\pi i}{\omega}\frac{\beta_2\beta_1\sinh[\beta_1(z'+d)]}{\epsilon_1\beta_2\cosh[\beta_1(z'+d)] + \epsilon_2\beta_1\sinh[\beta_1(z'+d)]},\\
\mathrm{B_\parallel} &= \frac{2\pi i}{\omega}\frac{\beta_2\beta_1 e^{-\beta_1 d}}{\epsilon_1\beta_2\cosh[\beta_1(z'+d)] + \epsilon_2\beta_1\sinh[\beta_1(z'+d)]},\\
\mathrm{C_\parallel} &= -\frac{2\pi i}{\omega}\frac{\beta_2\beta_1 e^{\beta_1 d}}{\epsilon_1\beta_2\cosh[\beta_1(z'+d)] + \epsilon_2\beta_1\sinh[\beta_1(z'+d)]},\\
\mathrm{D_\parallel} &= 0,\\
\mathrm{A_\perp} &= \frac{4\pi i\omega}{c^2}\frac{\mu_2\mu_1\sinh[\beta_1(z'+d)]}{\beta_1\mu_2\cosh[\beta_1(z'+d)] + \beta_2\mu_1\sinh[\beta_1(z'+d)]},\\
\mathrm{B_\perp} &= -\frac{2\pi i\omega}{c^2}\frac{\mu_2\mu_1 e^{\beta_1 d}}{\beta_1\mu_2\cosh[\beta_1(z'+d)] + \beta_2\mu_1\sinh[\beta_1(z'+d)]},\\
\mathrm{C_\perp} &= \frac{2\pi i\omega}{c^2}\frac{\mu_2\mu_1 e^{\beta_1 d}}{\beta_1\mu_2\cosh[\beta_1(z'+d)] + \beta_2\mu_1\sinh[\beta_1(z'+d)]},\\
\mathrm{D_\perp} &= 0.
\end{aligned}
\tag{A.22}
$$

## A.3 From Green's function to plasmons

With the Green's function obtained in the previous section we can finally obtain the components of the electric. Assuming a two-dimensional current distribution located at

$z = 0$, the current density can be written as $\boldsymbol{J}(q, z', \omega) = \boldsymbol{J}(q, \omega)\delta(z' - 0)$. Using the definition of the green functions defined in Eq. A.11 we obtain the expressions

$$\begin{aligned} E_{\mathrm{L}}(q, z, \omega) &= \int_{-d}^{\infty} dz' G_{\mathrm{L}}(q, z, z', \omega) J_{\mathrm{L}}(q, \omega)\delta(z' - 0) = G_{\mathrm{L}}(q, z, 0, \omega) J_{\mathrm{L}}(q, \omega), \\ E_{\mathrm{T}}(q, z, \omega) &= \int_{-d}^{\infty} dz' G_{\mathrm{T}}(q, z, z', \omega) J_{\mathrm{T}}(q, \omega)\delta(z' - 0) = G_{\mathrm{T}}(q, z, 0, \omega) J_{\mathrm{T}}(q, \omega). \end{aligned} \tag{A.23}$$

Now we assume that the current is given by the eletric field through the relation $J_i = \sigma_{ij} E_j(q, 0, \omega)$, where $\sigma_{ij}$ is the conductivity tensor and it is given by

$$\begin{aligned} &\sigma_{ij}(\boldsymbol{q}, \omega) = \\ &= \sigma_L(q, \omega)\frac{q_i q_j}{q^2} + \sigma_T(q, \omega)\left(\delta_{ij} - \frac{q_i q_j}{q^2}\right) + \sigma_{\mathrm{H}}(q, \omega)\varepsilon_{ijz}, \end{aligned} \tag{A.24}$$

Therefore, using this definition of the longitudinal and transverse components of the current and the expression for the conductivity tensor we finally obtain

$$\begin{aligned} J_{\mathrm{L}}(q, \omega) &= \sigma_{\mathrm{L}}(q, \omega) E_{\mathrm{L}}(q, \omega) - \sigma_{\mathrm{H}}(q, \omega) E_{\mathrm{T}}(q, 0, \omega), \\ J_{\mathrm{T}}(q, \omega) &= \sigma_{\mathrm{T}}(q, \omega) E_{\mathrm{T}}(q, \omega) + \sigma_{\mathrm{H}}(q, \omega) E_{\mathrm{H}}(q, 0, \omega). \end{aligned} \tag{A.25}$$

Finally by setting $z = 0$ in Eq. A.23 and replacing $J_{\mathrm{L}}$ and $J_{\mathrm{T}}$ from Eq. A.25 we obtain that the electric inside the plane has to satisfy the following

$$\begin{bmatrix} 1 - G_{\mathrm{L}}(q, 0, 0, \omega)\sigma_{\mathrm{L}}(q, \omega) & G_{\mathrm{L}}(q, 0, 0, \omega)\sigma_{\mathrm{H}}(q, \omega) \\ -G_{\mathrm{T}}(q, 0, 0, \omega)\sigma_{\mathrm{H}}(q, \omega) & 1 - G_{\mathrm{T}}(q, 0, 0, \omega)\sigma_{\mathrm{T}}(q, \omega) \end{bmatrix} \begin{bmatrix} E_{\mathrm{L}}(q, 0, \omega) \\ E_{\mathrm{T}}(q, 0, \omega) \end{bmatrix} = 0 \tag{A.26}$$

And the condition for the observation of plasmons is given by

$$\left(1 - G_{\mathrm{L}}(q, 0, 0, \omega)\sigma_{\mathrm{L}}(q, \omega)\right)\left(1 - G_{\mathrm{T}}(q, 0, 0, \omega)\sigma_{\mathrm{T}}(q, \omega)\right) + G_{\mathrm{L}}(q, 0, 0, \omega) G_{\mathrm{T}}(q, 0, 0, \omega)\sigma_{\mathrm{H}}^2(q, \omega) = 0 \tag{A.27}$$

# B

# Publications related with this thesis

- L. V. de Castro, D. J. P. de Sousa, 1 D. R. da Costa, Andrey Chaves, and J. Milton Pereira Jr., *AA-stacked bilayer graphene quantum dots: A comparison between tight-binding and continuum model.* (manuscript in preparation).

- I. torres, L. V. de Castro, B. Van Duppen, D. B. Ruiz, F. M. Peeters, F. H. L. Koppens and M. Polini,*Acoustic plasmons at the crossover between the collisionless and hydrodynamic regimes in two-dimensional electron liquids.* PHYSICAL REVIEW B **99**, 144307 (2019). DOI: 10.1103/PhysRevB.99.144307

- L. V. de Castro, I. torres, B. Van Duppen, D. B. Ruiz, F. M. Peeters, F. H. L. Kopppens and M. Polini, *Dynamical and nonlocal magnetoconductivity tensor of a two-dimensional Fermi liquid.* (Manuscript in preparation).

# C

# Publications not related with this thesis

- D. J. P. de Sousa, L. V. de Castro, D. R. da Costa, J. Milton Pereira Jr. *Boundary conditions for phosphorene nanoribbons in the continuum approach.* Physical Review B **94** , 235415 (2016). DOI:10.1103/PhysRevB.94.235415

- D. J. P. de Sousa, L. V. de Castro, D. R. da Costa, J. Milton Pereira Jr. and Tony Low. *Multilayered black phosphorus: From a tight-binding to a continuum description.* Physical Review B **96** , 155427 (2017). DOI:10.1103/PhysRevB.96.155427

# Bibliography


[1] M. Velický and P. S. Toth, Appl. Mat. today **9**, 68 (2017).

[2] K. S. Novoselov, A. K. Geim, S. V. Morozov, D. Jiang, Y. Zhang, S. V. Dubonos, I. V. Grigorieva, and A. A. Firsov, Science **306**, 666 (2004).

[3] S. Z. Butler, S. M. Hollen, L. Cao, Y. Cui, J. A. Gupta, H. R. Gutiérrez, T. F. Heinz, S. S. Hong, J. Huang, A. F. Ismach, E. Johnston-Halperin, M. Kuno, V. V. Plashnitsa, R. D. Robinson, R. S. Ruoff, S. Salahuddin, J. Shan, L. Shi, M. G. Spencer, M. Terrones, W. Windl, and J. E. Goldberger, ACS Nano **7**, 4, 2898-2926 (2013).

[4] J. Yang, J. Wu, S. Che, P. Stepanov, T. Taniguchi, K. Watanabe, H. Baek, D. Smirnov, R. Chen, and C. N. Lau, Nano Lett. **18**, 229 (2018).

[5] D. J. P. de Sousa, L. V. de Castro, D. R. da Costa, and J. M. Pereira, Jr., Phys. Rev. B **94**, 235415 (2016).

[6] A. N. Rudenko, M. I. Katsnelson, and R. Róldan Phys. Rev. B **95**, 081407 (2017)

[7] E. Van Veen, J. Yu, M. I. Katsnelson, R. Róldan, and S. Yuan Phys. Rev. Mat **2**, 114011 (2018)

[8] M. I. Katsnelson, *Graphene: carbon in two dimensions* (Cambridge University Press, New York, 2012).

[9] K. I. Bolotin, F. Ghahari, M. D. Shulman, H. L. Stormer, and P. Kim, Nat. **462**, 196 (2010)

[10] R. D. Mattuck, *A Guide to Feynman Diagrams in the Many-Body Problem* (Dover Publications, Inc., New York, 1967).

[11] A. L. Fetter and J. D. Walecka, Quantum Theory of Many-Particle Systems (Dover Publications, Inc., Mineola, New York, 1971)

[12] G.F. Giuliani and G. Vignale, *Quantum Theory of the Electron Liquid* (Cambridge University Press, Cambridge, 2005).

[13] N. W. Ashcroft and N. D. Mermin, Fí sica do Estado Sólido (Cengage Learning Ltda., São Paulo, 2011).

[14] P. Harrison *Quantum Wells, Wires and Dots* (John Wiley & Sons, LTD, Chichester, 2004)

[15] A. Atland and B. Simons Condensed Matter Field Theory (Cambridge University Press, New York, 2010)

[16] M. Sprinkle, D. Siegel, Y. Hu, J. Hicks, A. Tejeda, A. Taleb-Ibrahimi, P. Le Fèvre, F. Bertran, S. Vizzini, H. Enriquez, S. Chiang, P. Soukiassian, C. Berger, W. A. de Heer, A. Lanzara, and E. H. Conrad, Phys. Rev. Lett. **103**, 226803 (2009).

[17] S. Schnez, K. Ensslin, M. Sigrist, and T. Ihn, Phys. Rev. B **78**, 195427 (2008).

[18] M. Grujić, M. Zarenia, A. Chaves, M. Tadić, G. A. Farias, and F. M. Peeters, Phys. Rev. B **84**, 205441 (2011).

[19] D. R. da Costa, M. Zarenia, A. Chaves, G. A. Farias and F.M. Peeters, Carbon **78**, 392-400 (2014).

[20] J. M. Pereira Jr., F. M. Peeters, A. Chaves, and G. Farias, *Klein tunneling in single and multiple barriers in graphene* Semicond. Sci. Technol. **25** (2010) 033002

[21] A. H. Castro Neto, F. Guinea, N. M. R. Peres, K. S. Novoselov, and A. K. Geim, Rev. Mod. Phys. **81**, 109 (2009).

[22] M. I. Katsnelson, K. S. Novoselov, and A. K. Geim, Nature Physics **2**, 620 (2006).

[23] E. McCann and V. I. Falḱo, Phys. Rev. Lett. **96**, 086805 (2006).

[24] A. Matulis and F. M. Peeters, Phys. Rev. B **77**, 115423 (2008).

[25] J. M. Pereira, Jr., P. Vasilopoulos, and F. M. Peeters, Nano Lett. **7**, 946 (2007).

[26] D. P. Zebrowski, E. Wach, and B. Szafran, Phys. Rev. B **88**, 165405 (2013).

[27] L. J. P. Xavier, J. M. Pereira, Jr., Andrey Chaves, G. A. Farias, and F. M. Peeters, Appl. Phys. Lett. **96**, 212108 (2010).

[28] M. Zarenia, J. M. Pereira, Jr., F. M. Peeters, and G. A. Farias, Nano Lett. **9**, 4088 (2009).

[29] M. Zarenia, J. M. Pereira, Jr., A. Chaves, F. M. Peeters, and G. A. Farias, Phys. Rev. B **81**, 045431 (2010).

[30] J. M. Pereira, Jr., F. M. Peeters, P. Vasilopoulos, R. N. Costa Filho, and G. A. Farias, Phys. Rev. B **79**, 195403 (2009).

[31] P. Recher, J. Nilsson, G. Burkard, and B. Trauzettel, Phys. Rev. B **79**, 085407 (2009).

[32] S. Y. Zhou, G. -H. Gweon, A. V. Fedorov, P. N. First, W. A. de Heer, D. -H. Lee, F. Guinea, A. H. Castro Neto, and A. Lanzara, Nature Mater **6**, 770 (2007).

[33] M. V. Berry and R. J. Mondragon, Proc. R. Soc. London, Ser. A **412**, 53 (1987).

[34] M. Ramezani Masir, A. Matulis, and F. M. Peeters, Phys. Rev. B **84**, 245413 (2011).

[35] For negative integer values, *i. e.* $B = 0, -1, -2, ... = -n$, the regularized confluent hypergeometric function can be written as $\widetilde{M}(A, -n, x) = (a)_{n+1} x^{n+1} M(A, B, x)/(n+1)!$, where $(a)_{n+1}$ are the Pochhammer symbols.

[36] An important Kummer property is its derivate, given by $d\widetilde{M}(A, B, x)/dx = A\widetilde{M}(A+1, B+1, x)$.

[37] M. Ramezani Masir, A. Matulis, and F. M. Peeters, Phys. Rev. B **84**, 245413 (2011).

[38] A. Reina, S. Thiele, X. Jia, S. Bhaviripudi, M. Dresselhaus, J. Schaefer, and J. Kong, Nano Res. **2**, 509 (2009)

[39] C. Soldano, A. Mahmood, and E. Dujardin, Carbon **48**, 2127 (2010).

[40] G. Jo, M. Choe, S. Lee, W. Park, Y. H. Kahng, and T. Lee, Nanotechnology **23**, 112001 (2012).

[41] A. H. Castro Neto, F. Guinea, N. M. R. Peres, K. S. Novoselov, and A. K. Geim, Rev. Mod. Phys. **81**, 109 (2009).

[42] J. Güttinger, T. Frey, C. Stampfer, T. Ihn, and K. Ensslin, Phys. Rev. Lett. **105**, 116801 (2010).

[43] B. Trauzettel, D. V. Bulaev, D. Loss, and G. Burkard, Nat. Phys. **3**, 192 (2007).

[44] P. G. Silvestrov and K. B. Efetov, Phys. Rev. Lett. **98**, 016802 (2007).

[45] M. I. Katsnelson, K. S. Novoselov, and A. K. Geim, Nat. Phys. **2**, 620 (2006).

[46] D. A. Bahamon, A. L. C. Pereira, and P. A. Schulz, Phys. Rev. B **79**, 125414 (2009).

[47] Z. Z. Zhang, K. Chang, and F. M. Peeters, Phys. Rev. B **77**, 235411 (2008).

[48] M. Zarenia, A. Chaves, G. A. Farias, and F. M. Peeters, Phys. Rev. B **84**, 245403 (2011).

[49] F. Molitor, J. Güttinger, C. Stampfer, S. Dröscher, A. Jacobsen, T. Ihn, and K. Ensslin, J. Phys.: Condens. Matter **23**, 243201 (2011).

[50] H. P. Heiskanen, M. Manninen, and J. Akola, New J. Phys. **10**, 103015 (2008).

[51] A. V. Rozhkov, G. Giavaras, Y. P. Bliokh, V. Freilikher, and F. Nori, Phys. Rep. **503**, 77 (2011).

[52] M. Calvo, Phys. Rev. B **84**, 235413 (2011).

[53] J. H. Bardarson, M. Titov, and P. W. Brouwer, Phys. Rev. Lett. **102**, 226803 (2009).

[54] J. Park, S. B. Jo, Y.-J. Yu, Y. Kim, J. W. Yang, W. H. Lee, H. H. Kim, B. H. Hong, P. Kim, K. Cho, and K. S. Kim, Adv. Mater. **24**, 407 (2012).

[55] S. Dröscher, J. Güttinger, T. Mathis, B. Batlogg, T. Ihn, and K. Ensslin, Appl. Phys. Lett. **101**, 043107 (2012).

[56] E. V. Castro, K. S. Novoselov, S. V. Morozov, N. M. R. Peres, J. M. B. Lopes dos Santos, J. Nilsson, F. Guinea, A. K. Geim, and A. H. Castro Neto, Phys. Rev. Lett. **99**, 216802 (2007).

[57] F. Xia, D. B. Farmer, Y. M. Lin, and P. Avouris, Nano Lett. **10**, 715 (2010).

[58] M. T. Allen, J. Martin, and A. Yacoby, Nat. Commun. **3**, 934 (2012).

[59] A. M. Goossens, S. C. M. Driessen, T. A. Baart, K. Watanabe, T. Taniguchi, and L. M. K. Vandersypen, Nano Lett. **12**, 4656 (2012).

[60] E. McCann, Phys. Rev. B **74**, 161403(R) (2006).

[61] J. M. Pereira, Jr., P. Vasilopoulos, and F. M. Peeters, Nano Lett. **7**, 946 (2007).

[62] J. M. Pereira, Jr., F. M. Peeters, and P. Vasilopoulos, Phys. Rev. B **76**, 115419 (2007).

[63] A. Matulis and F. M. Peeters, Phys. Rev. B **77**, 115423 (2008).

[64] J. M. Pereira, Jr., F. M. Peeters, P. Vasilopoulos, R. N. Costa Filho, and G. A. Farias, Phys. Rev. B **79**, 195403 (2009).

[65] P. Recher, J. Nilsson, G. Burkard, and B. Trauzettel, Phys. Rev. B **79**, 085407 (2009).

[66] D. P. Zebrowski, E. Wach, and B. Szafran, Phys. Rev. B **88**, 165405 (2013).

[67] D. R. da Costa, M. Zarenia, Andrey Chaves, G. A. Farias, and F. M. Peeters, Carbon **78**, 392 (2014).

[68] D. R. da Costa, M. Zarenia, Andrey Chaves, G. A. Farias, and F. M. Peeters, Phys. Rev. B **92**, 115437 (2015).

[69] Y. B. Zhang, T. T. Tang, C. Girit, Z. Hao, M. C. Martin, A. Zettl, M. F. Crommie, Y. R. Shen, and F. Wang, Nature **459**, 820 (2009).

[70] E. McCann and M. Koshino, Rep. Prog. Phys. **76**, 056503 (2013).

[71] D. Wang and G. Jin, Europhys. Lett. **92**, 57008 (2010).

[72] G. Giavaras, P. A. Maksym, and M. Roy, J. Phys.: Condens. Matter **21**, 102201 (2009).

[73] Y. P. Bliokh, V. Freilikher, and F. Nori, Phys. Rev. B **81**, 075410 (2010).

[74] T. Champel and S. Florens, Phys. Rev. B **82**, 045421 (2010).

[75] G. Giavaras and F. Nori, Phys. Rev. B **85**, 165446 (2012).

[76] S. Y. Zhou, G.-H. Gweon, A. V. Fedorov, P. N. First, W. A. de Heer, D.-H. Lee, F. Guinea, A. H. Castro Neto, and A. Lanzara, Nat. Mat. **6**, 770 (2007).

[77] G. Giovannetti, P. A. Khomyakov, G. Brocks, P. J. Kelly, and J. van den Brink, Phys. Rev. B **76**, 073103 (2007)

[78] M. S. Nevius, M. Conrad, F. Wang, A. Celis, M. N. Nair, A. Taleb-Ibrahimi, A. Tejeda, and E. H. Conrad, Phys. Rev. Lett. **115**, 136802 (2015).

[79] S. Maëro, A. Torche, T. Phuphachong, E. Pallecchi, A. Ouerghi, R. Ferreira, L.-A. de Vaulchier, and Y. Guldner, Phys. Rev. B **90**, 195433 (2014).

[80] S. Schnez, F. Molitor, C. Stampfer, J. Güttinger, I Shorubalko, T. Ihn, and K. Ensslin, Appl. Phys. Lett. **94**, 012107 (2009).

[81] J. Güttinger, C. Stampfer, F. Libisch, T. Frey, J. Burgdörfer, T. Ihn, and K. Ensslin, Phys. Rev. Lett. **103**, 046810 (2009).

[82] D. Subramaniam, F. Libisch, Y. Li, C. Pauly, V. Geringer, R. Reiter, T. Mashoff, M. Liebmann, J. Burgdörfer, C. Busse, T. Michely, R. Mazzarello, M. Pratzer, and M. Morgenstern, Phys. Rev. Lett. **108**, 046801 (2012).

[83] I. torres, L. V. de Castro, B. Van Duppen, D. B. Ruiz, F. M. Peeters, F. H. L. Kopppens and M. Polini, Phy. Rev. B **99**, 144307 (2019)

[84] D. Pines and P. Nozières, *The Theory of Quantum Liquids* (W.A. Benjamin, Inc., New York, 1966).

[85] Z. Fei, A.S. Rodin, G.O. Andreev, W. Bao, A.S. McLeod, M. Wagner, L.M. Zhang, Z. Zhao, M. Thiemens, G. Dominguez, M.M. Fogler, A.H. Castro Neto, C.N. Lau, F. Keilmann, and D.N. Basov, Nature **487**, 82 (2012).

[86] J. Chen, M. Badioli, P. Alonso-González, S. Thongrattanasiri, F. Huth, J. Osmond, M. Spasenović, A. Centeno, A. Pesquera, P. Godignon, A. Zurutuza Elorza, N. Camara, F.J. García de Abajo, R. Hillenbrand, and F.H.L. Koppens, Nature **487**, 77 (2012).

[87] A. Woessner, M.B. Lundeberg, Y. Gao, A. Principi, P. Alonso-González, M. Carrega, K. Watanabe, T. Taniguchi, G. Vignale, M. Polini, J. Hone, R. Hillenbrand, and F.H.L. Koppens, Nature Mater. **14**, 421 (2015).

[88] L. Ju, B. Geng, J. Horng, C. Girit, M. Martin, Z. Hao, H.A. Bechtel, X. Liang, A. Zettl, Y.R. Shen, and F. Wang, Nature Nanotech. **6**, 630 (2011).

[89] P. Alonso-González, A.Y. Nikitin, A. Gao, A. Woessner, M.B. Lundeberg, A. Principi, N. Forcellini, W. Yan, S. Vèlez, A.J. Huber, K. Watanabe, T. Taniguchi, F. Casanova, L.E. Hueso, M. Polini, J. Hone, F.H.L. Koppens, and R. Hillenbrand, Nature Nanotech. **12**, 31 (2017).

[90] M.B. Lundeberg, Y. Gao, R. Asgari, C. Tan, B. Van Duppen, M. Autore, P. Alonso-González, A. Woessner, K. Watanabe, T. Taniguchi, R. Hillenbrand, J. Hone, M. Polini, and F.H.L. Koppens, Science **357**, 187 (2017).

[91] A.N. Grigorenko, M. Polini, and K.S. Novoselov, Nature Photonics **6**, 749 (2012).

[92] D.N. Basov, M.M. Fogler, and F.J. García de Abajo, Science **354**, aag1992 (2016).

[93] T. Low, A. Chaves, J.D. Caldwell, A. Kumar, N.X. Fang, P. Avouris, T.F. Heinz, F. Guinea, L. Martin-Moreno, and F.H.L. Koppens, Nature Mater. **16**, 182 (2017).

[94] D. Alcaraz Iranzo, S. Nanot, E.J.C. Dias, I. Epstein, C. Peng, D.K. Efetov, M.B. Lundeberg, R. Parret, J. Osmond, J.Y Hong, J. Kong, D.R. Englund, N.M.R. Peres, and F.H.L Koppens, Science **360**, 291 (2018).

[95] G.X. Ni, A.S. McLeod,Z. Sun, L. Wang, L. Xiong, K.W. Post, S.S. Sunku, B.Y. Jiang, J. Hone, C.R. Dean, M.M. Fogler, and D.N. Basov, Nature **557**, 530 (2018).

[96] H. Yan, X. Li, B. Chandra, G. Tulevski, Y. Wu, M. Freitag, W. Zhu, P. Avouris, and F. Xia, Nature Nanotech. **7**, 330 (2012).

[97] G.E. Santoro and G.F. Giuliani, Phys. Rev. B **37**, 937 (1988).

[98] A. Principi, R. Asgari, and M. Polini, Solid State Commun. **151**, 1627 (2011).

[99] A. Principi, E. van Loon, M. Polini, and M.I. Katsnelson, Phys. Rev. B **98**, 035427 (2018).

[100] V.N. Kotov, B. Uchoa, V.M. Pereira, F. Guinea, and A.H. Castro Neto, Rev. Mod. Phys. **84**, 1067 (2012).

[101] L. Wang, I. Meric, P.Y. Huang, Q. Gao, Y. Gao, H. Tran, T. Taniguchi, K. Watanabe, L.M. Campos, D.A. Muller, J. Guo, P. Kim, J. Hone, K.L. Shepard, and C.R. Dean, Science **342**, 614 (2013).

[102] G.F. Giuliani and J.J. Quinn, Phys. Rev. B **26**, 4421 (1982).

[103] Z. Qian and G. Vignale, Phys. Rev. B **71**, 075112 (2005).

[104] Q. Li and S. Das Sarma, prb **87**, 085406 (2013).

[105] M. Polini and G. Vignale, *The quasiparticle lifetime in a doped graphene sheet.* In *No-nonsense physicist: an overview of Gabriele Giuliani's work and life* (eds. M. Polini, G. Vignale, V. Pellegrini, and J.K. Jain) (Edizioni della Normale, Pisa, 2016). Also available as arXiv:1404.5728.

[106] A. Principi, G. Vignale, M. Carrega, and M. Polini, Phys. Rev. B **93**, 125410 (2016).

[107] I. Torre, A. Tomadin, A.K. Geim, and M. Polini, Phys. Rev. B **92**, 165433 (2015).

[108] D. Bandurin, I. Torre, R.K. Kumar, M. Ben Shalom, A. Tomadin, A. Principi, G.H. Auton, E. Khestanova, K.S. NovoseIov, I.V. Grigorieva, L.A. Ponomarenko, A.K. Geim, and M. Polini, Science **351**, 1055 (2016).

[109] F.M.D. Pellegrino, I. Torre and M. Polini, Phy. Rev. B **96**, 195401 (2017).

[110] R. Krishna Kumar, D.A. Bandurin, F.M.D. Pellegrino, Y. Cao, A. Principi, H. Guo, G.H. Auton, M. Ben Shalom, L.A. Ponomarenko, G. Falkovich, K. Watanabe, T. Taniguchi, I.V. Grigorieva, L.S Levitov, M. Polini, and A.K. Geim, Nature Phys. **13**, 1182 (2017).

[111] D.A. Bandurin, A.V. Shytov, L.S. Levitov, R. Krishna Kumar, A.I. Berdyugin, M. Ben Shalom, I.V. Grigorieva, A.K. Geim, and G. Falkovich, Nature Comm. **9**, 4533 (2018).

[112] J. Crossno, J.K. Shi, K. Wang, X. Liu, A. Harzheim, A. Lucas, S. Sachdev, P. Kim, T. Taniguchi, K. Watanabe, T.A. Ohki, and K.C. Fong, Science **351**, 1058 (2016).

[113] M.J.M. de Jong and L.W. Molenkamp, prb **51**, 13389 (1995).

[114] B.A. Braem, F.M.D. Pellegrino, A. Principi, M. Röösli, C. Gold, S. Hennel, J.V. Koski, M. Berl, W. Dietsche, W. Wegscheider, M. Polini, T. Ihn, and K. Ensslin, Phys. Rev. B **98**, 241304(R) (2018).

[115] P.J.W. Moll, P. Kushwaha, N. Nandi, B. Schmidt, and A.P. Mackenzie, Science **351**, 1061 (2016).

[116] S. Conti and G. Vignale, Phys. Rev. B **60**, 7966 (1999).

[117] L.D. Landau and E.M. Lifshitz, *Course of Theoretical Physics: Fluid Mechanics* (Pergamon, New York, 1987).

[118] R. Asgari, M.I. Katsnelson, and M. Polini, Ann. Phys. (Berl.) **526**, 359 (2014).

[119] S.H. Abedinpour, G. Vignale, A. Principi, M. Polini, W.K. Tse, and A.H. MacDonald, Phys. Rev. B **84**, 045429 (2011).

[120] L.S. Levitov, A.V. Shtyk, and M.V. Feigelman, Phys. Rev. B **88**, 235403 (2013).

[121] Note that we adopted the definition of Landau parameters given in Ref. [12]. We warn the reader that other authors use a definition that differs from ours by a factor of two for the parameters $F_l^{\rm s}$ with $l > 0$. The definition of $F_0^{\rm s}$ is instead universally accepted.

[122] R.N. Gurzhi, A.N. Kalinenko, and A.I. Kopeliovich, Phys. Rev. Lett. **74**, 3872 (1995).

[123] P.J. Ledwith, H. Guo, A.V. Shytov, and L. Levitov, arXiv:1708.02376.

[124] L. Lorentzend and H. Waadeland, *Continued Fractions with Applications* (Elsevier Science Publishers B.V., North Holland, 1992)

[125] M.S. Steinberg, Phys. Rev. **109**, 1486 (1958).

[126] G.F. Giuliani and J.J. Quinn, Phys. Rev. B **29**, 2321(R) (1984).

[127] F. Stern, Phys. Rev. Lett. **18**, 546 (1967).

[128] A. Tomadin, A. Principi, J.C.W. Song, L.S. Levitov, and M. Polini, Phys. Rev. Lett. **115**, 087401 (2015).

[129] T.V. Phan, J.C.W. Song, and L.S. Levitov, arXiv:1306.4972.

[130] F.H.L. Koppens, D.E. Chang, and F.J.G. de Abajo, Nano Lett. **11**, 3370 (2011).

[131] A. Woessner, A. Mishchenko, A. Misra, I. Torre, M.B. Lundeberg, K. Watanabe, T. Taniguchi, M. Polini, K.S. Novoselov, and F.H.L. Koppens, ACS Photon. **4**, 3012 (2017).

[132] U. Briskot, M. Schütt, I.V. Gornyi, M. Titov, B.N. Narozhny, and A.D. Mirlin, Phys. Rev. B **92**, 115426 (2015).

[133] D. Svintsov, Phys. Rev. B **97**, 121405(R) (2018).

[134] A.A. Abrikosov and I.M. Khalatnikov, Sov. Phys. JETP **6**, 84 (1958).

[135] A.A. Abrikosov and I.M. Khalatnikov, Rep. Prog. Phys. **22**, 329 (1959).

[136] W.R. Abel, A.C. Anderson, and J.C. Wheatley, Phys. Rev. Lett. **17**, 74 (1966).

[137] A. Lucas and S. Das Sarma, Phys. Rev. B **97**, 115449 (2018).

[138] Z. Sun, D.N. Basov, and M. Fogler, Proc. Natl. Acad. Sci. (USA) **115**, 3285 (2018).

[139] A. H. C. Neto, F. Guinea, N. M. Peres, K. S. Novoselov and A. K. Geim. Rev. Mod. Phys. **89**, 109 (2009)

[140] C. W. Groth, M. Wimmer, A. R. Akhmerov and X. Waintal. New J. Phys. **16**,063065 (2014)

[141] K. Wakabayashi, K. Sasaki, T. Nakanishi and T. Enoki, Sci. Technol. Adv. Mater. **11**, 054504 (2010).

[142] A. Carvalho, A.S.Rodin and A. H. Castro Neto, EPL **108**, 47005 (2014)

[143] W. Jones and N. H. March, *Theoretical Solid state physics Vol.2* (Dover publications, Inc., New York, 1973).

[144] S. J. Allen, H. L. Stormer, and J. C. M. Hwang, Phys. Rev. B **28**, 8 (1973).

[145] V. I. Talyanskii, A.V. Polisski, D. D. Arnone, M. Pepper, C. G. Smith, D. A. Ritchie J. E. F. Frost, and G. A. C. Phys. Rev. B **46**, 12427 (1992).

[146] E. Batke, D. Heitmann, J. P. Kotthaus and K. Ploog, Phys. Rev. Letters **54**, 2367

[147] N. B. Zhitenev, R. J. Haug, K. v. Klitzing, and K. Eberl, Phys. Rev. Lett. **71**, 2292 (1993).

[148] G. Sukhodub, F. Hols and R. J. Haug, Phys. Rev. Letters **93**, 19 (2004).

[149] I. Grigelionis, K. Nogajewski, G. Karczewski, T. Wojtowicz, M. Czapkiewicz, J. Wr. obel,H. Boukari, H. Mariette, and J. Lusakowski, Phys. Rev. B **91** 075424 (2015).

[150] Hugen Yan, Zhiqiang Li, Xuesong Li, Wenjuan Zhu, Phaedon Avouris, and Fengnian Xia, Nano Lett. 2012,12, 73766-3771

[151] K. W. Chiu and J. J. Quinn, Phys. Rev. B **9**, 11 (1974).

[152] P A D Gonçalves and N. M. R. Peres, *An Introduction to Graphene Plasmonics* (World scientific, 2016).

[153] R. Roldán, M. O. Goerbig, and J.-N. Fuchs, Phys. Rev. B **83**, 205406 (2011).

[154] R. S. Akzyanov, A. O. Sboychakov, A. V. Rozhkov, A. L. Rakhmanov, and Franco Nori, Phys. Rev. B **90** 55415 (2014).